Fall 1994

Shear strength and fatigue crack propagation in concrete by energy method

Wei Wang
New Jersey Institute of Technology

Copyright Warning & Restrictions

The copyright law of the United States (Title 17, United States Code) governs the making of photocopies or other reproductions of copyrighted material.

Under certain conditions specified in the law, libraries and archives are authorized to furnish a photocopy or other reproduction. One of these specified conditions is that the photocopy or reproduction is not to be "used for any purpose other than private study, scholarship, or research." If a, user makes a request for, or later uses, a photocopy or reproduction for purposes in excess of "fair use" that user may be liable for copyright infringement,

This institution reserves the right to refuse to accept a copying order if, in its judgment, fulfillment of the order would involve violation of copyright law.

Please Note: The author retains the copyright while the New Jersey Institute of Technology reserves the right to distribute this thesis or dissertation

Printing note: If you do not wish to print this page, then select "Pages from: first page # to: last page #" on the print dialog screen

ABSTRACT

SHEAR STRENGTH AND FATIGUE CRACK PROPAGATION IN CONCRETE BY ENERGY METHOD

Wei Wang

The limit analysis methods have been commonly used to predict the ultimate flexure strength of reinforced concrete members over 50 years. However, current design formulas for shear in structural concrete are mostly empirical. In part one of this dissertation, attempts are made to apply the theory of plasticity to predict the shear strengths of reinforced concrete structures.

The modified Coulomb-Mohr failure criterion is used as the constitutive law of concrete, and the plastic flow is assumed to be associated with this failure criterion. A generalized formulation for energy dissipation in accordance with the failure criterion and associated flow rule is proposed in this dissertation. The upper-bound method is used to predict the shear strengths of reinforced concrete members, including push-off shear transfer, bracket and deep beams. The proposed method is also used to predict the torsional strength of reinforced concrete beams. The theoretical solutions show a good agreement with the existing experimental results.

A structural coefficient of plasticity is proposed to consider the effect of hydrostatic pressure on the ductility of concrete materials. This structural coefficient of plasticity, namely ν_s, is found to be a function of reinforcement indexes and shear span ratios. Different ν_s' are given in this dissertation.

The fracture property of concrete structures becomes an increasingly important issue in the engineering practice because of the changing working of environment of reinforced concrete structures. Part two of this dissertation is designated to the study of the fracture and fatigue characteristics of structural concrete.

In part two, a generalized process zone theory based on the Paris' energy formula is proposed to study the inelastic fracture properties. This generalized process zone theory is capable of analyzing inelastic fracture characteristics of engineering materials in general. The so-called sized effect is formulated by this proposed generalized process zone theory for softening materials. A brittleness index is also proposed in this research based on the this generalized process zone theory. This brittleness index may be used to characterize the inelastic fracture properties of the structures.

A damage accumulation theory is proposed in this research to predict the fatigue crack propagation rate. The damage of the materials near crack tips caused by the cyclic load is characterized by the plastic component of J integral, or, the plastic fracture energy of the system. A fatigue crack propagation formula is proposed based on this damage accumulation theory. With the inelastic fracture properties predicted by the proposed generalized process zone theory, this fatigue crack propagation formula is capable of predicting the crack growth rate in metals and structural concrete. This theory is also able to predict the fatigue threshold of metals and concrete materials. Test results show that the proposed theory has a good accuracy in both metals and structural concrete.

SHEAR STRENGTH AND FATIGUE CRACK PROPAGATION IN CONCRETE BY ENERGY METHOD

by
Wei Wang

A Dissertation
Submitted to the Faculty of
New Jersey Institute of Technology
in Partial Fulfillment of the Requirements for the Degree of
Doctor of Philosophy in Civil Engineering

Department of Civil and Environmental Engineering

January 1995

APPROVAL PAGE

SHEAR STRENGTH AND FATIGUE CRACK PROPAGATION IN CONCRETE BY ENERGY METHOD

Wei Wang

Dr. C.T. Thomas Hsu, Dissertation Advisor Professor of Civil and Environmental Engineering, NJIT	Date
Dr. William Spillers, Committee Member Professor and Chairman of Civil and Environmental Engineering, NJIT	Date
Dr. Farhad Ansari, Committee Member Professor of Civil and Environmental Engineering, NJIT	Date
Prof. Namunu Meegoda, Committee Member Associate Professor of Civil and Environmental Engineering, NJIT	Date
Dr. Denis Blackmore, Committee Member Professor of Applied Mathematics, NJIT	Date

BIOGRAPHICAL SKETCH

Author: Wei Wang

Degree: Doctor of Philosophy in Civil Engineering

Date: January, 1995

Undergraduate and Graduate Education:

Doctor of Philosophy in Civil Engineering,
New Jersey Institute of Technology, Newark, NJ 1995

Bachelor of Science in Civil Engineering,
Tongji University,Shanghai, China, 1984

Major: Structural Engineering

Publications:

Invited Articles:

Wang, W. and Hsu, C.T.T.(1994). "Generalized process zone and accumulative damage theory in fatigue crack propagation." Chapter in the *Handbook of Fatigue Crack Propagation in Metallic Structures*, edited by Andrea Carpinteri, to be published by Elsevier Science Publishers.

Wang, W. (1988). "No-fine concrete." chapter in *Modern Concrete and Construction Methods*. National Civil Engineering Publishing House, Beijing, China, (in Chinese).

Journal Papers:

Wang, W. and Hsu, C.T.T.(1994). "Fatigue crack growth rate of metal by plastic energy damage accumulation theory." *Journal of Engineering Mechanics,* ASCE, Vol. 120, No. 4, April, pp. 776-795.

Wang, W., Jiang, D.H. and Hsu, C.T.T. (1993). "Shear strength of reinforced concrete deep beams." *Journal of Structural Engineering*, ASCE, Vol. 119, No. 8, August, pp. 2294-2312.

Wang, W. (1986). "Ultimate Strength of T/L Shaped Columns Under Biaxial Loading." *Journal of Structural Engineer*, Vol. 1, No.2, Shanghai, China,(in Chinese).

ACKNOWLEDGMENT

The author wishes to express his sincere gratitude to his advisor, Professor C.T. Thomas Hsu, for his guidance, friendship, and constant support throughout this research.

Special thanks are expressed to Professors Farhad Ansari, Denis Blackmore, Namunu Meegoda and William Spillers for serving as the members of the advisory committee.

The author wishes to express his sincere gratefulness and respect to his former advisor, Professor Da-Hua Jiang at Tongji University, Shanghai, China. It would have been impossible for the author to begin his research career without his guidance, support and friendship. His style, spirit and attitude towards his academic life have influenced the author significantly during the past ten years.

Sincere thanks are expressed to Professor Paul C. Chan for his support during the course of the preparation of this dissertation.

The author is grateful to Liaison Committee of Rectors Conference of European Economic Community Countries for providing the initial funding for this research project, and also to the Department of Civil and Environmental Engineering and the Office of Graduate Studies at the New Jersey Institute of Technology for the financial support in pursuit of this degree.

Special thanks are expressed to a fellow doctoral student, Mr. Haitao Bian, for his help in preparing this dissertation.

This dissertation is dedicated
to my family

TABLE OF CONTENTS
(Part I)

TABLE OF CONTENTS
(**Part I** Continued)

TABLE OF CONTENTS
(Part II)

TABLE OF CONTENTS
(Part II Continued)

LIST OF TABLES

LIST OF FIGURES

LIST OF FIGURES
(Continued)

LIST OF FIGURES
(Continued)

LIST OF FIGURES
(Continued)

PART I

CHAPTER 1

INTRODUCTION

1.1 General

The research on shear strength related failures of reinforced concrete structures was a focal point during the past 30 years. In the 70's, the application of the theory of plasticity started a new chapter of reinforced concrete mechanics. Several constitutive models were developed exclusively for concrete material. These constitutive models made the application of the nonlinear finite element analysis method in reinforced concrete structures possible. The nonlinear finite element analysis method provides detailed structural analysis which would not have been possible in the past. A carefully constructed model may be able to analyze the crack initiation, propagation and ultimate load of reinforced concrete structures(Okaemure and Maekawa, 1991). However, because of its higher cost, nonlinear analysis methods may not be considered as a conventional engineering practice.

As a practical, simple, and effective method, the limit analysis has been used to predict the ultimate strength of reinforced concrete structures for over fifty years. Rather than elastic approach, the limit analysis method is based on the theory of plasticity, thus, it

provides a solid theoretical background in describing structures made of reinforced concrete which is well-known to be a reasonably ductile composite material. In the 30's Johansen (1932) established the plastic theory for slabs. Known as the yield line theory, his attempt in applying the classical theory of plasticity to reinforced concrete structures was a complete success and it initiated a new age of the mechanics of reinforced concrete structures.

A generalized theory of plasticity was postulated by Gvozdev in 1938 (Gvozdev, 1938) and Prager (1952) independently. Gvozdev's work was not known to the west until 1960 when his original paper was translated into English. Similar research was conducted at Brown University in USA. Their work formed a so called "Prager School" in the field of plasticity. Most of their researches are considered as fundamentals in modern theory of plasticity(Nielsen, 1971).

One of the most important improvements during the development of the theory of plasticity was undoubtedly the establishment of the so called upper- and lower-bound theorems. The contents of these theorems indeed known by intuition long before Gvozdev's work and those of the "Prager School" appeared. However, a complete precise formulation was given by Gvozdev (1938) and Drucker, Greenberg, and Prager (1952), independently. The upper- and lower-bound theories have been proved to be very valuable tools in the engineering practice.

In the 70's and 80's, the generalized formulation for limit analysis of reinforced concrete structures was initiated by applying the theory of plasticity. Different constitutive laws for concrete material were developed during this period of time (Kupffer, 1969, Ottosen, 1977). These constitutive laws provide a solid base of the modern limit analysis method for reinforced concrete structures. Several research groups worked on this field during this period of time. Among them are Nielsen's work on reinforced concrete disk and beams (Nielsen, 1971), Chen's work on splitting specimen (Chen, 1982), Bræstrup (1978) and Jiang's (Jiang and Shen, 1986) punching shear of slabs. These studies together with researches conducted by others in this area have all contributed significantly to the development of limit analysis in reinforced concrete structures.

1.2 Scope and Objective of Research

In spite of the progress made in the 70's and 80's, the research and application of the theory of limit analyses of reinforced concrete structures subjected to multi-axial stresses is still a challenging task. Progress in this field will influence the future design and analysis method of reinforced concrete structures.

The theory of limit analysis for reinforced concrete flexural members has become well established since the development of both the yield line theory and the stripe

theory (Johensen, 1932, Helloborg's 1953, 1956). However, researches on shear strength of different reinforced concrete structural elements only began in the 70's and 80's (Nielsen, 1971, Bræstrup and Nielsen 1978, Jiang and Shen, 1986). These research problems included shear strength of slender beams, shear strength of reinforced concrete panels, and punching shear strength of slabs, etc. These studies were essentially important in initiating researches in this field.

Like all the other pioneer researches in the history, these studies lacked relevance. A generalized or unified method must be developed to reveal the fundamental shear properties of reinforced concrete structures. Progress in such an attempt may provide possibilities for a more consistent and efficient reinforced concrete design code based on limit analysis methods. The scope and objective of this research is to seek the possibility of establishing such a unified theory, and apply it to different problems, thus leading to a series of consistent solutions to these problems.

1.3 Brief Review of Limit Analysis

1.3.1 Stress Tensor

A Stress tensor may be defined as follows in Cartesian coordinates(Chen and Han, 1988)

$$\sigma_{ij} = \begin{bmatrix} \sigma_{11} & \sigma_{12} & \sigma_{13} \\ \sigma_{21} & \sigma_{22} & \sigma_{23} \\ \sigma_{31} & \sigma_{32} & \sigma_{33} \end{bmatrix} \qquad 1.1$$

This stress tensor can be written using Von Karman's notation in the form

$$\sigma_{ij} = \begin{bmatrix} \sigma_x & \tau_{xy} & \tau_{xz} \\ \tau_{yx} & \sigma_y & \sigma_{yz} \\ \tau_{zx} & \tau_{zy} & \sigma_z \end{bmatrix} \qquad 1.2$$

Principal directions are defined as the directions of the Cartesian coordinates that satisfy the following relation

$$\sigma_{ij} \equiv 0 \text{ if } i \neq j \qquad 1.3$$

As shown in Equation 1.3, the stress tensor has only normal component in a principal direction $\mathbf{n_i}$. Thus the principal direction shall have the following form

$$\sigma_{ij} n_j = \sigma n_i \qquad 1.4$$

Using the Kronecker Delta δ_{ij}, the above equation yields

$$(\sigma_{ij} - \sigma\delta_{ij})n = 0 \qquad 1.5$$

which implies

$$\begin{cases} (\sigma_{11} - \sigma)n_1 + \sigma_{12}n_2 + \sigma_{13}n_3 = 0 \\ \sigma_{21}n_1 + (\sigma_{22} - \sigma)n_2 + \sigma_{23}n_3 = 0 \\ \sigma_{31}n_1 + \sigma_{32}n_2 + (\sigma_{33} - \sigma)n_3 = 0 \end{cases} \qquad 1.6$$

In order to obtain a nontrivial solution from the above simultaneous linear equations, the determinant of the coefficient must vanish

$$\begin{vmatrix} (\sigma_{11}-\sigma) & \sigma_{12} & \sigma_{13} \\ \sigma_{21} & (\sigma_{22}-\sigma) & \sigma_{23} \\ \sigma_{31} & \sigma_{32} & (\sigma_{33}-\sigma) \end{vmatrix} = 0 \qquad 1.7$$

or in the abbreviated notation

$$\left|\sigma_{ij}-\sigma\delta_{ij}\right| = 0 \qquad 1.8$$

Equation 1.8 yields

$$\sigma^3 - I_1\sigma^2 + I_2\sigma - I_3 = 0 \qquad 1.9$$

where

$$I_1 = \sigma_{11}+\sigma_{22}+\sigma_{33} \qquad 1.10$$

$$I_2 = \begin{vmatrix} \sigma_{22} & \sigma_{23} \\ \sigma_{32} & \sigma_{33} \end{vmatrix} + \begin{vmatrix} \sigma_{11} & \sigma_{13} \\ \sigma_{31} & \sigma_{33} \end{vmatrix} + \begin{vmatrix} \sigma_{11} & \sigma_{12} \\ \sigma_{21} & \sigma_{22} \end{vmatrix} \qquad 1.11$$

$$I_3 = \begin{vmatrix} \sigma_{11} & \sigma_{12} & \sigma_{13} \\ \sigma_{21} & \sigma_{22} & \sigma_{23} \\ \sigma_{31} & \sigma_{32} & \sigma_{33} \end{vmatrix} \qquad 1.12$$

Here, I_1, I_2 and I_3 are referred to as *invariants of the stress tensor* since they are independent of the rotation of the coordinate axes. In principal directions, the stress invariant can be written as

$$\begin{aligned} I_1 &= \sigma_1+\sigma_2+\sigma_3 \\ I_2 &= \sigma_1\sigma_2+\sigma_2\sigma_3+\sigma_3\sigma_1 \\ I_3 &= \sigma_1\sigma_2\sigma_3 \end{aligned} \qquad 1.13$$

A stress state at a point may be described by a *hydrostatic (spherical) stress* tensor and *stress deviatoric* tensor. The hydrostatic stress tensor

indicates the mean stress level that the material is subjected to. The stress deviatoric tensor represents the shear related properties of a stress state. The hydrostatic stress tensor has elements of $p\delta_{ij}$, where p is the mean stress and is given by

$$p = \frac{1}{3}\sigma_{kk} = \frac{1}{3}(\sigma_1 + \sigma_2 + \sigma_3) = \frac{1}{3}I_1 \qquad 1.14$$

The stress deviatoric tensor is defined by subtracting the hydrostatic stress tensor from the actual stress tensor,

$$s_{ij} = \sigma_{ij} - p\delta_{ij} \qquad 1.15$$

The procedure used in deriving the formulation of stress invariant may be applied to obtain the invariant of the stress deviator s_{ij}. To ensure a nontrivial solution for principal stress deviator, the following must be satisfied

$$\left|s_{ij} - s\delta_{ij}\right| = 0 \qquad 1.16$$

or

$$s^3 - J_1 s^2 - J_2 s^2 - J_3 = 0 \qquad 1.17$$

where J_1, J_2, and J_3 are the invariant of the stress deviator tensor. Similar to the stress invariant, the invariant of the stress deviator tensor can be found as follows

$$\begin{aligned} J_1 &= s_{ii} = s_{11} + s_{22} + s_{33} = s_1 + s_2 + s_3 = 0 \\ J_2 &= \frac{1}{2}s_{ij}s_{ji} = \frac{1}{6}[(s_1 - s_2)^2 + (s_2 - s_3)^2 + (s_3 - s_1)^2] \\ J_3 &= \frac{1}{3}s_{ij}s_{jk}s_{ki} = s_1 s_2 s_3 \end{aligned} \qquad 1.18$$

where s_{ij} is the stress deviator tensor.

The invariant of the stress deviator tensor may also be written in terms of invariants I_1, I_2, and I_3, which leads to:

$$J_1 = 0$$
$$J_2 = \frac{1}{3}(I_1^2 + 2I_2) \qquad 1.19$$
$$J_3 = \frac{1}{27}(2I_1^3 - 9I_1I_2 + 27I_3)$$

And also, these invariants may be written in terms of principal stresses. For example, the second invariant has the form of

$$J_2 = \frac{1}{6}\left[(\sigma_1 - \sigma_2)^2 + (\sigma_2 - \sigma_3)^2 + (\sigma_3 - \sigma_1)^2\right] \qquad 1.20$$

As shown in Equation 1.58, the second invariant of stress deviator tensor J_2 is a shear stresses and specific strain energy related parameter. It has been widely accepted that the ductile failure of material is mainly caused by shear stresses and dissipation of strain energy. Thus the majority of the postulated failure criteria are proposed as functions of J_2 for a three-dimensional stress state. (Hsieh, et al. 1982) (Willam and Warnke, 1975)

1.3.2 Failure Criteria of Engineering Material

Engineering materials may be classified into two major categories, namely pressure independent and pressure dependent ones. Most metals are of the first category, or, pressure independent. Failure criteria for these materials are functions of J_2. In contrast, the

strengths of cementitious materials, such as concrete and mortar, are hydrostatic pressure dependent. Their failure criteria shall be functions of J_2 and I_1 simultaneously.

Different failure criteria for both hydrostatic dependent and independent materials were postulated in the past. Several well developed criteria have been widely used in engineering practice. Among them are the Tresca maximum shear stress model and von Mises' maximum specific strain energy criterion (Hill, 1950) for pressure independent materials, and Coulomb's internal friction criterion for pressure dependent materials (Coulomb, 1773).

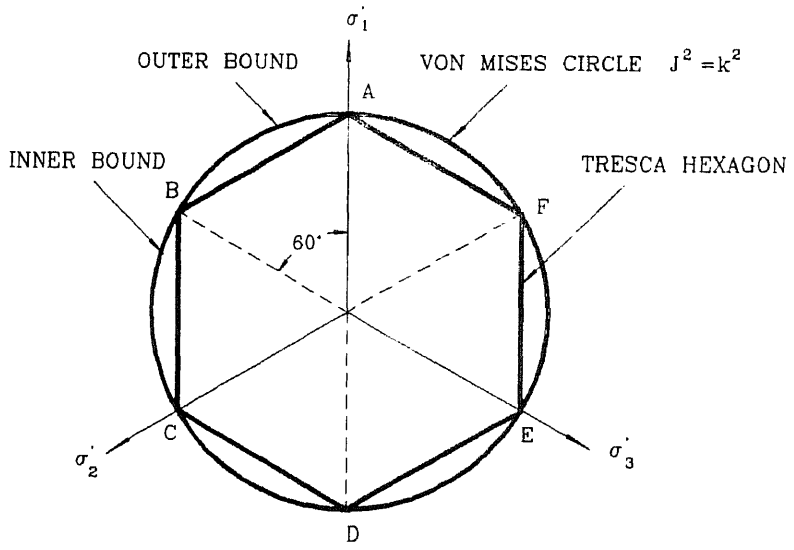

Figure 1.3.1 Yield Criteria Matched in Tension in a Deviatoric Plane (Chen and Han, 1988)

Pressure Independent Yield Criteria: In the theory of plasticity, failure criteria may be defined in terms of surfaces in a stress space, known as Haigh-Westgaard stress-spaces (Chen and Han, 1988). For a pressure independent material, its failure surface has a cyclinderial shape along the hydrostatic axis (see Figure 1.3.1 and 1.3.2) since the surface is a pressure independent function.

The Tresca yield criterion defines that the failure of the material as the applied maximum shear strength reaches a critical value **k**. This critical values may be determined by the uniaxial yield strength σ_0, namely

$$k = \frac{\sigma_0}{2} \qquad 1.21$$

Tresca's maximum shear criterion has the form of

$$\text{Max}\left(\frac{1}{2}|\sigma_1 - \sigma_2|,\ |\sigma_2 - \sigma_3|,\ \frac{1}{2}|\sigma_3 - \sigma_1|\right) = k \qquad 1.22$$

in terms of principal stresses. It defines a regular hexagonal prism surface in the principal stress space as shown in Figure 1.3.1. Tresca's yield criterion can also be expressed in terms of the invariant J_2 and J_3

$$f(J_2, \theta) = 2\sqrt{J_2}\sin\left(\theta + \frac{\pi}{3}\right) - \sigma_0 = 0 \ (0 \le \theta \le 60^0) \qquad 1.23$$

where θ is the direction of the stress tensor with respect to the first principal stress in the π-plane.

Von Mises' Failure criterion is based on the maximum specific strain energy dissipated by the material. The failure of materials occurs when the specific strain energy in the material reaches the critical value, namely

$$f(J_2) = J_2 - k^2 = 0 \qquad 1.24$$

or in principal stresses

$$(\sigma_1 - \sigma_2)^2 + (\sigma_2 - \sigma_3)^2 + (\sigma_3 - \sigma_1)^2 = 6k^2 \qquad 1.25$$

where

$$k = \frac{\sigma_0}{\sqrt{3}} \qquad 1.26$$

Von Mises' yield criterion defines a circular cylinder in the principal stress space as shown in Figure 1.3.2. These two pressure independent yield criteria have been widely used in the analysis and design of metallic structures for decades.

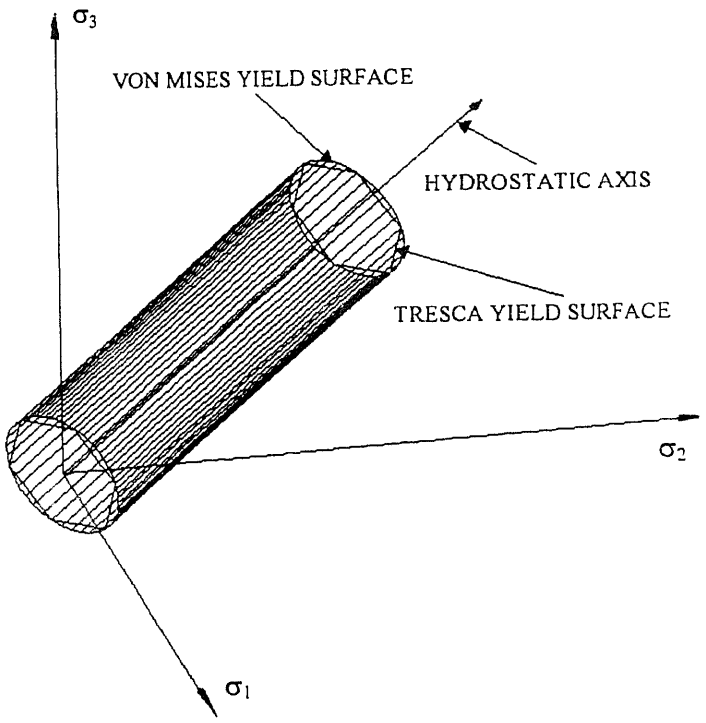

Figure 1.3.2 Yield Surfaces in Principal Stress Space(Chen and Han, 1988)

Pressure Dependent Failure Criteria: Strengths of most cementitious composites, such as concrete, mortar and rock, are hydrostatic pressure dependent. In contrast, the failure surface of a hydrostatic dependent material varies in accordance with different values of the hydrostatic pressure. Higher negative hydrostatic pressures may increase the yield strength of the material, thus, the failure surfaces shall have a larger cross section perpendicular to the hydrostatic pressure axis.

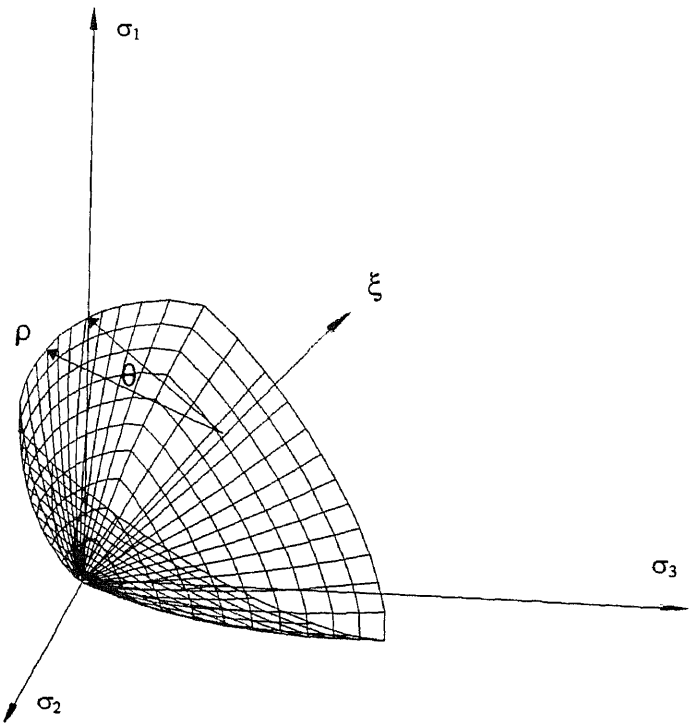

Figure 1.3.3 Ottosen Failure Criterion for Concrete Materials

Most cementitious materials are hydrostatic pressure dependent. Their failure surfaces are convex and have a closed end at the higher positive hydrostatic pressure side. Physically, the closed end on failure surfaces indicates that the material may fail due to positive (tensile) hydrostatic pressure.

Ottosen's four-parameter failure criterion (Ottosen, 1977) defines a typical failure surface (Figure 1.3.3) for cementitious material. It has a closed end at the tension side and opens at the compression side. These materials are referred to as Coulomb materials occasionally since their strength can be considered as internal-friction dependent. The Mohr-Coulomb criterion defines the critical shear stress as a function of cohesion c and internal-friction angle ϕ.

$$|\tau| = c - \sigma \tan\phi \qquad 1.27$$

In principal stress space, the Mohr-Coulomb criterion reads

$$\sigma_1 \frac{1+\sin\phi}{2c\cos\phi} - \sigma_3 \frac{1-\sin\phi}{2c\cos\phi} = 1 \qquad 1.28$$

Where ϕ is the internal friction angle. Define

$$f_c' = \frac{2c\cos\phi}{1-\sin\phi}, \text{ and}$$
$$f_t' = \frac{2c\cos\phi}{1+\sin\phi} \qquad 1.29$$

Equation 1.28 may be simplified as

$$\frac{\sigma_1}{f_t'} - \frac{\sigma_3}{f_c'} = 1 \qquad \text{for} \quad \sigma_1 \geq \sigma_2 \geq \sigma_3 \qquad 1.30$$

If expressed in terms of the invariant, the Mohr-Coulomb failure criterion yields

$$f(I_1, J_2, \theta) = \frac{1}{3} I_1 \sin\phi + \sqrt{J_2}\sin(\theta + \frac{\pi}{3}) + \frac{\sqrt{J_2}}{\sqrt{3}}\cos(\theta + \frac{\pi}{3})\sin\phi - c\cos\phi = 0 \qquad 1.31$$

As expected, the Mohr-Coulomb failure surface has a hexagonal section that is similar to the Tresca yield criterion since they all define the failure of the material in terms of maximum shear stress. Indeed, the Mohr-Coulomb criterion becomes identical with Tresca's yield criterion when $\phi = 0$ as it should be.

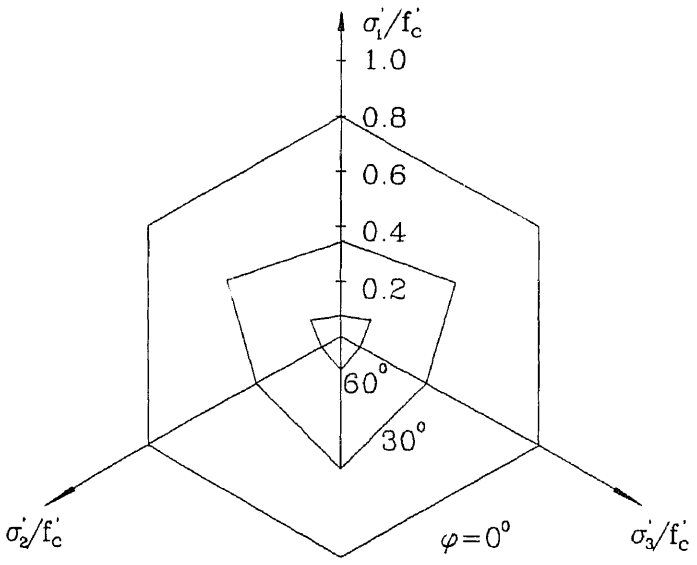

Figure 1.3.4 Coulomb Failure Criteria in the Deviatoric Plane for Different ϕ's (Chen and Han, 1988)

The Coulomb failure criterion assumes a constant internal friction angle for a given material. As a matter of fact, the internal friction depends on the hydrostatic pressure in the material. On a macro-level, the strength of the material appears to be a function of hydrostatic pressure. Larger hydrostatic stresses may lead to a higher strength of the material. However, the increment in strength is not a linear function of the hydrostatic pressure. A higher negative hydrostatic stress increases the internal friction, and so the strength of the material. However, it may also damage the inter-lock system in the material and lead to a lower internal friction angle. Thus, the incremental strength becomes smaller.

In fact, the failure of a cementitious material is more likely to be both internal-friction and specific plastic strain energy dependent. Thus, its failure surface has a rounder sectional shape, especially when the material is subjected to a higher negative hydrostatic pressure.

Concrete is a most commonly used cementitious material. When it is subjected to a lower negative hydrostatic pressure, its strength is mostly dependent upon the maximum tensile strength. Thus, its failure surface has a triangle section corresponding to a high ϕ value (see Figure 1.3.4). For stress states with high negative hydrostatic pressure, the strength of concrete

is more likely to be dominated by strain energy dissipation. Therefore, the cross section of the failure surface at high negative hydrostatic pressure has a shape closer to a circle defined by von Mises criterion.

Ottosen (1977) suggested the following criterion to define a failure surface having the above properties. His equation is classified as a four parameter formula, and has the form of:

$$f(I_1,J_2,\theta) = aJ_2 + \lambda\sqrt{J_2} + bI_1 - 1 = 0 \qquad 1.32$$

where λ is a function of $\cos 3\theta$

$$\lambda = \begin{cases} k_1 \cos[\frac{1}{3}\cos^{-1}(k_2 \cdot \cos 3\theta)] \\ k_1 \cos[\frac{\pi}{3} - \frac{1}{3}\cos^{-1}(-k_2 \cdot \cos 3\theta)] \end{cases} \qquad 1.33$$

a, b, k_1, and k_2 are constants that may be determined by the so-called membrane analogy. The values of these constants for different f_t/f_c' ratios are given in Table 1.3.1

Table 1.3.1 Parameters and their dependence on f_t/f_c' ratios

f_t/f_c'	a	b	k_1	k_2
0.08	1.8076	4.0962	14.4863	0.9914
0.10	1.2759	3.1962	11.7365	0.9801
0.12	0.9218	2.5969	9.9110	0.9647

Ottosen's criterion successfully described the general shape of a failure surface of cementitious

material. It is valid for a wide range of stress combinations. With its explicit formulation, his criterion is easily applied in finite element analysis methods.

1.3.3 Plastic Flow and Associated Flow Rule

A perfectly plastic material has no strain hardening beyond the yield surface. Thus, plastic deformation (*plastic flow*) occurs under a constant flow stress (yield strength). In terms of the theory of plasticity, plastic flow occurs if

$$f(\sigma_{ij}, k) = 0 \qquad 1.34$$

where σ_{ij} is the stress tensor, and k is a constant. In case of materials undergoing plasticity, the stress tensor can only move on the yield surface, therefore, the increment of the yield function is equal to zero, i.e.

$$f(\sigma_{ij}, k) = 0 \quad \text{and} \quad df = \frac{\partial f}{\partial \sigma_{ij}} d\sigma_{ij} = 0 \qquad 1.35$$

The criteria for unloading is

$$f(\sigma_{ij}, k) = 0 \quad \text{and} \quad df = \frac{\partial f}{\partial \sigma_{ij}} d\sigma_{ij} < 0 \qquad 1.36$$

A so called plastic flow rule was postulated to define the incremental plastic strain tensor $d\varepsilon^{p}_{ij}$. Von Mises (1928) proposed a plastic potential function $g(\sigma_{ij})$ which is a scalar function of the stress tensor σ_{ij}.

Then the incremental plastic strain tensor may be found as

$$d\varepsilon_{ij}^{p} = d\lambda \frac{\partial g}{\partial \sigma_{ij}} \qquad 1.37$$

This relation was later known as the flow rule in the theory of plasticity. Assume that $f = g$, or the plastic potential function and the yield function coincide, the flow rule yields

$$d\varepsilon_{ij}^{p} = d\lambda \frac{\partial f}{\partial \sigma_{ij}} \qquad 1.38$$

where $d\lambda$ is a positive scalar factor of proportionality, which is non-zero only when plastic flow occurs.

Equation 1.38 is called the associated the flow rule since the plastic flow is associated with the yield surface (Hill, 1950). In contrast, Equation 1.37 is defined as the non-associated flow rule in case of $f \neq g$. Geometric interpretation of Equation 1.38 leads to the following: the incremental plastic strain has the same direction as the normal of the yield surface of the material since $d\lambda$ is a constant during the course of undergoing plastic flow. This concept will be used in the following section to derive the strain energy dissipation rate.

1.3.4 Lower-and Upper-Bound Theorems

The basic theorem of limit analysis has been used for decades and can be established directly for a structure with the following properties (Chen 1982):

1. The material exhibits perfect or ideal plasticity, i.e. work hardening or work softening does not occur. This implies that stress states cannot move outside the yield surface along any loading path, so that stress vectors in the yield zone of a structures must be tangential to the surface whenever the plastic-strain rate are occurring.
2. The yield surface is convex, and the plastic-strain are derivable from the yield function through the associated flow rule.
3. Changes in geometry of the structure that occur at the collapsed load are insignificant, i.e. the principle of virtual work can be used.

The collapsed load of an idealized structure having the ideal properties listed above is called *limit load*. The basic theories construct the base *limit analysis*, namely *upper and lower bound theorems*.

The upper-bound theorem states that a structure will collapse if there is any compatible pattern of plastic deformation for which the external forces do work that exceed the internal dissipation. It is a formal statement which explains that in all the possible collapsed paths, the external force will find the

optimal path that requires the least amount of work done to destroy a structure.

In contrast the lower bound method states that if an equilibrium of stress can be found to balance the applied load and is everywhere within yielding or at yielding, the structure will not collapse or will be just at the point of collapse. In other words, from the point of view of a system, it always finds its maximum capacity to carry the external load to maintain the integrity of the system. However, the external loads always find the way to destroy the system with the least energy. In this sense, the two basic theorems of limit analysis explains, at least from the point of view of mechanics, the basic and delicate law of the nature, i.e., the nature always finds the best way to maintain or destroy a system as it wishes.

A solution from limit analysis is said to be exact if the upper bound solution matches the lower bound solution. However, it is difficult in general to find both lower- and upper-bound solution for a system, especially for reinforced concrete structures. In practice, either a lowest upper-bound solution with a compatible failure mechanism or an uppermost lower bound solution which satisfies the force boundary condition may provide a satisfactory estimation of the ultimate strength of the structure. The analyses of shear strengths in reinforced concrete structures provided in

part I of this dissertation are based on the upper-bound theorem.

1.4 Constitutive Laws

Failure criteria for general engineering materials have been discussed in section 1.3.2. Hereafter, a modified Coulomb-Mohr failure criterion is discussed in details. This failure criterion is used intensively throughout this investigation on the shear strengths of different reinforced concrete structural elements.

In solving punching shear problems, Jiang and Shen (1986) used a parabolic Coulomb-Mohr intrinsic curve as the yield criterion for concrete. The parabola shown in Figure 1.4.1 gives the following relation between shear stress τ_{nt} and normal stress σ_n on the yield surface,

$$\frac{\sigma_n}{f_t^*}+\frac{1}{K}\left(\frac{\tau_{nt}}{f_t^*}\right)^2=1 \qquad 1.39$$

$$K=\frac{1}{4}[m+2(1-\sqrt{m+1})], \text{ and} \qquad 1.40$$

$$m=\frac{f_c^*}{f_t^*}=\frac{\nu_c f_c'}{\nu_t f_t'} \qquad 1.41$$

where

f_t^*, f_c^* = plastic (or effective) tensile and compressive strengths of concrete,

f_t', f_c' = uniaxial tensile and compressive strengths of concrete, and

ν_t, ν_c = plastic or effective factors for tensile and compressive strengths.

The reason for using the plastic , or reduced effective strength of material rather than the ultimate strength of the material will be discussed in details later.

The value of **K** is determined by allowing the parabolic intrinsic curve tangent to Mohr's circle for simple compression. Due to symmetry, the parabola is also tangent to the Mohr's cycle for simple tension.

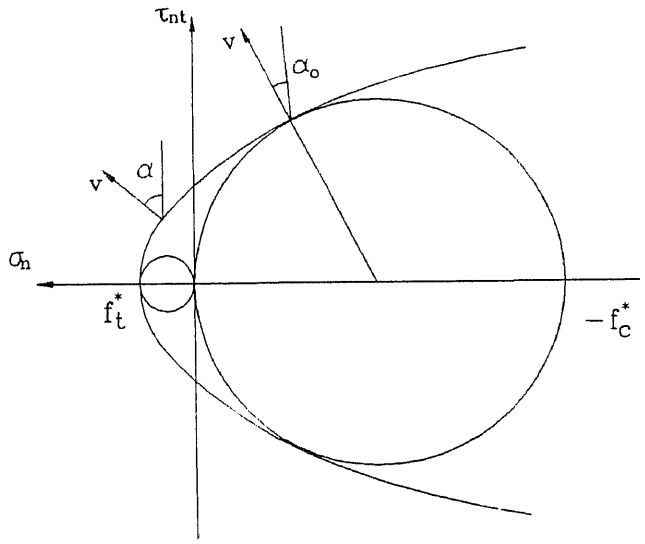

Figure 1.4.1 Modified Coulomb-Mohr Failure Criteria(Jiang and Shen, 1986)

The material yields when a certain stress $M(\sigma_n, \tau_{nt})$ reaches the parabolic curve, thus the corresponding stresses σ_n and τ_{nt} must satisfy Equation 1.39. The associated flow rule requires that the direction of plastic flow be normal to the yield surface. Thus

$$\tan\alpha = 2K\frac{f_t^*}{\tau_{nt}} \qquad 1.42$$

where α is illustrated in Figure 1.4.1.

When the direction of plastic strain rate is given, the value of the shear and normal stresses on a yield surface can be uniquely determined as

$$\sigma_1 = [1 - K(\mathrm{cosec}\alpha - 1)^2]f_t^* \qquad 1.43$$

$$\sigma_3 = [1 - K(\mathrm{cosec}\alpha + 1)^2]\, f_t^* \qquad 1.44$$

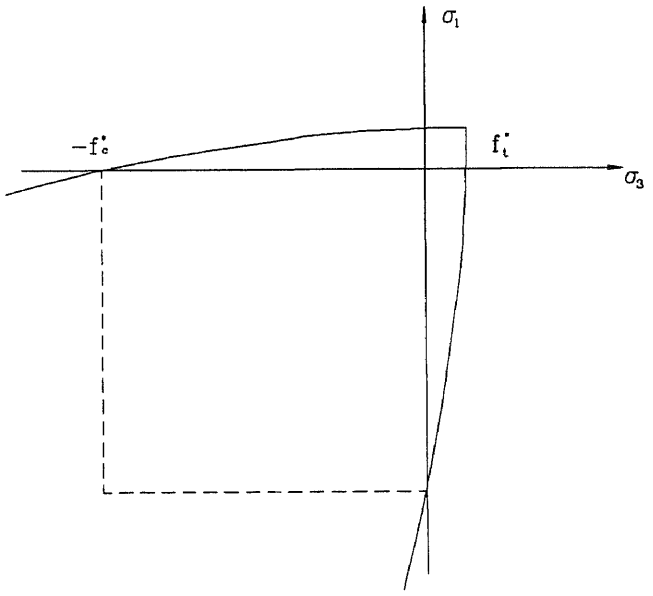

Figure 1.4.2 Yield Locus in Principal Stress Space

Figure 1.4.2 shows the yield locus of the failure criterion in a principal stress space. The curves representing Equation 1.43, and 1.44 are hyperbolic in the principal stress space.

In case of α less than α_o (see Figure 1.4.1) the concrete fails in simple compression. Here, α_o is in the normal direction of the parabola at the point where the curve tangent to the Mohr's circle for simple compression.

By assuming that the minimum third principal stress is $-f_c^*$, the yield surface shown in Figure 1.4.2 is simply capped, and it leads to the following simple relations

$$\sigma_1 = 0 \qquad 1.45$$

$$\sigma_3 = -f_c^* \qquad 1.46$$

In principal stress space, Equation 1.45 and 1.46 correspond to the dotted line in Figure 1.4.2.

The work equation will be used to find the upper-bound solution. In a work equation the rate of work done by external load in a permissible failure mechanism is set to be equal to the energy dissipation rate of the material, namely $D(\dot{\varepsilon}_{ij}^p)$. The general formulation of the energy dissipation rate for von Mises and Mohr-Coulomb criteria are given by Chen (1975). Hereafter, a generalized energy dissipation rate in accordance with the above parabolic failure surface is proposed(Wang,

1988). This generalized formulation of energy dissipation rate is applicable to both plane stress and strain conditions.

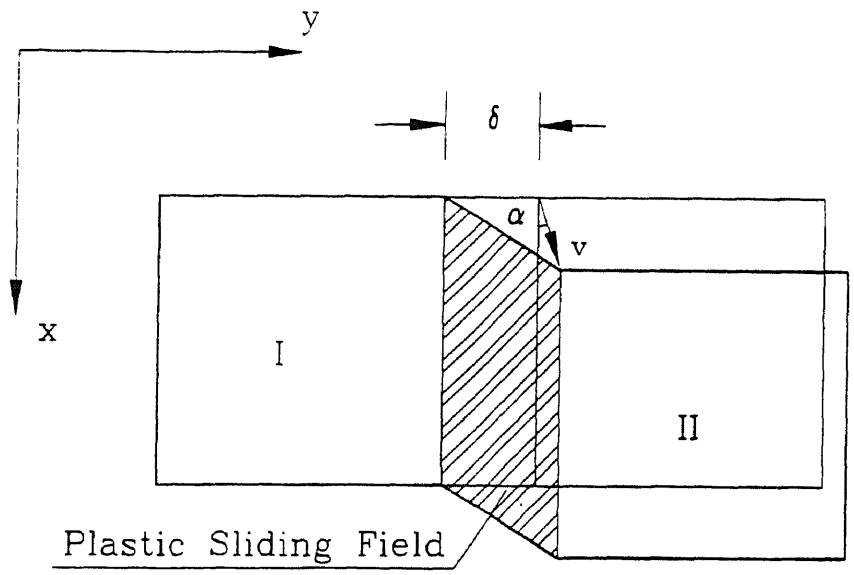

Figure 1.4.3 Discontinuous Displacement Field (Wang, 1988)

Consider a plane, homogenous displacement field in a narrow zone of a depth of d between two rigid bodies I and II as shown in Figure 1.4.3. The strain rate in the deforming zone is

$$\begin{cases} \dot{\varepsilon}_x^p = 0 \\ \dot{\varepsilon}_y^p = \dfrac{v}{\delta}\sin\alpha \\ \dot{\gamma}_{xy}^p = 2\dot{\varepsilon}_{xy}^p = \dfrac{v}{\delta}\cos\alpha \end{cases} \qquad 1.47$$

where v is the relative displacement of the rigid body I and II, δ is the width of the yield zone, and α is the direction of the displacement. The principal stresses are found to be equal to

$$\begin{Bmatrix} \dot{\varepsilon}_1^p \\ \dot{\varepsilon}_3^p \end{Bmatrix} = \begin{cases} \dfrac{\dot{\varepsilon}_x^p + \dot{\varepsilon}_y^p}{2} + \sqrt{\left(\dfrac{\dot{\varepsilon}_x^p - \dot{\varepsilon}_y^p}{2}\right)^2 + \dot{\varepsilon}_{xy}^{p^2}} \\ \dfrac{\dot{\varepsilon}_x^p + \dot{\varepsilon}_y^p}{2} - \sqrt{\left(\dfrac{\dot{\varepsilon}_x^p - \dot{\varepsilon}_y^p}{2}\right)^2 + \dot{\varepsilon}_{xy}^{p^2}} \end{cases} \qquad 1.48$$

Substituting Equation 1.47 into 1.48, the principal stresses in such a yield zone may be found as

$$\begin{Bmatrix} \dot{\varepsilon}_1^p \\ \dot{\varepsilon}_3^p \end{Bmatrix} = \frac{v}{2\delta} \begin{Bmatrix} \sin\alpha + 1 \\ \sin\alpha - 1 \end{Bmatrix} \qquad 1.49$$

The corresponding direction of the first principal stress with respect to the x-axis is

$$\tan 2\theta = \frac{\dot{\gamma}_{xy}^p}{\dot{\varepsilon}_x^p - \dot{\varepsilon}_y^p} = -\cot\alpha = \tan\left(\alpha + \frac{\pi}{2}\right) \qquad 1.50$$

or

$$\theta = \frac{\alpha}{2} + \frac{\pi}{4} \qquad 1.51$$

Thus, the energy dissipation rate in a unit volume of the concrete within the yield zone may be written as

$$D_c(\dot{\varepsilon}_{ij}^p) = \delta(\sigma_1 \dot{\varepsilon}_1^p + \sigma_3 \dot{\varepsilon}_3^p) \qquad 1.52$$

This general equation leads to the following equation for proposed strain rate in the yield zone

$$D_c(\dot{\varepsilon}_{ij}^p) = \frac{1}{2} v\sigma_1(1 + \sin\alpha) - \frac{1}{2}(1 - \sin\alpha) \qquad 1.53$$

Equation 1.53 shows that the energy dissipation rate in a unit length of the yield zone is independent of its width. Thus, theoretically speaking, the yield zone may be referred to as a yield line, or a yield surface in a three dimensional body. Since this yield zone physically indicates the discontinuity of the displacement in a solid object, therefore, it is also referred to as a *surface of discontinuity*.

According to the associated flow rule, the direction of the plastic strain rate is solely dependent upon the stress state and normal to the yield surface. Therefore, the direction of the plastic flow shown in Figure 1.4.3 must be equal to the normal direction of the yield surface indicated in Figure 1.4.1.

For a plane strain condition, the direction of plastic flow α must be greater than 0. However, it may vary between $\pi/2$ and $-\pi/2$ for materials subjected to plane stress condition. In case of α being less than α_o, the material will fail in compression.

The energy dissipation in a unit length of yield line can be obtained by substituting Equation 1.43 and 1.44 into Equation 1.53.

$$D_c(\dot{\varepsilon}_{ij}^p) = v f_t^* (\sin\alpha + K\cot\alpha\cos\alpha),\ \alpha \geq \alpha_o \qquad 1.54$$

$$D_c(\dot{\varepsilon}_{ij}^p) = v f_t^* \frac{m}{2}(1 - \sin\alpha),\ \alpha < \alpha_o \qquad 1.55$$

Equations 1.54 and 1.55 give the energy dissipation per unit length of a yield line in a plane stress condition.

As mentioned previously, Equations 1.43 and 1.44 can also be applied to a plane strain condition even if α is less than α_o. Thus, the energy dissipation in a unit length of yield line in a plane strain condition can be written as

$$D_c(\dot{\varepsilon}_{ij}^p) = vf_t^*(\sin\alpha + K\cot\alpha\cos\alpha),\ 0 \le \alpha \le \frac{\pi}{2} \qquad 1.56$$

The above equations for energy dissipation rate form the basis for the limit analysis of reinforced concrete structures subjected to shear stresses. They will be used in the following chapters to attain the the ultimate shear strengths of reinforced concrete structures.

1.5 Coefficient of Plasticity

The above formulas are derived by assuming that the materials are all rigid-perfectly plastic. However, concrete is not a perfectly plastic material. In contrast, it is often referred to as a typical brittle material with nonlinear ascending and descending parts as shown in Figure 1.5.1.

As shown in Figure 1.5.1, the slope of the descending part in a stress-stain curve of concrete depends on the strength of the material. The higher the strength, the larger the slope, thus the less the ductility. A coefficient ν_c is defined to account for

the effective strength of concrete, and it reads (Exner 1979, Nielsen 1984):

$$\nu_c = \frac{f_c^*}{f_c'} = \int_0^1 \left(\frac{\sigma}{f_c'}\right) d\left(\frac{\varepsilon}{\varepsilon_u}\right) \qquad 1.57$$

where, ε_u is the ultimate strain of concrete under uniaxial compression.

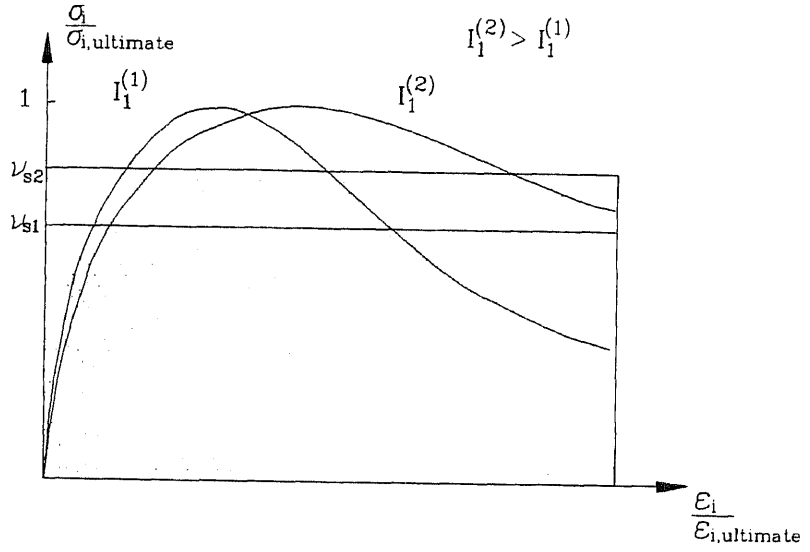

Figure 1.5.1 Factor of Plasticity of Concrete (Wang, et. al. 1992)

This definition of ν_c is based on the assumption that an equivalent ideal rigid perfectly plastic material has the same toughness as the actual concrete material. If a material has a very flat stress-strain curve beyond the yield point, its ν_c is expected to be close to 1. Obviously, this value is equal to 1 for a perfectly rigid-plastic material, and 0.5 for a brittle,

non-softening elastic material. The value of ν_c may even drop below 0.5 for softening materials.

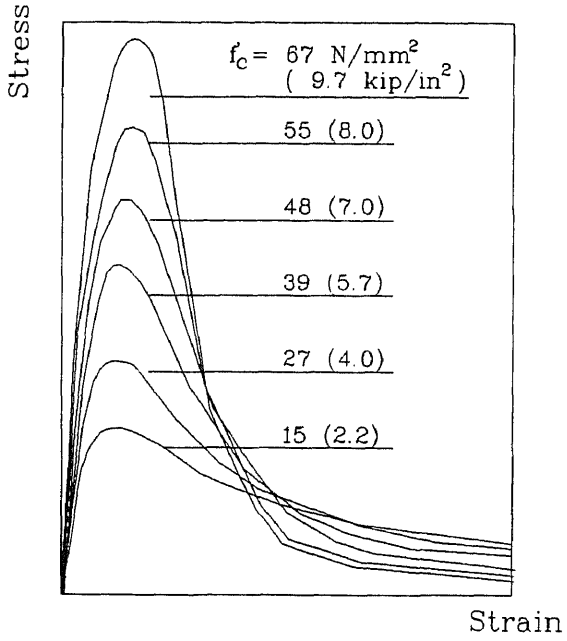

Figure 1.5.2 Stress-Strain Curves of Concrete Materials with Different Strengths

As shown in Figure 1.5.2, the shape of stress-strain curves for normal concrete varies in accordance with its strength. Concrete of higher strength may have a steeper descending part, thus a lower value of ν_c shall be used in the analysis. In contrast, a higher value of ν_c shall be used for lower strength concrete because of their flatter descending part. In general, the value of ν_c is proportional to the ductility of the material. Thus, ν_c may be referred to as the factor of plasticity of the material.

Using statistical analysis, the factor of plasticity of concrete in slender beams was found to be equal to (Nielsen et. al, 1978)

$$\nu_c = 0.8 - \frac{f_c'(\text{MPa})}{200} \qquad 1.58$$

Equation 1.58 indicates the decrease in ductility for concrete materials as its strength increases.

For different structural elements, the material may be subjected to different stresses. For example, the biaxial stresses state within the shear span of a deep beam varies in accordance with the changing shear span ratio. A smaller shear span ratio may cause a higher negative hydrostatic pressure in the material. In such a case, the stress-strain curve is very much different from that of the one in slender beams. Thus the plastic coefficient ν_c should be modified by another constant which depends upon structurally related parameters and loading conditions.

For deep beams subjected to concentrated loads, this coefficient of plasticity may be found as a function of the shear span ratio λ , or a/d, where a is the distance between the load and the support, and d is the effective depth of a deep beam. For deep beams with smaller shear span ratios, its stress field within the shear span has a greater tendency to be compressive, or in terms of the theory of plasticity, the stress field has a smaller first invariant of stress tensor I_1 (Wang

et. al, 1992). Generally speaking, a smaller I_1 indicates a flatter descending part of the stress-strain curve of concrete (see Figure 1.5.1). This phenomenon was first illustrated by Richartm et al. in 1928 with a series of triaxial compression tests of concrete (Richartm et al 1928) and was supported by Kupfer's biaxial test of concrete in later 60's (Kupfer et al 1969). The test results showed that the concrete behaves more plastically under compressive load than under tensile load. Therefore, another coefficient corresponding to the structural behavior ν_s should be introduced to modify the ν_c value for different structures.

ν_s is primarily designed to reflect the different plastic behavior for various types of structures. Formulas of ν_s will be proposed in the following section for different structural elements in accordance with their structural characteristics.

CHAPTER 2

LIMIT ANALYSIS OF SHEAR TRANSFER AND REINFORCED CONCRETE BRACKETS

2.1 Introduction

A shear transfer specimen assures an indisputable failure surface, and it has a simple stress field along the failure surface. Therefore, it is an ideal specimen in measuring the ultimate shear strength of plain and reinforced concrete structures. Figure 2.1.1 shows a typical shear transfer specimen.

Earlier researches in this area were more empirical than analytical(Mast 1968, Mattock and Hawkins 1972, and Paulay and Locker 1974). These earlier researches have formed a solid base of the so called shear friction theory. This theory assumes that the direct shear strength of reinforced concrete material is a linear function of the internal friction angle of concrete and the reinforcement ratio. This shear friction theory has been adopted by ACI in the design specification of reinforced concrete joints since 1971 (ACI, 1971).

Several analytical methods have also been developed since the late 60's using different approaches. Some of them achieved very good results, such as the limit

analysis method by Nielsen et. al (1978), and the softening truss theory by Hsu et. al (1987).

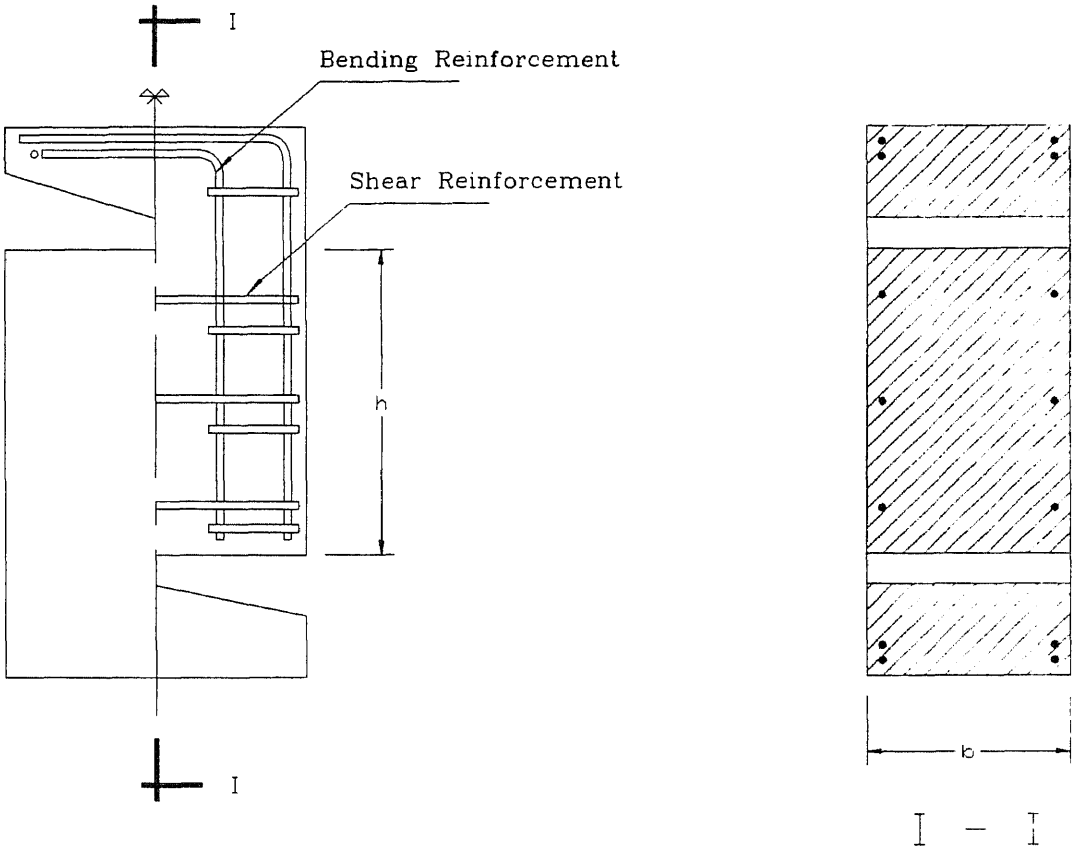

Figure 2.1.1 Failure Mechanism of Reinforced Concrete Push-Off Shear Transfer Specimens

Designs of reinforced or plain concrete joints in precast concrete segmental bridges are the typical practical applications of the shear transfer related researches (Buyukozturk et. al, 1990).

The failure of a push-off shear transfer specimen occurs after a through slip line is formed in the center

of the specimen. The ultimate shear strength of such a failure mechanism may be formulated using upper-bound method by balancing the energy dissipated in concrete and reinforcing bars crossing the failure surface. In the following section in this chapter, an analytical shear strength formula is developed based on this failure mechanism.

2.2 Limit Analyses of Plain and Reinforced Concrete Shear Transfers

2.2.1 Energy Dissipation

Energy dissipation of a reinforced concrete shear transfer specimen includes two parts, namely, the energy dissipated by concrete and reinforcing bars crossing the failure surface.

The energy dissipated by concrete my be computed by the equations derived in Section 1.3 of Chapter one. Considering a shear transfer specimen shown in Figure 2.2.1, the energy dissipation in concrete D_c is

$$D_c = \begin{cases} vbhf_t^*(\sin\alpha + k\cot\alpha\cos\alpha), & \text{if } \alpha \geq \alpha_0 \\ \dfrac{mv}{2}bhf_t^*(1-\sin\alpha), & \text{if } \alpha < \alpha_0 \end{cases} \qquad 2.1$$

and the energy dissipation in reinforcement D_s is

$$D_s = A_{sh}f_y v\sin\alpha \qquad 2.2$$

where,

v is the rate of plastic flow;

α is the direction of plastic flow;

α_o is the transition plastic flow direction, below which, the concrete material fails in compression;

b and **h** are the dimensions of the shear resisting section;

m and **k** are the material constants to be used in the failure criterion;

f_t^* is the effective tensile strength of concrete;

f_y is the yield strength of reinforcement.

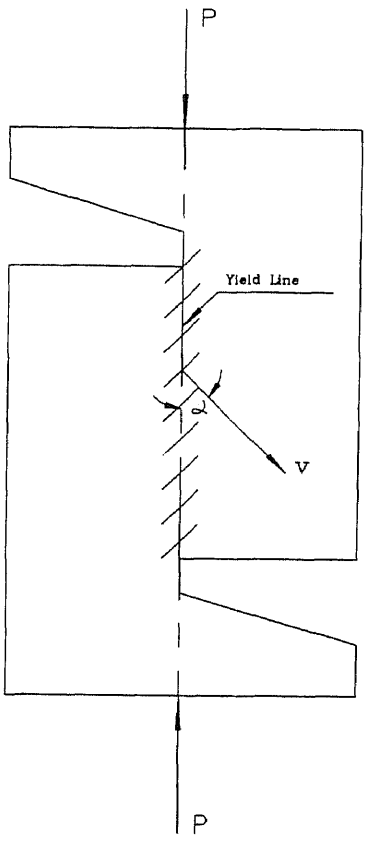

Figure 2.2.1 Reinforced Concrete Shear Transfer and Its Failure Mechanism

The total dissipated energy along the yield line in a shear transfer specimen is

$$D = D_c + D_s \qquad 2.3$$

or

$$D = \begin{cases} vbhf_t^*(\sin\alpha + K\cot\alpha\cos\alpha) + A_{sh}f_y v\sin\alpha & \text{if } \alpha \geq \alpha_0 \\ \dfrac{mv}{2}bhf_t^*(1-\sin\alpha) + A_{sh}f_y v\sin\alpha & \text{if } \alpha < \alpha_0 \end{cases} \qquad 2.4$$

The rate of work done by the applied load P in this case is

$$W = vP\cos\alpha \qquad 2.5$$

In case of $\alpha \geq \alpha_o$, the work equation can be written as

$$vP\cos\alpha = vbhf_t^*(\sin\alpha + K\cot\alpha\cos\alpha) + A_{sh}f_y\sin\alpha \qquad 2.6$$

Denoted by ψ, the index of reinforcement is defined as

$$\psi = \frac{A_{sh}}{bh}\frac{f_y}{f_t^*} \qquad 2.7$$

and it leads to a simplified work equation as

$$P = bhf_t^*(\tan\alpha + K\cot\alpha + \psi\tan\alpha) \qquad 2.8$$

The reinforcement index is a dimensionless parameter that indicates the level of reinforcement in a structure. This parameter determines the load resisting characteristics of a reinforced concrete structure. In comparison with the reinforcement ratio, this reinforcement index shows the reinforcement level of a structure in a more comprehensive manner. A straight forward implementation of this reinforcement index is the ratio between the load resisting capacities of concrete and steel. And also, it indicates the

hydrostatic pressure level in the concrete material, and thus influences the overall ductility of the structure.

The lowest upper-bound solution can be found when

$$\frac{dP}{d\alpha} = bhf_t^*(\sec^2\alpha - K\csc^2\alpha + \psi\sec^2\alpha) = 0 \qquad 2.9$$

Equation 2.24 yields an explicit solution for the stationary value of α that leads to the lowest upper-bound solution of P

$$\alpha = \arctan\sqrt{\frac{K}{1+\psi}} \qquad 2.10$$

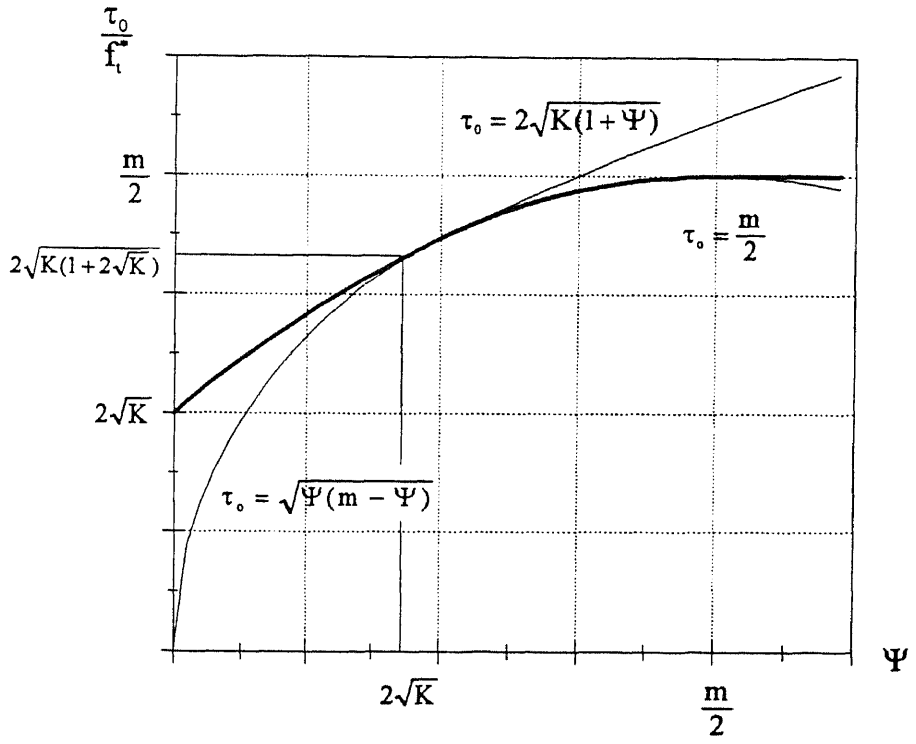

Figure 2.2.2 Lowest Upper-Bound Solution for Shear Trasfer

The lowest upper-bound, therefore, can be written as

$$\tau_o = \frac{P}{bhf_t^*} = 2\sqrt{K(1+\psi)} \qquad 2.11$$

where τ_o is the normalized ultimate shear strength. The normalized shear strength τ_o vs. reinforcement index ψ curve is parabolic (see Figure 2.2.2) according to Equation 2.24.

A similar work equation may be derived in case of $\alpha < \alpha_o$ using the second part of Equation 2.4

$$vP\cos\alpha = \frac{vm}{2} bhf_t^*(1-\sin\alpha) + A_{sh} f_y v \sin\alpha \qquad 2.12$$

where A_{sh} is the sectional area of reinforcement. Equation 2.24 may be simplified as follows

$$P = vbhf_t^*\left(\frac{m}{2}\frac{1-\sin\alpha}{\cos\alpha} + \psi\tan\alpha\right). \qquad 2.13$$

its lowest upper-bound solution may be obtained by letting $\frac{dP}{d\alpha} = 0$, which yields

$$\tau_o = \frac{P}{bhf_t^*} = \sqrt{\psi(m-\psi)}, \quad (\alpha < \alpha_o) \qquad 2.14$$

Equation 2.24 indicates a semicircular arc in a $\tau_o - \Psi$ coordinate system. Its radius is m/2 as shown in Figure 2.2.2. In cases of a overreinforced structure the predicted normalized ultimate shear strength from Equation 2.24 may decrease as the reinforcement index exceeds m/2. However, the increasing of reinforcement ratio should never reduce its strength in reality. Thus, Equation 2.24 should not be used for a specimen with reinforcing index higher than m/2. In such a case, the reinforcing bars can not reach their yield strength,

and undergo elasticity while the concrete fails due to compression. The above formulas are not applicable to this case since the reinforcement does not yield and undergoes elasticity. Therefore, the normalized shear strength for specimen with higher reinforcement index than m/2 shall be equal to the maximum value of m/2.

The value of m/2 may be referred to as the critical reinforcement index, above which a structure shall be considered as overreinforced. Different structures may have different definitions of reinforcement indexes. However, the analytical results from this investigation show that the critical reinforcement index of m/2 is applicable to all different structures.

Solutions for shear transfer may be summarized as follows

$$\tau_o = \begin{cases} 2\sqrt{K(1+\psi)}, & \psi < 2\sqrt{K} \\ \sqrt{\psi(m-\psi)}, & \frac{m}{2} \geq \psi \geq 2\sqrt{K} \\ \frac{m}{2}, & \psi > \frac{m}{2} \end{cases} \qquad 2.15$$

in which, the plastic flow direction constrain $\alpha<\alpha_o$ is replaced by the reinforcement index $\psi<2\sqrt{K}$. This relation may be obtained by letting Equation 2.10 to be equal to α_o. Figure 2.2.2 shows the analytical results in a $\tau_o - \Psi$ coordinate system.

An empirical study was conducted in order to verify the validity of the proposed analytical method. Test results from elsewhere were also analyzed using the

proposed formula. These studies show that the proposed ultimate shear strength formula for reinforced concrete shear transfer has good accuracy. Details of a testing program and comparison are discussed in Chapter 5 of Part I of this dissertation.

2.2.2 Discussions

The ultimate shear strength of shear transfers estimated from Equation 2.15 shows a nonlinear relation between the reinforcing index and the normalized shear strength, which is different from the shear friction theory being used in ACI (1989). According to ACI building code, the ultimate shear strength may be transferred by reinforced concrete shear connection is

$$V_n = A_{vf} f_y (\mu \sin\alpha_f + \cos\alpha_f) \qquad 2.16$$

where α_f is the angle between the shear-friction reinforcement and shear plane, μ is a coefficient of friction, it varies from 1.4 to 0.6 depending on the types of concrete and reinforcing bars, A_{vf} is the area of shear-friction reinforcement and f_y is its yield strength. This ultimate shear strength may not exceed $0.2f_c'A_c$ nor $800A_c$ in pounds according to ACI, where A_c is the shear resisting area.

The ACI's specification on shear friction is conservative in comparison to the theoretical solution from limit analysis. The maximum shear strength by limit

analysis is $0.5\nu_c f'_c A_c$. For concrete with a strength of 3000 psi, the factor of plasticity ν_c is about 0.7, thus leads to a maximum shear strength of $0.35 f'_c A_c$. However, for concrete with higher strength, this maximum shear strength is closer to the ACI specification. For instance, for concrete with a strength of 6000 psi, this maximum shear strength may decrease to $0.30 f'_c A_c$.

Compared to the limit analysis result, specifications in the ACI Building Code are not too conservative. Knowing that the shear failures of structures are most likely to be brittle and sudden, such structures shall be designed with extreme caution. On the other hand, the test data on the subject may have relatively larger deviation, which is common for shear strength tests. Therefore, in order to have the same low failure probability, a lower estimated shear strength must be used in the design.

The limit analysis of the push-off shear transfer specimen shows the load resisting mechanism of reinforced concrete structural elements. For a slightly reinforced concrete structure, concrete failure is due to combined shear and compressive stresses. For a heavily reinforced structure concrete, it may fail due to compressive stress as the direction of plastic flow changes from $\alpha > \alpha_o$ to $\alpha < \alpha_o$ in order to minimize the energy dissipation in shear reinforcement.

2.3 Shear Strength of Reinforced Concrete Brackets

A direct application of the theory developed in this research is to predict the shear strength of bracket. Brackets are designed to transfer vertical load to columns. They are very short in span and high in depth. They behave like deep cantilever beams under vertical load. Therefore, the shear strength analysis of such structures is of the first priority in the design routine.

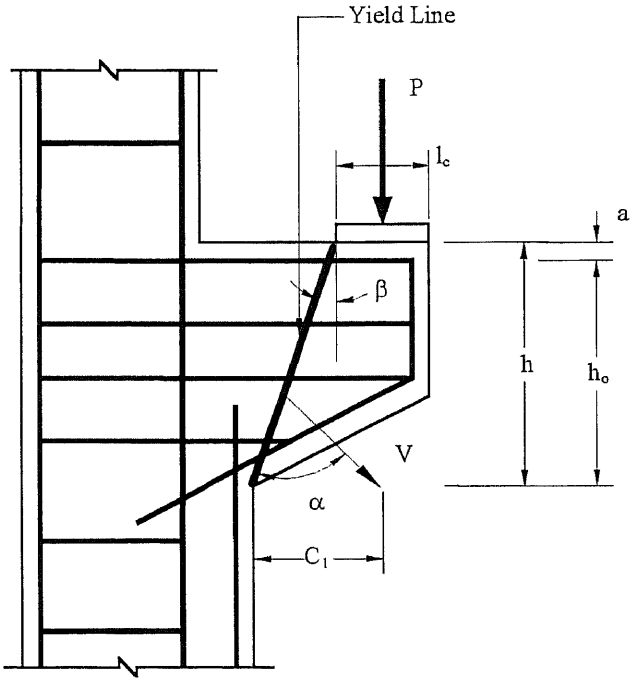

Figure 2.3.1 Typical Shear Failure of Reinforced Concrete Brackets

A reinforced concrete bracket is illustrated in Figure 2.3.1. Several horizontal reinforcing bars are

placed near the top surface of the bracket to carry the tension caused by bending.

A bracket shall not use the vertical shear reinforcement. This is because potential vertical cracks may eliminate the effect of having vertical reinforcement to resist shear. Use vertical shear reinforcement in bracket design may cause serious problems in engineering practice (See Figure 2.3.2).

Figure 2.3.2 Shear Failure in Concrete Bracket Caused by a Conceptual Error in the Original Design (Source: Hayden/Wegman Consulting Engineers, NY City)

The failure of the bracket is assumed to be caused by the formation of a critical diagonal crack in the Bracket. Assume the direction of the critical slip line (diagonal crack) is β with respect to the vertical, and the direction of plastic flow v forms an angle of α from the crack. The energy dissipation rate in this failure mechanism may be found as

$$D_c = \begin{cases} vbhf_t^* \sec\beta(\sin\alpha + K\cot\alpha\cos\alpha) + vA_{sh}f_y\sin(\alpha-\beta), & \alpha \geq \alpha_o \\ vbhf_t^* \sec\beta\left(\frac{m}{2}(1-\sin\alpha)\right) + vA_{sh}f_y\sin(\alpha-\beta), & \alpha < \alpha_o \end{cases} \quad 2.17$$

where A_{sh} is the cross-sectional area of horizontal reinforcing bars. The rate of work done by the applied load is

$$W = Pv\cos(\alpha+\beta) \quad 2.18$$

where P is the external load. Thus, the work equation may be written as

$$P = \frac{bhf_t^*}{\cos\alpha\cos(\alpha-\beta)} \cdot \begin{cases} \sin\alpha + K\cot\alpha\cos\alpha + \psi_h\cos\beta\sin(\alpha-\beta), & \alpha \geq \alpha_o \\ \frac{m}{2}(1-\sin\alpha) + \psi_h\cos\beta\sin(\alpha-\beta), & \alpha < \alpha_o \end{cases} \quad 2.19$$

where the reinforcing index is defined as

$$\psi_h = \frac{A_{st}}{bh} \cdot \frac{f_y}{f_t^*} \quad 2.20$$

In order to find the lowest upper-bound solution, let $\frac{dP}{d\alpha} = 0$, which yields:

$$\tan\alpha = \begin{cases} \frac{K\tan\beta}{1+\psi_h} + \sqrt{\left(\frac{K\tan\beta}{1+\psi_h}\right)^2 + \frac{K}{1+\psi_h}}, & \alpha \geq \alpha_o \\ \frac{\tan\beta + \varsigma_h\sec\beta}{1-\varsigma_h^2}, & \alpha < \alpha_o \end{cases} \quad 2.21$$

where

$$\varsigma_h = 1 - \frac{2\psi_y}{m} \qquad 2.22$$

Equation 2.19 shows that P is a function of α and β; thus, the lowest value shall be determined by letting $\frac{dP}{d\alpha} = 0$ and $\frac{dP}{d\beta} = 0$. However these two simultaneous equations will not lead to an explicit formulation of the problem.

In order to find an explicit equation to predict the ultimate shear strength of a bracket, a numerical analysis method is used. By varying β from 0 to 90°, a series values of α and P may be found through Equations 2.19 and 2.21. The minimum P in this series values of P's must satisfy the equation of $\frac{dP}{d\beta} = 0$. Thus, this minimum value of P may be considered as the lowest upper bound solution since it satisfies both $\frac{dP}{d\alpha} = 0$ and $\frac{dP}{d\beta} = 0$.

The β corresponding to the lowest upper-bound is found to be a function of reinforcing index ψ_h. Regression of the results from numerical analysis shows

$$\sqrt[3]{\beta} = c_1 + c_2\psi_h, \ \beta \le \frac{\pi}{4} \qquad 2.23$$

where

$$\begin{cases} C_1 = 0.74 + 0.1m \\ C_2 = 0.058 - 0.006m \end{cases} \qquad 2.24$$

β predicted by the above equation is expected to have an accuracy better than 0.5%. Figure 2.3.3 shows the comparison between the "exact" solution from numerical analysis and the one predicted by Equation 2.24.

Test results from about one hundred specimens reported in the literature were analyzed using the proposed formula. The concrete strength of these specimens varies from 2000 psi to 5000 psi, and the reinforcement ratio varies from 0.32% to 2.7%. The comparison of the measured and predicted ultimate strength ratio has an average of 0.973 and standard deviation of 0.130. Details of the specimens and analysis are listed in Chapter 5.

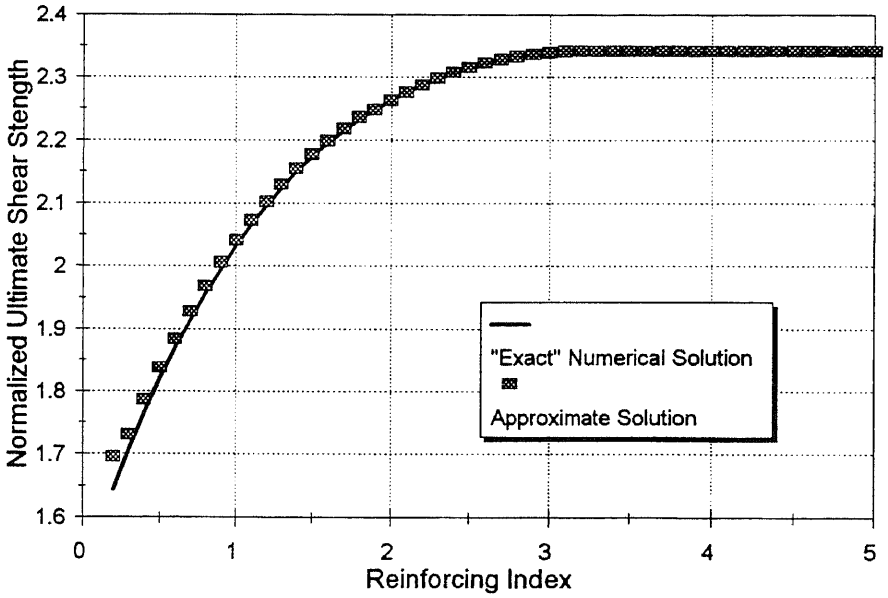

Figure 2.3.3 Comparison Between "Exact" and Approximate Solutions

CHAPTER 3

SHEAR STRENGTH OF REINFORCED CONCRETE DEEP BEAMS

3.1 Introduction

Designs of reinforced concrete deep beams are usually controlled by shear strength. For past decades, many theoretical and empirical researches have been conducted on predicting the shear strength of reinforced concrete deep beams (Klingroth 1942, De Paiva and Siess 1965, Zsutty 1971, Nielsen 1971, Smith & Fereig 1974, Mau & Hsu 1987). Several empirical studies reveled some of the important results and provided deeper understanding of the problem. However, theoretical researches on this topic were more or less limited because of the complexity of the problem. Developments on computational analysis technology provide possibilities of performing very detailed nonlinear finite element analysis. However, with its case-by-case fashion, the finite element analysis is too expensive to perform as a regular design routine. Closed form solutions are always desirable in engineering practice.

Theoretical analysis of the shear strength of deep beams is not yet well developed yet. Most of the formulas to predict shear strength of deep beams in design codes adopted by different countries and academic institutes are empirical. It is of utmost importance to

provide these formulas with an analytical interpretation and necessary improvement.

The perfect or ideal plasticity concept has been used recently to find reinforced concrete problems in Denmark, Switzerland, USA and China for the past decades (Nielsen 1961, 1971, 1984, Nielsen et al 1978, Marti 1980, Chen 1982, Jiang & Shen 1986), and it shows a high potential for solving the problem of shear strength of reinforced concrete deep beams. In the following sections, the upper-bound method is used to find the ultimate shear strength of concrete deep beams with horizontal and vertical reinforcements. Tests results published in the literature are used to verify the proposed formulas.

3.2 Upper-Bound Solution for Reinforced concrete Deep Beams

Consider a simply supported reinforced concrete deep beam which is shown in Figure 3.2.1 with both horizontal and vertical web reinforcements of ratios ρ_h and ρ_v. A critical inclined crack (yield line) occurs under the external load **P**. The direction of the yield line is β with respect to the vertical axis. The plastic flow on the slip line forms an angle of α with respect to the yield line (see Figure 3.2.2). In this case, the energy dissipation along the crack or yield line can be written as

$$\delta D = D_c + D_{sh} + D_{sv} \qquad 3.1$$

The total energy dissipation along the yield line contains three parts, they are the contributions from concrete D_c, horizontal web reinforcement D_{sh}, and vertical web reinforcement D_{sv}, respectively. According to the energy dissipation formula developed in Chapter one, the contribution of concrete can be written as

$$D_c = \begin{cases} \dfrac{vbh}{\cos\beta} f_t^* (\sin\alpha + K\cot\alpha\cos\alpha), & \alpha \geq \alpha_o \\ \dfrac{vbh}{\cos\beta} f_t^* \dfrac{m}{2}(1-\sin\alpha), & \alpha < \alpha_o \end{cases} \qquad 3.2$$

where a plane stress condition is assumed.

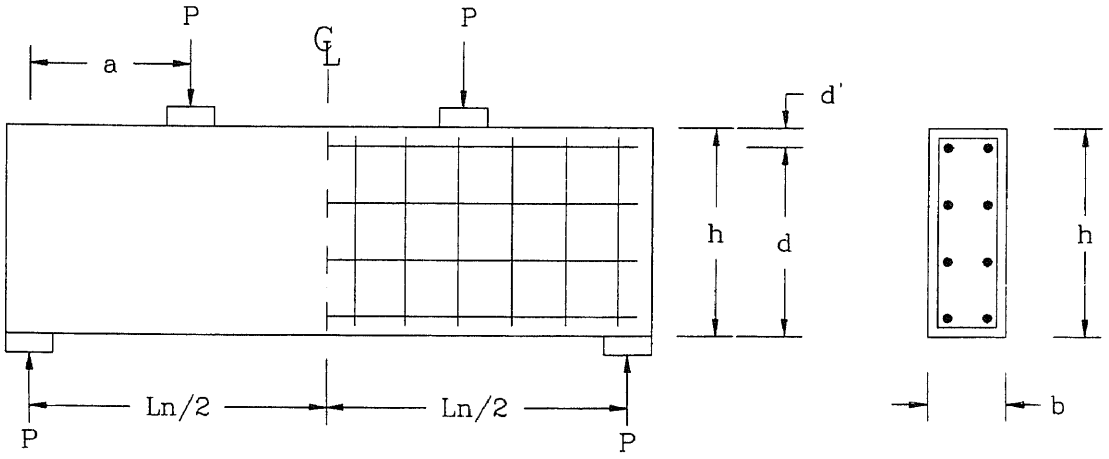

Figure 3.2.1 Geometry of Reinforced Concrete Deep Beam

By considering the deformation of the reinforcements in horizontal and vertical directions,

the energy dissipation of reinforcements can be written as,

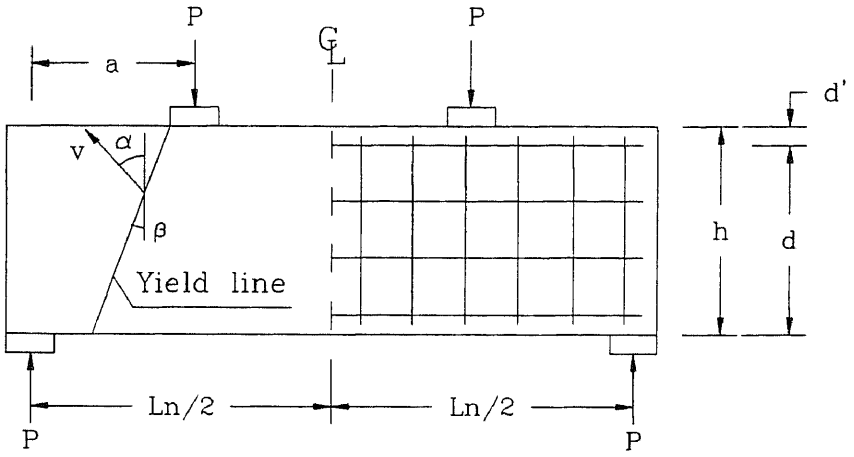

Figure 3.2.2 Failure Mechanism of Deep Beam

$$D_{sv} = v\frac{A_{sv}}{S_v} f_{vy} h \tan\beta \cos(\alpha - \beta) \qquad 3.3$$

$$D_{sh} = v\frac{A_{sh}}{S_h} f_{vh} h \sin(\alpha - \beta) \qquad 3.4$$

where, A_{sv} and A_{sh} are the cross-sectional areas of vertical and horizontal reinforcements; S_v and S_h are the vertical and horizontal spacings of the reinforcement net as indicated in Figure 3.2.1; f_{vy} and f_{hy} are the yield strengths of the reinforcing bars; and v is the rate of displacement.

The rate of work done by the external load is:

$$\delta W = Pv\cos(\alpha - \beta) \qquad 3.5$$

The work equation can be written as

$$\delta W = \delta D \tag{3.6}$$

which leads to

$$P = \frac{bhf_t^*}{\cos\beta\cos(\alpha-\beta)}\begin{cases}(\sin\alpha + K\cot\alpha\cos\alpha + \psi_v \sin\beta\cos(\alpha-\beta) + \psi_h \cos\beta\sin(\alpha-\beta)), & \alpha \geq \alpha_o \\ \frac{m}{2}(1-\sin\alpha) + \psi_v \sin\beta\cos(\alpha-\beta) + \psi_h \cos\beta\sin(\alpha-\beta)), & \alpha < \alpha_o\end{cases} \tag{3.7}$$

where ψ_v and ψ_h are reinforcement indexes in horizontal and vertical directions.

$$\begin{cases}\psi_v = \dfrac{A_{sv}f_{vy}}{S_v bf_t^*} \\ \psi_h = \dfrac{A_{sh}f_{hy}}{S_v bf_t^*}\end{cases} \tag{3.8}$$

The lowest upper-bound solution in this case can be written as

$$\min[P(\alpha,\beta)] \quad \text{subjected to: } \alpha \geq \beta \geq 0 \tag{3.9}$$

This is a typical optimal problem. Thus, the necessary condition for (α,β) to be the abscissa of the optimum is that

$$\frac{\partial P}{\partial \alpha} = 0 \tag{3.10}$$

and

$$\frac{\partial P}{\partial \beta} = 0 \tag{3.11}$$

Substituting Equation 3.7 into Equations 3.10 and 3.11, the critical (stationary) point (α,β) may be found by solving the following non-linear simultaneous equations

$$\tan\alpha = \frac{K\tan\beta}{1+\psi_h} + \sqrt{\left(\frac{K\tan\beta}{1+\psi_h}\right)^2 + \frac{K}{1+\psi_h}} \tag{3.12}$$

and

$$\psi_v \sec^2\beta - \psi_h \sec^2(\alpha-\beta) = \sin^2\alpha - K\cos^2\alpha, \quad \text{for} \quad \alpha \geq \alpha_o \qquad 3.13$$

In case of $\alpha < \alpha_o$, the abscissæ α and β of the optimum must satisfy the following

$$\tan\alpha = \frac{\tan\beta + \varsigma_h\sqrt{\sec^2\beta - \varsigma_h^2}}{1-\varsigma_h^2} \qquad 3.14$$

and

$$(1-\sin\alpha)\sin\alpha = \psi_h\cos^2\beta - \psi_v\cos^2(\alpha-\beta) \qquad 3.15$$

where

$$\varsigma_h = 1 - \frac{2\psi_h}{m} \qquad 3.16$$

As illustrated in Figure 3.2.2, α should be greater than or equal to β, otherwise the horizontal web reinforcement in the deep beam will be in compression rather than in tension under shear.

3.3 Numerical Solution

The above analysis provides a possibility of solving the problem mathematically. However, the solution for a stationary point (α,β) may not be explicit. A feasible approach to this problem is to use numerical methods. Different numerical methods are available for solving this kind of problem, such as, Newton-Raphson approximation and different search techniques for linear and nonlinear systems (Spillers, 1975) (Stark and Nicholls, 1972)

In this investigation, a short FORTRAN program was written to search for the lowest upper-bound solution directly. The algorithm of the program is simple and straight forward: by varying β from zero to 45°, find the stationary points of α with Equations 3.14 and 3.15 using the chosen value of β. Different P's may be found using Equation 3.7 with the chosen values of α and β. The lowest upper-bound solution may be obtained by sorting out the minimum value of **P** in accordance with the given value of β. This minimum value of **P** may be considered as the "exact" solution of the problem since $\partial P/\partial\beta$ and $\partial P/\partial\alpha$ vanish simultaneously at that point. The accuracy of this approach solely depends on the increment of β used.

The numerical solution is expected to form rather smooth continuous curves since the abscissæ of optimum itself must be continuous, at least within certain limits. Therefore, regression of the numerical solution may lead to an approximate solution.

By fitting the data from numerical analysis, the stationary point of β may be found as a function of the vertical and horizontal reinforcement indexes:

$$\sqrt{\beta} = c_1 - c_2\psi_v + c_3\psi_h \qquad 3.17$$

where

$$\begin{cases} c_1 = 0.6523 + 0.0135m \\ c_2 = 0.233 - 0.0125m \\ c_3 = 0.1687 - 0.01m \end{cases}$$

The lowest upper bound solution predicted by using the above β value is accurate for all practical purposes. The error in this method is less than 1%.

3.4 Discussions of Solution

In case that a deep beams is not equally reinforced in the horizontal and vertical directions, the reinforcement in the stronger direction may not yield. In such cases, the reinforcement in the stronger direction will not have energy dissipation. Its structural function is not to dissipate energy, but to supply a constraint to the concrete in that direction, and thus to increase the strength of concrete. In this case, the work equation derived in the above section may be simplified. Explicit solutions are available in such cases.

CASE I. Longitudinal Shear Reinforcement Is Over Reinforced

In this case the horizontal reinforcement may not yield at the time of failure. Therefore, the plastic energy dissipation by the horizontal reinforcement shall be equal to zero, or in terms of plastic flow,

$$\alpha=\beta \qquad 3.18$$

The work equation becomes

$$P=\frac{bhf_t^*}{\cos\alpha}(\sin\alpha+K\cot\alpha\cos\alpha+\psi_v\sin\alpha), \quad \alpha\geq\alpha_o$$
$$P=\frac{bhf_t^*}{\cos\alpha}\left[\frac{m}{2}(1-\sin\alpha)+\psi_v\sin\alpha\right], \quad \alpha<\alpha_o \qquad 3.19$$

The lowest upper bound solution may be found as follows:

$$\frac{P}{bhf_t^*}=\begin{cases}2\sqrt{K(1+\psi_v)}, & \psi_v<2\sqrt{K}\\ \sqrt{\psi_v(m-\psi_v)}, & \frac{m}{2}\geq\psi_v>2\sqrt{K}\\ \frac{m}{2}, & \psi_v>\frac{m}{2}\end{cases} \qquad 3.20$$

and

$$\alpha=\begin{cases}\arctan\sqrt{\frac{K}{1+\psi_v}}, & \psi_v\leq 2\sqrt{K}\\ \arcsin\left(1-\frac{2\psi_v}{m}\right), & \frac{m}{2}\geq\psi_v>2\sqrt{K}\end{cases} \qquad 3.21$$

By comparing Equations 3.21 and 3.12, explicit conditions for horizontally over-reinforced deep beams may be derived by comparing Equations 3.21 and 3.12. In the case of $\alpha\leq\alpha_o$, or $\psi_v\leq 2\sqrt{K}$, the direction of plastic flow is

$$\tan\alpha=\frac{K\tan\alpha}{1+\psi_h}+\sqrt{\left(\frac{K\tan\alpha}{1+\psi_h}\right)^2+\frac{K}{1+\psi_h}} \qquad 3.22$$

according to Equation 3.12. Rearranging Equation 3.22, one has,

$$\tan^2\alpha=\frac{K}{1+\psi_h-2K} \qquad 3.23$$

The critical horizontal reinforcement index may be found by letting Equation 3.22 equal to Equation 3.21, that is

$$\frac{K}{1+\psi_v}=\frac{K}{1+\psi_h^c-2K} \qquad 3.24$$

or

$$\psi_h^c\geq\psi_v+2K \qquad \text{for } \psi_v\leq 2\sqrt{K} \qquad 3.25$$

where ψ_h^c is the critical horizontal reinforcing index. Deep beams with higher horizontal reinforcement index

should be considered as over-reinforced in horizontal direction, and their horizontal reinforcement will not yield at the time of failure.

A similar approach may be used in order to find the critical horizontal reinforcing index in the case of $\psi_v \geq 2\sqrt{K}$. Notice that $\alpha = \beta$ when a deep beam is over-reinforced, thus Equation 3.14 may be re-written as

$$-\varsigma_h^2 \tan\alpha = \varsigma^2 \sqrt{\sec^2\alpha - \varsigma_h^2} \qquad 3.26$$

Since ζ_h and $\tan\alpha$ are non-negtive, the only solution of the above equation is that ζ_h is equal to zero, or ψ_h^c is equal to m/2 according to Equation 3.16.

The above analyses yield the following conclusion: *the horizontal reinforcement will not contribute to the plastic energy dissipation when it is greater than or equal to either* $\psi_v + 2K$ *or* $m/2$. In these cases, the simplified solution of Equation 3.20 may be applied to compute the ultimate shear strength of reinforced concrete deep beams.

CASE II. Vertical Stirrup Is Over Reinforced

In this case, the vertical reinforcement may not yield, implying that it has no contribution to the plastic energy dissipation; whence

$$\beta = 0 \qquad 3.27$$

If $\beta=0$, the work equation becomes

$$P = bhf_t^* \begin{cases} \tan\alpha + K\cot\alpha + \psi_h \tan\alpha, & \psi_h \le 2\sqrt{K} \\ \frac{m}{2}\left(\frac{1-\sin\alpha}{\cos\alpha}\right) + \psi_h \tan\alpha, & \frac{m}{2} \ge \psi_h > 2\sqrt{K} \end{cases} \qquad 3.28$$

which gives the lowest upper bound solution as follows

$$\frac{P}{bhf_t^*} = \begin{cases} 2\sqrt{K(1+\psi_h)}, & \psi_h \le 2\sqrt{K} \\ \sqrt{\psi_h(m-\psi_h)}, & \frac{m}{2} \ge \psi_h > 2\sqrt{K} \\ \frac{m}{2}, & \psi_h > \frac{m}{2} \end{cases} \qquad 3.29$$

The displacement vector angle is determined by,

$$\alpha = \begin{cases} \arctan\sqrt{\frac{K}{1+\psi_h}}, & \psi_h \le 2\sqrt{K} \\ \arcsin\left(1-\frac{2\psi_h}{m}\right), & \frac{m}{2} \ge \psi_h > 2\sqrt{K} \end{cases} \qquad 3.30$$

- **Effective Strength Factor For Deep Beams**

As mentioned in Chapter One, the effective strength of concrete in the above equations shall be modified in order to reflect the changes in ductility of concrete under different hydrostatic pressures. In the case of deep beams subjected to shear, the hydrostatic pressure varies according to the shear span ratio.

Smaller shear span ratios indicate that the concrete material within the shear span is more likely subjected to higher negative compressive stresses than that with larger shear span ratios. In terms of the theory of plasticity, larger compressive stresses means higher negative hydrostatic pressure, or smaller first stress invariant I_1, and thus higher ductility. Consequently, the effective strength of concrete to be

used in the above computation shall be modified with a factor ν_s to indicate this effect. The factor of ν_s is referred to as *structural factor of plasticity*. Combined with the material factor of plasticity ν_c, the effective strength of concrete may be found as

$$f_c^* = (\nu_s \cdot \nu_c) f_c' \qquad 3.31$$

Unfortunately, due to the complexity of the problem, there is not an analytical solution available for this proposed ν_s in general. Statistical analysis is the only practical approach to this problem, and it shows that for deep beams ν_s can be expressed as follows:

$$\nu_s = 1.25 - 0.25\lambda \qquad 3.32$$

where λ is the shear span ratio which can be expressed as a/h in Figure 3.3.1.

Equation 3.32 will be used in the following analysis of existing test data reported in the past to verify the proposed formulation.

A total of 64 test specimens reported by Mau and Hsu(1989) are used herein to verify the present theoretical solution. The average of the ratio between the testing data and the predicted ultimate strength is 1.02, and the standard deviation is 0.130. Details of comparison are shown in Chapter 5.

Chapter 4

ULTIMATE STRENGTH OF REINFORCED CONCRETE BEAMS SUBJECTED TO PURE TORSION

4.1 Introduction

In the previous chapters, two-dimensional problems are discussed using the theory of plasticity in reinforced concrete structures. Basic theorems such as failure criterion of concrete, energy dissipation in unit length of a yield line, and coefficient of plasticity of concrete are developed, and they are proved to be effective in solving the two dimensional problems in reinforced concrete structures. Hereafter, these theorems and concepts will be applied to the problem of torsional strength of reinforced concrete beams.

As a three-dimensional problem, practice of the proposed limit analysis method may extend its application, and therefore, show the effectiveness and theoretical significance of the proposed theory.

As a general case in the theory of plasticity, solving of three-dimensional problems requires a precise three-dimensional yield surface in a stress-space. And also, a generalized energy dissipation rate over a unit yield surface is required to compute the energy dissipation rate.

For the problem of torsional strength of reinforced concrete beams with free ends, the formula of energy dissipation rate derived in Chapter One is still applicable. However, the failure surface discussed in Chapter One shall be modified in solving three-dimensional problems in general. As an exception, this failure criterion may be used in plane strain and symmetrical problems with simple modifications(Jiang and Shen, 1987, Wang, et. al., 1992)

Two different approaches have been used in the past for the problem of torsional strength of reinforced concrete beams. One is the so-called space truss theory and another is the skew bending theory.

The space truss model was first proposed by Raush in 1929. It became the basic formula to calculate the torsional strength of reinforced concrete structural members. However, this model was considered as over-conservative, especially for under-reinforced members(Hsu, 1968a and 1968b).

The space truss model has undergone two major developments. First, the introduction of the variable-angle truss model and the discovery of the bending phenomenon in the diagonal concrete struts were developed by Lampert and Thurlimann (1968, 1969). In the early 70's, the compatibility equations derived by Collins (1973) made it possible to determine the angle of concrete struts. Second, the softening concept was

introduced to concrete materials by Vecchio and Collins (1981). Hsu (1988) combined equilibrium, compatibility and softening strain-stress relation together, and proposed a so-called softening truss theory to solve the torsional strength of reinforced concrete members.

The skew bending model was first proposed by Lessig and Yudin(Lessig, 1958, Yudin,1962). By a assuming a unique yield surface, their theory is capable of explaining some of the observed phenomena that can not be clarified with classical theories (Hsu, 1968b). However, the failure surface proposed in their theory is much more complicated and is not easy to apply. And also, this theory is more likely to over-estimate the ultimate torsional strength. A simplified version of this theory was proposed by Hsu in 1968(Hsu, 1968b) and it was proved to be able to give more promising results.

A new approach to finding the torsional strength of concrete torsional member is proposed here using the limit analysis method. This method is consistent with the previous chapters, and therefore, the formulation for a torsional member will enhance the applicability of the proposed limit analysis method.

4.2 Torsional Strength of Reinforced Concrete Beams

Torsional failure of reinforced concrete structures may be classified as a special case in the shear failure category. In case of pure torsion, shear stresses will

be developed in the member to resist the external torque. The application of the theory of plasticity may successfully lead to analytical solutions of ultimate torsional strength of prismatic elements made of homogeneous and isotropic materials. Known as the sand-heap analogy(Sadowsky, 1949), this method is based upon the theory of plasticity, and has been proved to be effective for estimating the ultimate torsional strength of metal elements. However, the same approach for structures of reinforced cementitious composites seems to be less promising.

A limit analysis approach based on the upper-bound method is presented in the following sections. The analytical results agree well with the experimental result reported in the literature (see Chapter 5).

4.2.1. Failure Mechanism And Energy Dissipation

Consider a prismatic square reinforced concrete beam subjected to pure torsion as shown in Figure 4.2.1 . A possible failure mechanism is assumed as illustrated in the figure. Let θ be the twisting angle, and v be the plastic flow rate, thus

$$v = \theta \times \sec(\alpha - \beta) \qquad 4.1$$

Denote dA as the differential area of the yield surface,or

$$dA = 2x \sec\beta dx \qquad 4.2$$

where x is the distance between the centroid of the section and the differential area. The assumed failure mechanism and the plastic flow field as specified above lead to the following equations for computing the corresponding energy dissipation rate on the yield surface

$$dD_c = f_c'\theta \sec(\alpha-\beta)2x\sec\beta dx(\sin\alpha + K\cot\alpha), \text{ for } \alpha \geq \alpha_o \qquad 4.3$$

and

$$dD_c = f_t^*\theta x \sec(\alpha-\beta)2x\sec\beta dx\frac{m}{2}(1-\sin\alpha), \text{ for } \alpha < \alpha_o \qquad 4.4$$

The total energy dissipated in the surface of discontinuity may be found through the integration of Equations 4.3 and 4.4, which leads to

$$D_c = \frac{\theta}{3}a^3\sec\beta\sec(\alpha-\beta)f_t^*(\sin\alpha + K\cot\alpha\cos\alpha), \text{ for } \alpha \geq \alpha_o \qquad 4.5$$

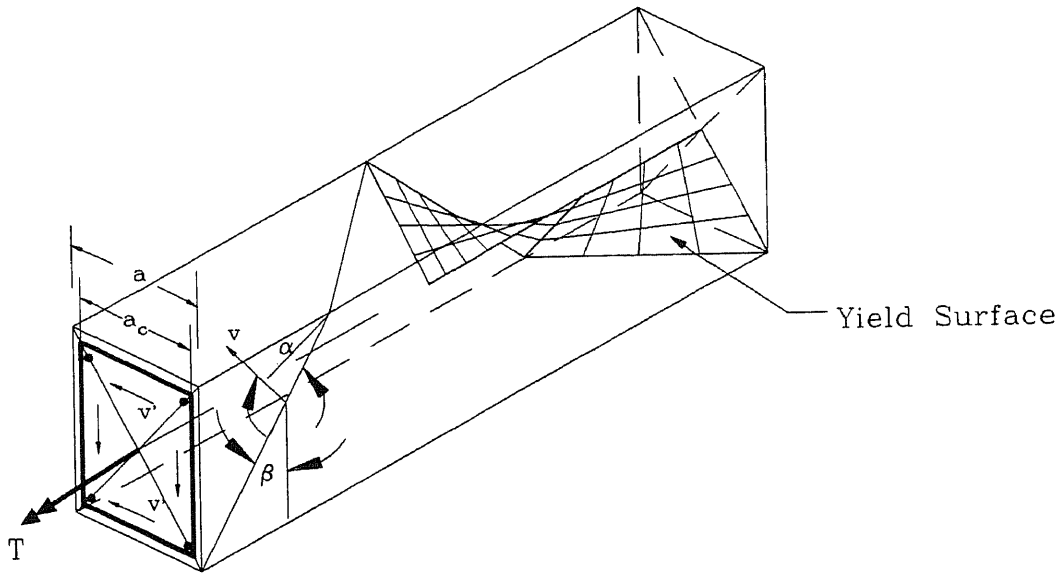

Figure 4.2.1 Square Reinforced Concrete Torsional Member

For a reinforced concrete torsional element, its reinforcement also dissipates energy at the time of yielding. The energy dissipated by reinforcing bars located on one side of the section may be written as

$$D_s = \rho_{sl} a f_{sl} v \sin(\alpha-\beta) + \rho_{st} f_{yt} v \cos(\alpha-\beta), \text{ and}$$

$$v = \frac{a_c \theta}{2} \sec(\alpha-\beta)$$

By counting all reinforcing bars on the section in question, the total energy dissipated by the steel may be represented in the form of

$$D_s = 2A_c\theta\left[\rho_{sl} f_{yl} \tan(\alpha-\beta) + \rho_{st} f_{yt} \tan\beta\right] \qquad 4.6$$

where

$A_c = a_c^2$, is the core sectional area;

$\rho_{sl} = \frac{A_{sl}}{s_l}$ and $\rho_{st} = \frac{A_{st}}{s_t}$ are reinforcement ratioes;

a_c is the length of one side of the core section,

A_{sl}, A_{st} are cross-sectional areas of a single longitudinal or transverse reinforcing bars, and

f_{sl}, f_{st} are the corresponding yield strengths of longitudinal and transverse rebars.

Thus, the total energy dissipation rate for a reinforced torsional concrete member may be found as

$$D = \frac{\theta f_t^*}{6} a^3 \sec\beta \sec(\alpha-\beta)(\sin\alpha + K\cos\alpha\cot\alpha) + 2a_c^2\theta\left[\rho_{sl} f_{yl} \tan(\alpha-\beta) + \rho_{st} f_{yt} \tan\beta\right], \text{ for } \alpha \geq \alpha_o \qquad 4.7$$

Here, a and a_c are the gross and core lengths of the section in question.

Note that the first term in Equation 4.7 is the contribution from the concrete material, and second term

is from the reinforcement in both longitudinal and transverse directions. Also, $f_t a^3/6$ is the fully-plastic torsional strength of a square beam made of Von Mises or Tresca material.

The same analogy may apply to the rectangular reinforced concrete torsional members. The failure mechanism of the square member is slightly different from the rectangular ones in the formation of a permissible plastic flow (see Figure 4.2.2).

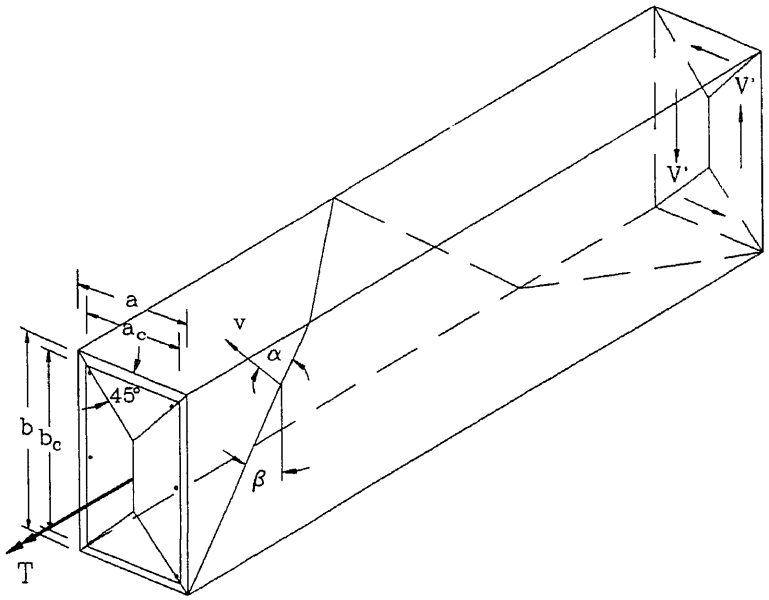

Figure 4.2.2 Failure Mechanics of Rectangular Reinforced Concrete Beams

The corresponding energy dissipation rate for rectangular reinforced concrete torsional members is

$$D=\frac{\theta f_t^*}{12}a^2(3b-a)\sec\beta\sec(\alpha-\beta)(\sin\alpha+K\cos\alpha\cot\alpha)$$
$$+a_c b_c(1+\frac{a_c}{b_c})\theta\left[\rho_{sl}f_{yl}\tan(\alpha-\beta)+\rho_{st}f_{yt}\tan\beta\right],\ \text{for}\ \alpha\geq\alpha_o \qquad 4.8$$

where a_c and b_c are the width and depth of the core section ($b_c \geq a_c$).

4.2.2 Work Equation And Its Solution

The work done by the external torque T is

$$W = T\cdot\theta \qquad 4.9$$

Thus, the work equation yields

$$T=\frac{f_t^*}{12}a^2(3b-a)\sec\beta\sec(\alpha-\beta)(\sin\alpha+K\cos\alpha\cot\alpha)$$
$$+a_c b_c(1+\frac{a_c}{b_c})\left[\rho_{sl}f_{yl}\tan(\alpha-\beta)+\rho_{st}f_{yt}\tan\beta\right],\ \text{for}\ \alpha\geq\alpha_o \qquad 4.10$$

and

$$T=\frac{f_t^*}{12}a^2(3b-a)\sec\beta\sec(\alpha-\beta)\frac{m}{2}(1-\sin\alpha)$$
$$+a_c b_c(1+\frac{a_c}{b_c})\left[\rho_{sl}f_{yl}\tan(\alpha-\beta)+\rho_{st}f_{yt}\tan\beta\right],\ \text{for}\ \alpha<\alpha_o \qquad 4.11$$

Define longitudinal and transverse reinforcing indexes Ψ_{sl} and Ψ_{st} as follows

$$\Psi_{sl}=\frac{\rho_{sl}f_{yl}}{f_t^*}\frac{a_c b_c(1+a_c/b_c)}{I_p}=\frac{A_{sl}}{S_l}\frac{f_{yl}}{f_t^*}\frac{a_c b_c(1+a_c/b_c)}{I_p} \qquad 4.12$$

and

$$\Psi_{st}=\frac{\rho_{st}f_{yt}}{f_t^*}\frac{a_c b_c(1+a_c/b_c)}{I_p}=\frac{A_{st}}{S_t}\frac{f_{yt}}{f_t^*}\frac{a_c b_c(1+a_c/b_c)}{I_p} \qquad 4.13$$

Where I_p is the plastic torsional inertia which is $a^2(3b-a)/12$ for a rectangular section. The lowest upper-bound solution may be found by letting

$$\left(\frac{T}{f_t^* I_p}\right)' = 0 \qquad 4.14$$

or

$$1 - K\cot^2\alpha - 2K\tan\beta\cot\alpha + \Psi_{sl} = 0 \qquad 4.15$$

which leads to

$$\tan\alpha = \frac{K\tan\beta + \sqrt{(K\tan\beta)^2 + K(1+\Psi_{sl})}}{(1+\Psi_{sl})} \qquad 4.16$$

The same approach may be applied to the case of $\alpha < \alpha_o$, which yields

$$\frac{T}{f_t^* l_p} = \frac{m}{2}\sec\beta\sec(\alpha-\beta)(1-\sin\alpha) + \Psi_{sl}\tan(\alpha-\beta) + \Psi_{si}\tan\beta \qquad 4.17$$

and

$$\alpha = \arcsin\left[\left(1 - \frac{2\Psi_{sl}}{m}\right)\cos\beta\right] + \beta \qquad 4.18$$

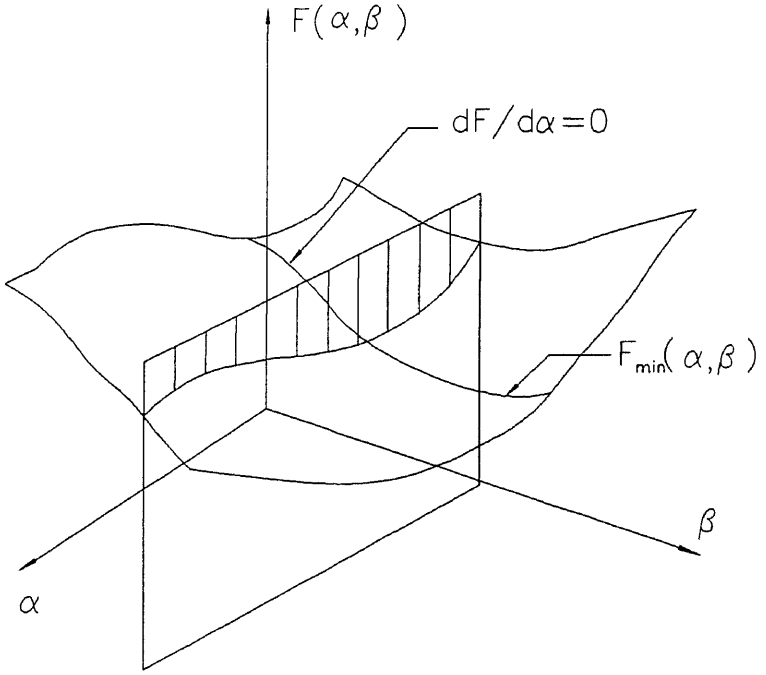

Figure 4.2.3 Numerical Method for Lowest Upper-Bound Solution

It is also necessary to set up the equation of $dT/d\beta$. However, this equation does not lead to an explicit closed form solution for β. In practice, the α values found from Equations 4.16 and 18 actually define a valley of the surface defined by Equations 4.9 and 4.11 (see Figure 4.2.3).

Thus, by changing the value of β from 0 to 90° with a small increment, a series of α may be found with Equations 4.16 and 4.18. The minimum value of the T corresponding to the α and β are the desired lowest upper-bound solution.

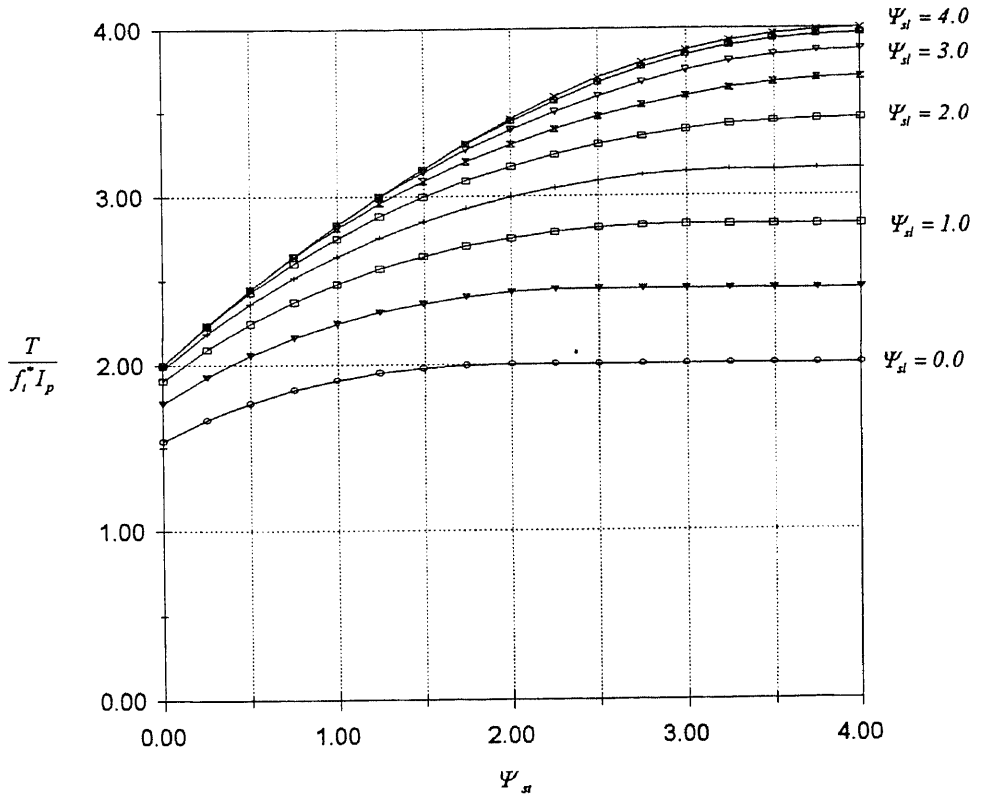

Figure 4.2.4 Ultimate Torsional Strength of Reinforced Concrete Beams (2D)

Numerical analysis shows that the direction of plastic flow depends on the difference of longitudinal and transverse reinforcement indexes as well as their absolute values. A larger reinforcement index will yield a smaller component of plastic flow in its direction. As a matter of fact, the reinforcing bars in a over-reinforced direction will not yield during the course of loading. In such a case, the failure of the element may be caused by either yielding of the reinforcement on the other direction or the crushing of concrete under biaxial compressive stresses.

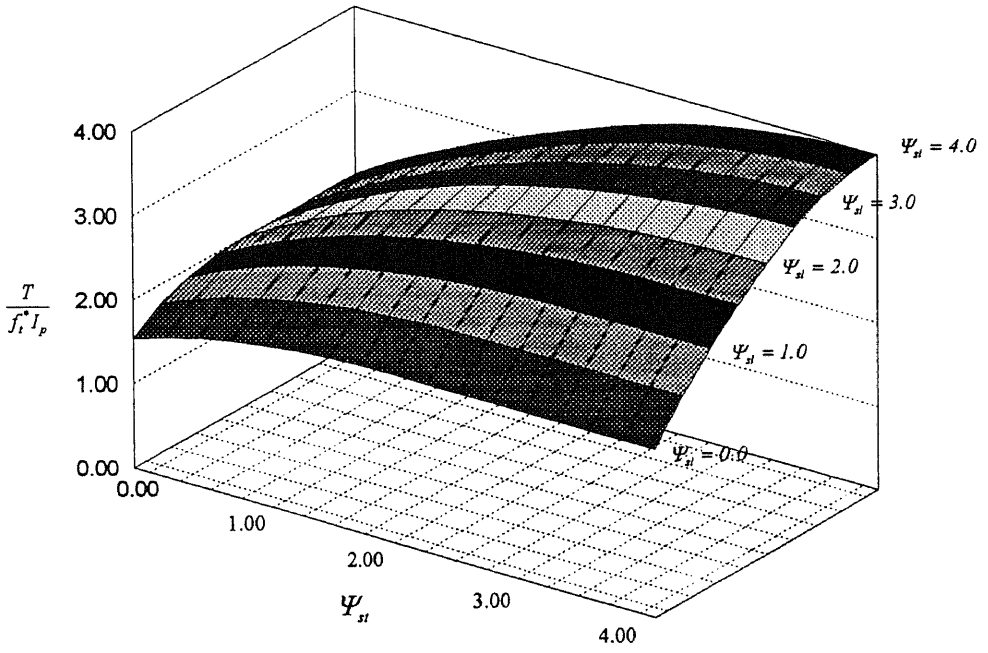

Figure 4.2.5 Ultimate Torsional Strength of Reinforced Concrete Beams (3D)

To attain the contribution from the longitudinal reinforcement, the direction of plastic flow α shall be larger than β, or the direction of the inclined yield line with respect to the vertical axis (see Figure 4.2.1 and 4.2.2). The assumption of having a larger β in comparison to α indicates that a longitudinal bar shall never be subjected to compressive stress.

Based on the work equation and the constraint of the direction of plastic flow, a numerical analysis was performed using the methods mention previously and MathCAD, an integrated mathematical utility software. The result is illustrated in Figure 4.2.4.

The result of the ultimate strength of reinforced concrete beams is also presented in a three dimensional space as shown in Figure 4.2.5.

4.3 Discussions of Solution

It is important to realize that the concrete material in a torsional member fails due to shear under most circumstances. This phenomenon can be found by comparing the direction of the plastic flow in the member with the critical value of α_o. The direction of plastic flow α is found to be a function of the reinforcement indexes Ψ_{st} and Ψ_{sl} (see Figure 4.3.1).

Results shown in Figure 4.3.1 indicate that the failures of a properly reinforced concrete torsional member

are caused by the yielding of reinforcement and shear failure of the concrete.

The lowest upper-bound solution, therefore, may be divided into four areas in accordance with directions of the plastic flow and the yield line.

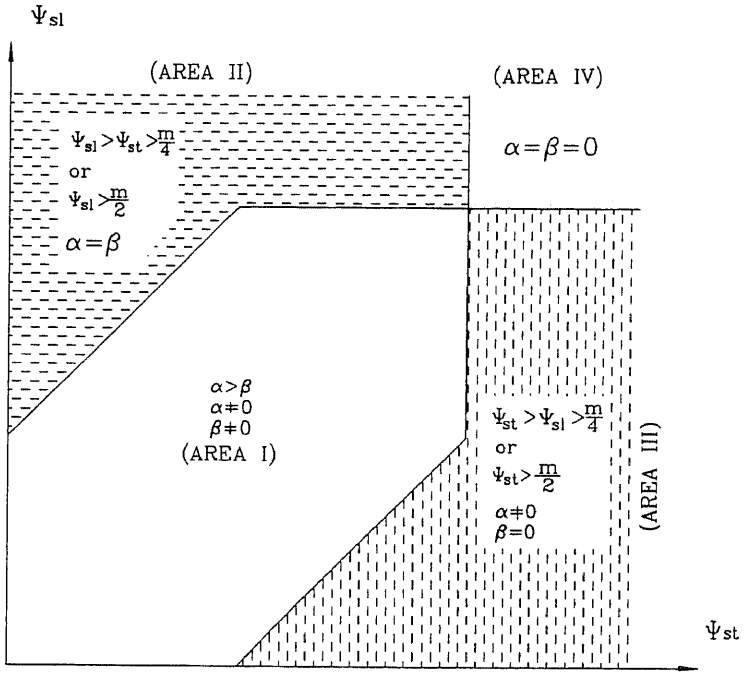

Figure 4.3.1 Directions of Plastic Flow and Yield Line vs. Reinforcement Indexes

Area I presents the load resisting characteristics of properly reinforced concrete members. For beams located in this area, the directions of plastic flow and yield lines are non-zero and unequal, thus their reinforcing bars in both longitudinal and transverse directions may yield at the time of failure.

Area II is designated to the members with over-reinforcement in longitudinal direction. The longitudinal reinforcement in these members will not yield during the course of failure. In terms of directions of plastic flow and yield lines, members located in this area will have the same value of α and β.

Area III is designated to the members with overreinforcement in transverse direction. A vertical yield line will be developed to avoid any plastic energy dissipation in transverse direction. It is because the steels will not yield in this direction.

Area IV indicates the cases that members are over-reinforced in both transverse and longitudinal directions. In such a case, both α and β are zero since the reinforcements in neither directions yields. The members located in this area shall have the maximum normalized strength as indicated in figure 4.2.3 and 4.2.4 of $\frac{m}{2} f_t^* I_p$.

As mentioned in the above discussions, these areas are directly influenced by the amount of reinforcements in longitudinal and transverse directions, or the confinement

in both longitudinal and transverse directions. The analysis shows the following boundaries for these areas:

For Area I:

$$\begin{cases} |\Psi_{st} - \Psi_{sl}| < \dfrac{m}{4} \\ 0 < \Psi_{sl} < \dfrac{m}{2}, \text{ and} \\ 0 < \Psi_{st} < \dfrac{m}{2} \end{cases} \qquad 4.19$$

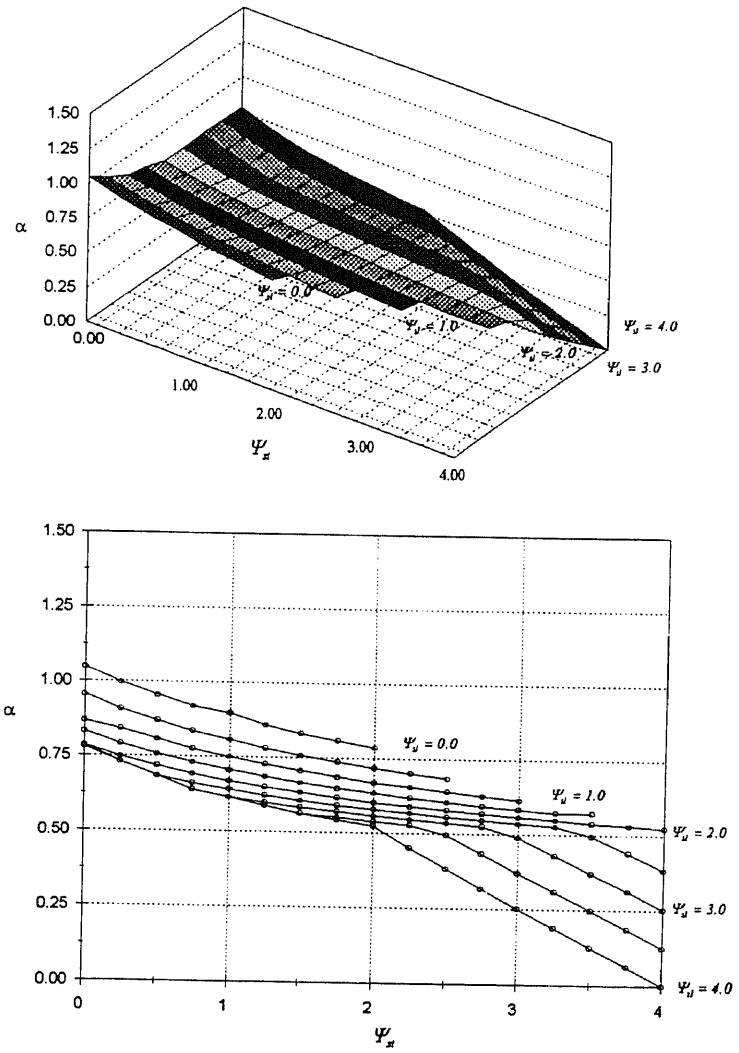

Figure 4.3.2 Directions of Plastic Flow vs. Reinforcement Indexes

For area II

$$\begin{cases} |\Psi_{st} - \Psi_{sl}| \geq \frac{m}{4} \\ \Psi_{sl} \geq \frac{m}{2}, \text{ and} \\ \Psi_{st} < \frac{m}{2} \end{cases} \qquad 4.20$$

For area III

$$\begin{cases} |\Psi_{st} - \Psi_{sl}| \geq \frac{m}{4} \\ \Psi_{st} \geq \frac{m}{2}, \text{ and} \\ \Psi_{sl} < \frac{m}{4} \end{cases} \qquad 4.21$$

For area IV

$$\begin{cases} \Psi_{st} \geq \frac{m}{2}, \text{ and} \\ \Psi_{sl} \geq \frac{m}{2} \end{cases} \qquad 4.22$$

The torsional strength of reinforced concrete members may be found by using numerical analysis methods. Figure 4.2.4 shows the nominal torsion strength vs. reinforcing indexes. It indicates that the torsional strength of a plain reinforced concrete member is about $1.54f_t^*I_p$, which is approximately equal to $0.32f_t^*a^2b$ for a rectangular section with b to a ratio of 2:1. The coefficient varies from 0.257 to 0.38 for different b to a ratios. According to ACI, this coefficient is said to have an average value of 0.3 for sections with various b to a ratios (ACI, 1989).

The solution also shows that a reinforced concrete member has a peak torsional strength of $mf_t^*I_p/2$ or $f_c^*I_p/2$ regardless of the values of reinforcement indexes exceeding

the maximum value of m/2. This result is consistent with the previous results for shear transfer, deep beams and brackets. Therefore, m/2 may be considered as a unified criterion to determine the maiximum reinforcement ratio of reinfroced cocnrete structures.

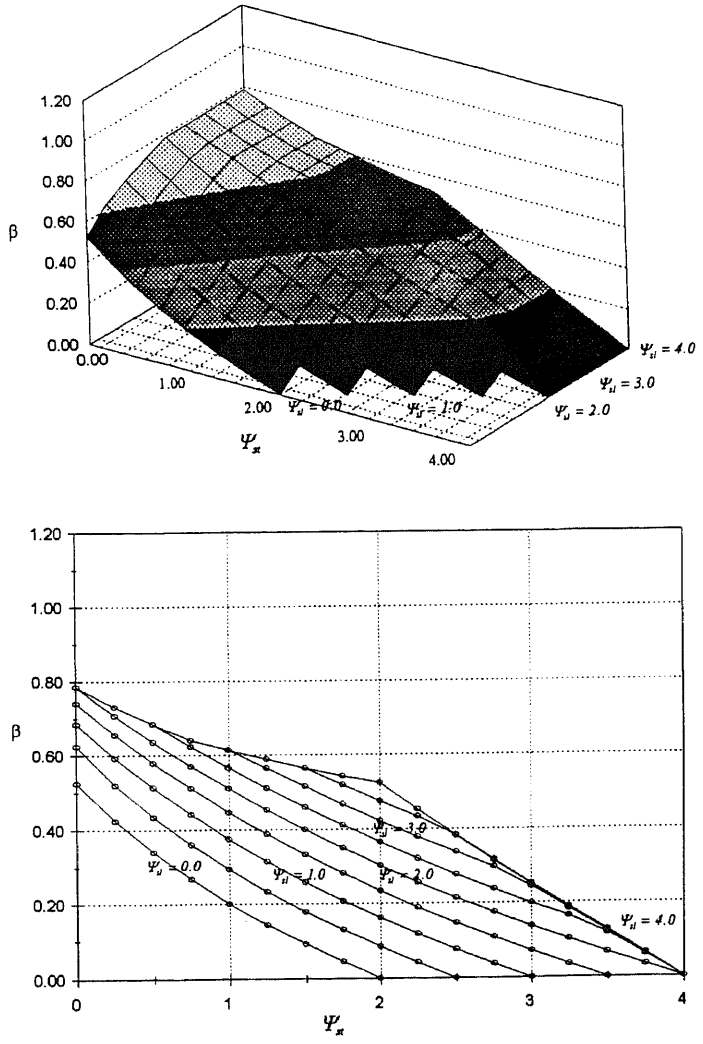

Figure 4.3.3 Directions of Yield Line vs. Reinforcement Indexes

4.4. Simplified Solution for Longitudinally Constrained Members

In engineering practice, a torsional member is always designed with additional longitudinal reinforcing bars to withstand the bending moment which may apply to the member. Thus, from the viewpoint of resisting torque, the member is most likely to be over-reinforced in the longitudinal direction. Therefore, the longitudinal reinforcement may not yield or just at the point of yielding at the time of failure. In terms of plastic flow, these members are constrained longitudinally. In such a case, the directions of plastic flow and the yield line may have the following relation:

$$\alpha = \beta \tag{4.23}$$

Thus, the previous solution may be simplified as

$$\tan\alpha = \sqrt{\frac{K}{1+\Psi_{st}}}, \quad \alpha \geq \alpha_o \tag{4.24}$$

and

$$\alpha = \arcsin(1-\frac{2}{m}\Psi_{st}), \quad \alpha < \alpha_o \tag{4.25}$$

The corresponding lowest upper-bound solution may be found as

$$\frac{T}{f_t^* I_p} = \begin{cases} 2\sqrt{K(1+\Psi_{st})}, & \alpha \geq \alpha_o \\ \sqrt{\Psi_{st}(m-\Psi_{st})}, & \alpha < \alpha_o \end{cases} \tag{4.26}$$

where $I_p = a^2(3b-a)/12$ is the torsional plastics modulus of the section.

This solution may fall back to the classical plastic solution for torsional problems. Well-known as the "send heap analogy" (Sadowsky, 1949), the classical

approach to the torsional strength of a rectangular section leads to the following solution

$$T=\frac{a^2k}{6}(3b-a) \qquad 4.27$$

where

$$k=\begin{cases}\frac{f_y}{\sqrt{3}}, & \text{von Mises failure criterion}\\ \frac{f_y}{2}, & \text{Tresca failure criterion}\end{cases} \qquad 4.28$$

The failure criterion used in this research may be referred to as a modified Coulomb criterion. The Coulomb criterion will become the Tresca criterion if the internal friction angle is zero (see Figure 1.3.3). Thus, the derived equation is expected to have the similar format as the classical solution. Indeed, as a matter of fact, the proposed formulation in this research may be considered as the factored classical solution to consider the properties of concrete and the reinforcing indexes as shown in Equation 4.26. The formulas derived in this chapter may be considered as the theorical solution for torsional strength of structural members made of reinforced cementitious composites.

Section 4 of Chapter 5 shows the comparison of the proposed formula with 39 experimental results reported by Hsu (1968b). The average value of the measured to predicted strength ratio is 0.98, and its standard deviation is 0.09.

CHAPTER 5

EMPIRICAL STUDY AND VERIFICATION OF PROPOSED SHEAR STRENGTH FORMULAS FOR REINFROCED COCNRETE STRUCTURES

Experimental results from the author's tests and several other test results are analyzed herewith to verify the proposed formulas from the limit analysis method. These test data include shear transfer, shear strengths of brackets and deep beams, as well as the torsional strengths of reinforced concrete rectangular beams. The comparison between the measured and the predicted strength of these members show that the proposed formulas have an acceptable accuracy and may be used for design purposes.

5.1 Empirical Study and Verification of Analytical Strength Formula for Shear Transfer

As a part of the fundamental study of this research, the experiment of reinforced concrete shear transfer was conducted to study its shear resistant behavior. And also, the test results are used here to verify the theoretical formula by the limit analysis proposed in Chapter 2.

5.1.1 Design of Specimens

Four different groups of specimens were used in the experiment. They are:

1. Group D0. Plain concrete without reinforcement;
2. Group D4. Reinforced concrete with shear reinforcing bars of d=4mm by 70mm (reinforcement ratio ≈ 0.21%);
3. Group D6.5 Reinforced concrete with shear reinforcing bars of d=6.5mm by 70mm (reinforcement ratio ≈ 0.56%);
4. Group D8. Reinforced concrete with shear reinforcing bars of d=8mm by 70mm (reinforcement ratio ≈ 0.77%).

To prevent the potential size effect, these specimens were designed to have the dimensions similar to those used in the engineering practice. The maximum size of coarse aggregate is less than 0.6 in. The overall shear resisting area has a nominal dimension of 16×24(cm^2) (6.3×9.45 sq. in.). Two notches were designed in order to assure a vertical yield (slip) line. This simple failure mechanism is exactly the same as the one being used in the limit analysis presented in Chapter 2. Thus, the proposed upper-bound solution may be considered to be an exact solution for a shear transfer of this kind.

5.1.2 Material Properties

Concrete Mix Design

The content of cement and fine aggregates of the mix design in this investigation were higher than that of normal concrete. Its maximum size of coarse aggregates is less than 15mm (0.6 in) in order to improve the workability, as well as the quality of the specimens. The same mix design was also used in the other investigations on the shear strength of fiber reinforced concrete shear transfer so that the results from the two studies are compatible (Wang, 1988).

Materials used per cubic meter concrete are (in Kg):

Cement (Type I)	Sand	coarse aggregates	Water
350	1185	790	>175

The water cement ratio for the concrete was 0.6.

The compressive strength of the concrete was 15.73 MPa (2280 psi). The tensile strength of the concrete was measured by the splitting test.

The setup of the splitting test is shown in Figure 5.1.1. This setup allows the splitting specimen to have a similar failure mechanics of push-off shear transfer. Thus for plain concrete, the ultimate splitting strength may be found as

$$f_t^* = \frac{P}{2a^2\sqrt{K}} \qquad 5.1$$

where, P is the applied ultimate load, a is the length of each side of the cubic specimen, and K is a material constant which is defined by Equation 1.40. Equation 5.1 may be written in a short form of

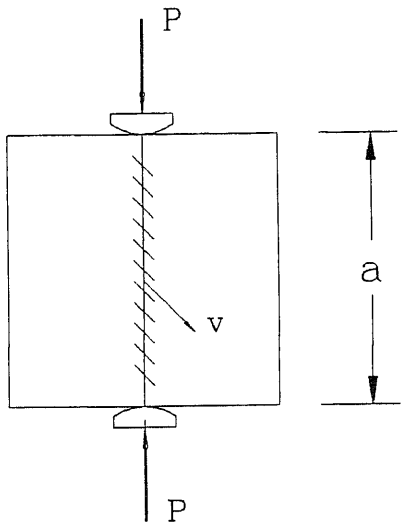

Figure 5.1.1 Splitting Test Setup for concrete Material

$$f_t^* = K_s \frac{P}{a^2} \qquad 5.2$$

where

$$K_s = \frac{1}{2\sqrt{K}} = \frac{1}{\sqrt{m + 2(1 - \sqrt{m+1})}} \qquad 5.3$$

K_s descends as the compressive strength of concrete increases (See Figure 5.1.2).

Figure 5.1.2 shows the equivalent tensile strength of concrete decreases as the compressive strength

increases. The measured equivalent tensile strength for the concrete used in this investigation was 1.204 MPa (174.58 psi).

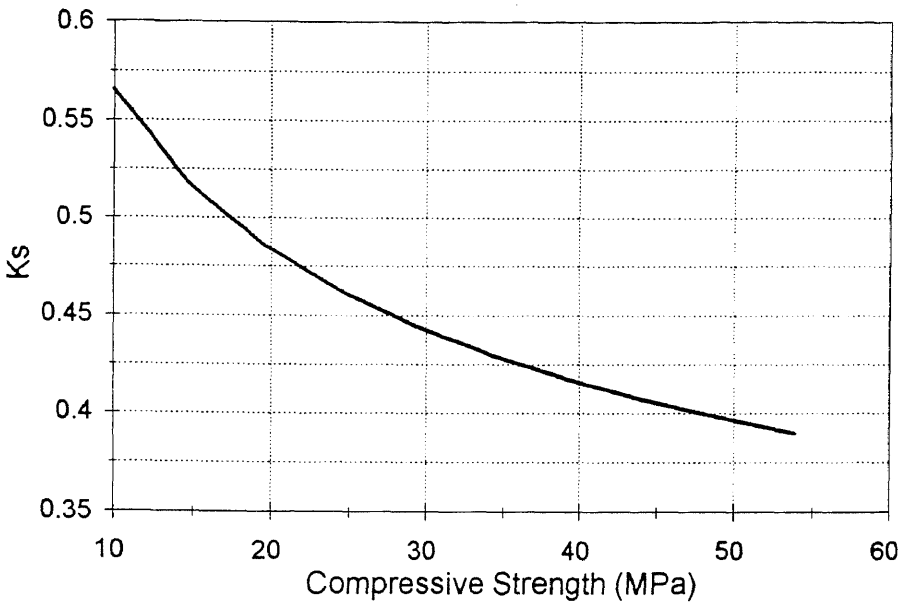

Figure 5.1.2 k_s vs. f_c'

Strength of reinforcing bars

Three different types of reinforcing bars were used in the test. They have strength of 484.1 MPa (71.3 ksi), 220.61 MPa (32.2 ksi), and 231.7 MPa (34.1 ksi), respectively.

5.1.3 Test Results and Comparisons

A systematic difference was found in comparison between the measured and the predicted ultimate shear strength. For plain or slightly reinforced push-off shear transfer

specimen, the predicted ultimate shear strength is larger than the measured ones. In contrast, for specimens with higher reinforcement indexes, their measured shear strengths are slightly higher than the predicted ones. This is because that the effectiveness factor ν_c mentioned in Chapter one is proposed based on the tests on normally reinforced concrete slender beams (Nielsen, 1978). The hydrostatic pressure of the stress fields in these beams are most likely larger than those in the push-off shear transfer specimens.

According to previous researches, concrete material becomes more ductile when it is subjected to higher hydrostatic pressures(Wang, et. al, 1992). Therefore, the factor of plasticity for concrete shall be modified according to the hydrostatic pressure level in a structural element. For any structures that are different from slender beams, their effective strengths shall be modified by an additional factor which reflects the hydrostatic pressure level in the material. This factor considers the structural effects on the plasticity of the material, and therefore, may be called the structural factor of plasticity and denoted as ν_s. In contrast, the factor ν_c indicates the material effects on the ductility, and may be referred to as the material factor of plasticity.

For a push-off shear transfer specimen, the effective strength of concrete may be found as

$$\nu = \nu_c \nu_s \qquad 5.4$$

where

$$\nu_s = 0.9 + 0.03\psi \qquad 5.5$$

in which, Ψ is the reinforcement index of the specimen.

Equation 5.5 indicates that the effective strength of concrete is slightly less than that in reinforced concrete beams. It increases as the shear reinforcement index increases. The reason for a push-off shear transfer specimen to have a lower effective strength is due to the stress state in the specimen. A push-off shear transfer specimen is supposed to have a higher tensile strength than a beam. In terms of the theory of plasticity, the stress field in a shear transfer specimen has a higher hydrostatic pressure (positive for tensile stress). Thus, a lower effective strength shall be used for the push-off shear transfer specimens.

As the reinforcement index increases, the reinforcing bars may supply an additional confinement to the concrete to increase the hydrostatic pressure level. Due to this confined stress, the concrete material becomes more ductile, thus, a higher effective strength of concrete may be used in the analysis. This effect can be clearly seen from Equation 5.5.

Table 5.1.1 in Appendix A shows the comparison between the measured and the predicted shear strengths of push-off shear transfers. Statistical analysis shows that the predicted shear strength matches the measured strength with a good accuracy.

The mean value of the ratios between the measured and predicted shear strengths is 0.985 and the corresponding standard deviation is 0.07. The errors of the majority of predicted shear strengths are less than ±15% in comparison to the test results. (see Figure 5.1.3) The results are based om the analyses of 34 experimental results, of which 12 were tested by the author and the rest of them were collected by Hsu et. al (1986).

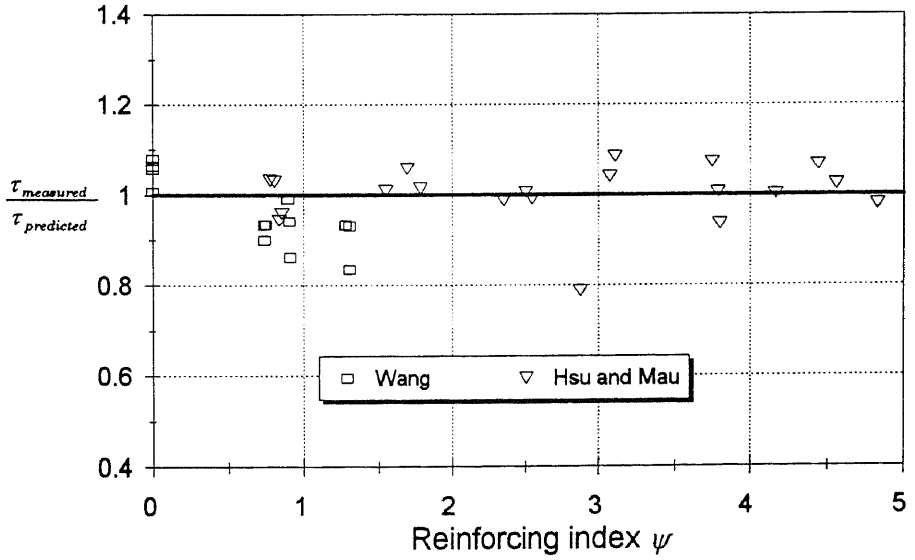

Figure 5.1.3 Comparison Between Measured and Predicted Shear Strengths of Push-off Shear Transfer Specimen

5.2 Brackets

Brackets or corbels are widely used in precast or prestressed concrete structures. They are used as beam seats in buildings and bridges. Shear failures are most common cases among these types of elements.

Theoretical analysis in Chapters 2 leads to an explicit formula for the ultimate shear strength of brackets. Also several test results were gathered by the Shear Strength Committee at the Chinese Institute of Building Technology. These data were initially collected for verifying the proposed articles for the shear strength design in the 1986 edition of the Chinese Reinforced Concrete Building Code. The test data included the experimental results from about 100 specimens that were tested in China and U.S.A. These data are carefully chosen for present study and they are believed to have a good reliability.

The concrete strength of these specimens varies from 15 MPa (2000 psi) to 45 MPa (5000 psi) and the reinforcement ratio varies from 0.32% to 2.70%. Thus, these test data covers a wide range both in terms of concrete strength and reinforcement ratio. Table 5.2.1 in Appendix A shows the list of the material properties of the specimens and Table 5.2.2 in Appendix A gives the analysis results and the comparison with the measured ultimate shear strength.

The so called structural factor of plasticity for brackets was found to be equal to

$$\nu_s = 0.94 - 0.16\lambda \qquad 5.6$$

where λ is the shear span ratio.

Figure 5.2.1 shows the ratio between the measured and predicted ultimate shear strengths of reinforced concrete brackets and/or corbels without considering the structural factor of plasticity. Figure 5.2.2 shows the result after considering the structural factor of plasticity.

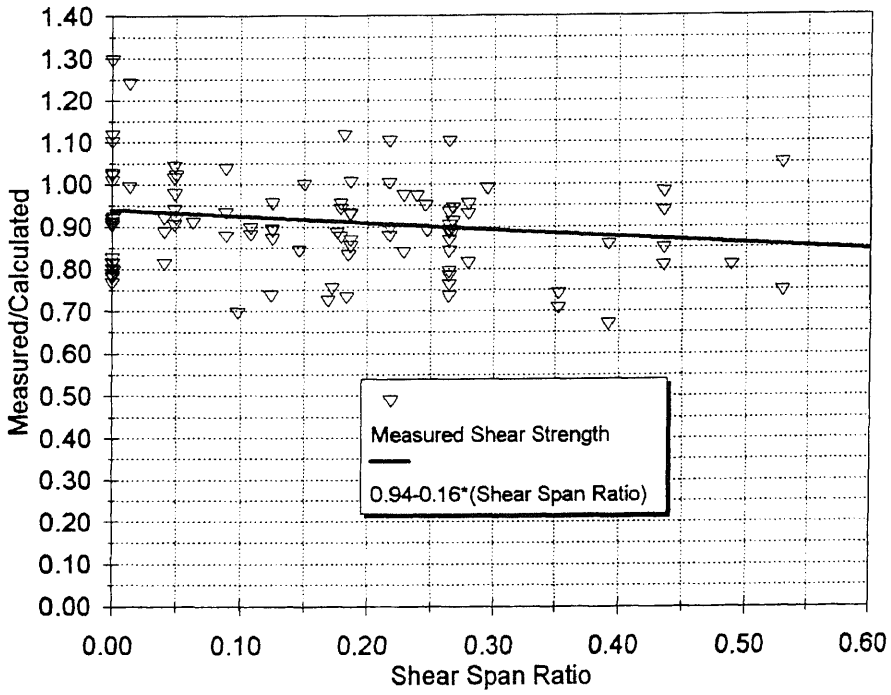

Figure 5.2.1 Comparison of Measured and Predicted Shear Strengths of Brackets (without ν_s)

Figure 5.2.1 clearly shows a consistent decrease of the measured nominal shear strength as the shear span ratio increases. Physically, the shear span ratio indicates the tensile stress level in a reinforced concrete beam. Higher shear span ratio means a higher tensile stress, thus, higher positive hydrostatic pressure value. In this case, the concrete material behaves more brittle and the proposed structural factor of plasticity, therefore, is a decreasing function of the shear span ratio.

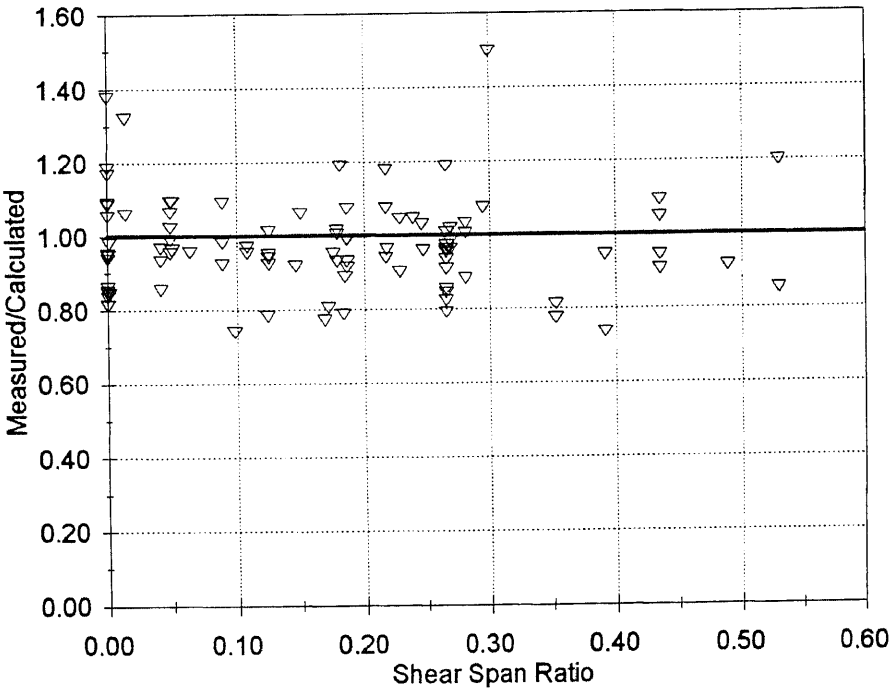

Figure 5.2.2 Comparison of Measured and Predicted Shear Strengths of Brackets.(with ν_s)

The ratios between the measured and predicted ultimate shear strengths of brackets yield an average value of 0.973 and a standard deviation of 0.130.

5.3 Shear Strength of Deep Beams

A total of 64 test specimens reported by Mau and Hsu(1989) are used here to verify the present theoretical solution. These data were originally reported by Smith and Vantsiotis(1982), Kong, Robins and Cole(1970), and De Paiva and Siess(1965). The above test data were selected due to the following reasons:

1) The specimens must fail in web shear mode, not in bearing or flexural modes;
2) the test specimens must contain at least a minimum amount of transverse web reinforcement specified in the ACI Code(1989) to render the truss model applicable;
3) the span-depth ratio a/h must be less than 2; and
4) the specimens must be simply supported.

Table 5.3.1 in Appendix A shows the material properties and dimensions of the specimens used in this investigation. Details of computation and the comparison of measured and predicted ultimate shear strength are listed in the Table 5.3.2 in Appendix A.

A total of 64 specimens were used to verify the proposed ultimate shear strength formula for reinforced concrete deep beams. Using the ratio of predicted

ultimate shear strength to the measured ones as an indicator, the comparison gives a mean value of 1.02 and standard deviation of 0.128, respectively.

The effective strength is used to consider both material and structural effects on the plasticity of the concrete material. The structural factor of plasticity is found to be equal to

$$\nu_s = 1.25 - 0.15\lambda \qquad 5.7$$

where λ is the shear span ratio which can be expressed as a/h in for simply supported beams.

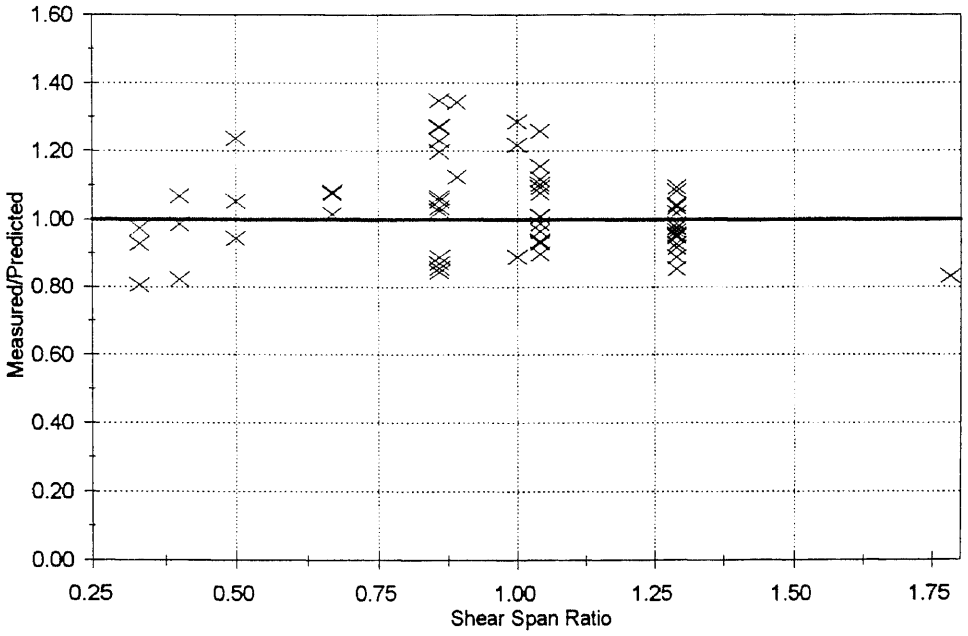

Figure 5.3.1 Comparison Between Measured and Predicted Ultimate Shear Strengths of Deep Beams

As expected, the structural factor of plasticity of deep beams is found to be a function of shear span

ratio. Just as in brackets, this factor decreases as the shear span increases (Wang, et. al, 1992). The comparison between the measured and predicted ultimate shear strengths of 64 Specimens is illustrated in Figure 5.3.1. Details of the specimens and calculations are listed in Table 5.3.1 in Appendix A.

5.4 Torsional Strength

About 40 test results from previous empirical study conducted at the University of Houston are used to verify the proposed ultimate torsional strength of reinforced concrete beams (Hsu, 1968b). A typical specimen is shown in Figure 5.4.1.

The length of all beams was 122 in. A length of 14 inch at each end of the beam was threaded into the clamping head of the test rig, through which the torsional moments were applied. The clear span subjected to torsion was 96 in. to avoid local failure close to the clamping heads due to stress concentration, a length of 25 in. at each end of the beams was reinforced with bout 30% additional stirrups. Details of each beam series are shown in Fig 5.4.1.

As shown in Figure 5.4.1, the beams of series S were hollow. However, a length of 14 in. at each end of the beams was solid to prevent crushing of the wall from the clamping heads of the test rig.

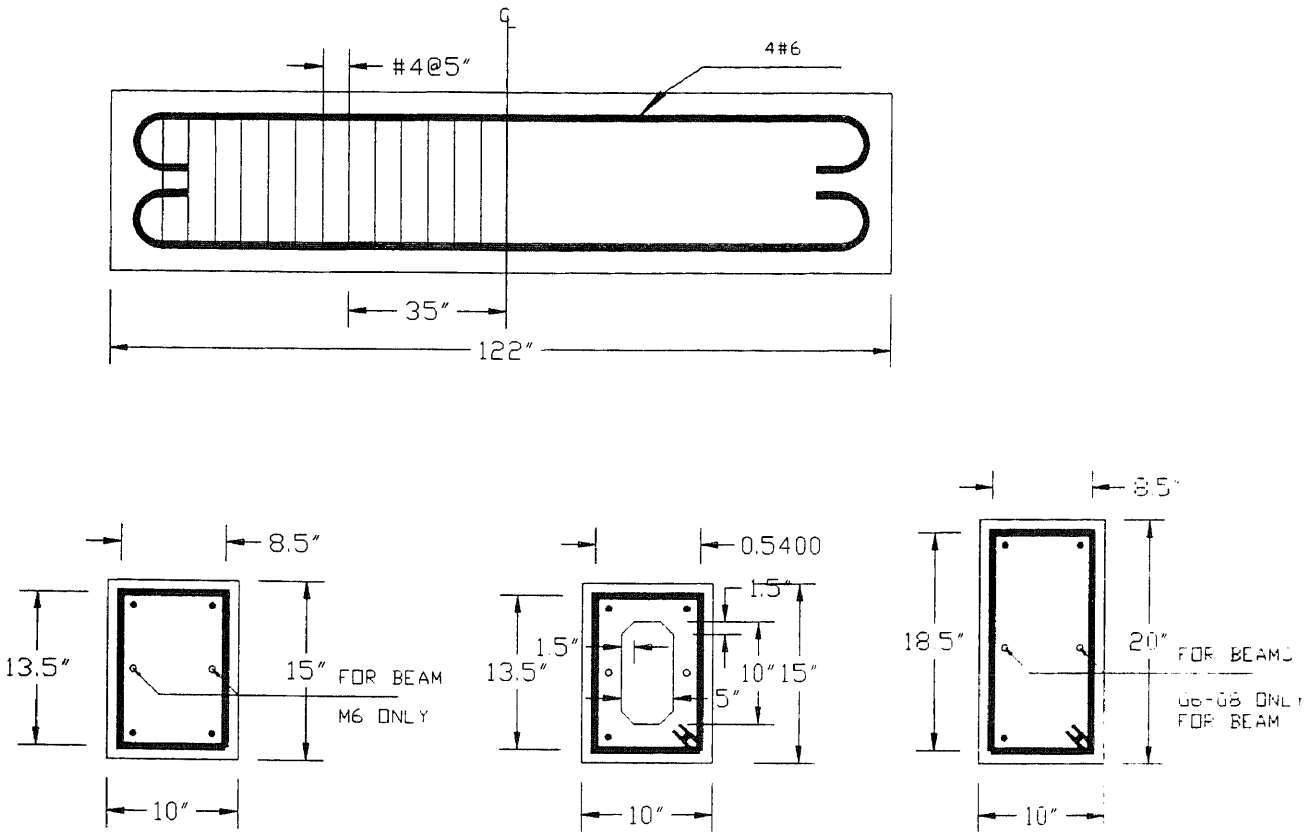

Figure 5.4.1 Typical Torsional Specimen

All reinforcements were intermediate grade deformed bars having yield strengths from 45 ksi to 52 ksi as listed in Table 5.4.1 in Appendix A.

The reinforcing cages for the beams usually consisted of four longitudinal corner bars and closed stirrups tied together by soft steel wire. However, several beams in the Group G and M were added two

additional longitudinal reinforcing bars. Details of reinforcing of each beam are listed in Table 5.4.1 in Appendix A.

Concrete mixture used in the test was 1:3.5:4 (Cement:Sand:Coarse Aggregate) and had an average compressive strength of 4000 psi.

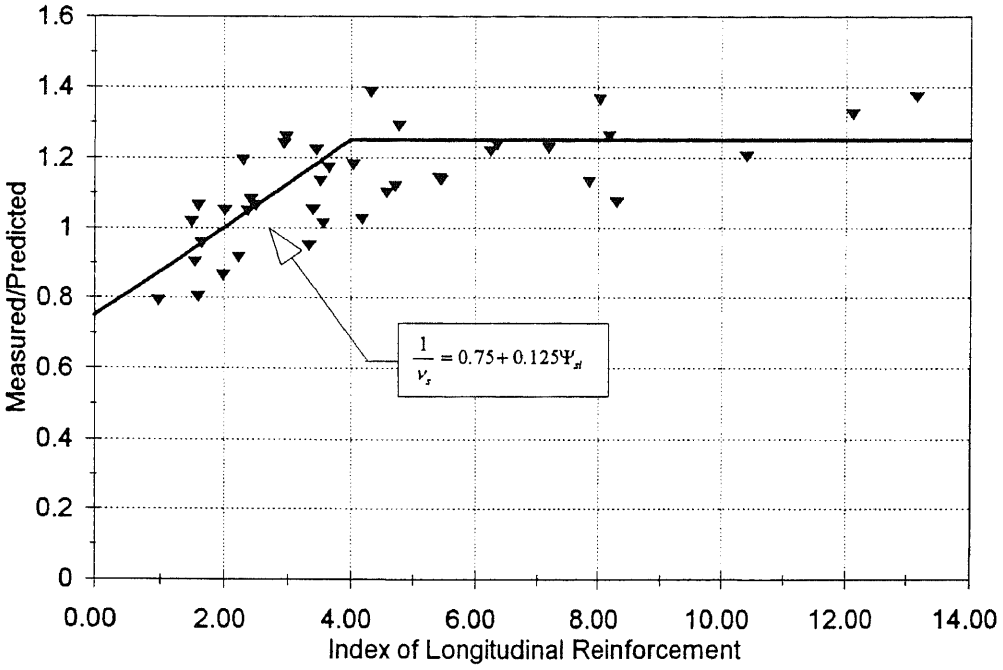

Figure 5.4.2 Comparison of Measured and Predicted Torsional Strengths of Reinforced Concrete (Without ν_s)

All specimens were cured for four days under polyethylene sheets in the forms and then stripped and stored at 70F and 50 percent relative humidity until tested at the age of 11 to 14 days. Strengths of the concrete are listed in Table 5.4.1.

Torsional beams were tested in especially designed torsion test rig. The measured ultimate torsional strengths are listed in Table. 5.4.2 in Appendix A.

Comparison between the measured and the predicted ultimate torsional strengths is listed in Table 5.4.2 in Appendix A. Figure 5.4.2 shows the ratio between the measured and predicted torsional strengths vs. the longitudinal reinforcement index.

A consistent increase of this ratio within the range of $0<\Psi_{sl}<4$ is observed, because the effective strength of concrete is assumed to be constant in the computation. As a matter of fact, the effective strength of concrete is expected to vary in accordance with the level of the hydrostatic pressure. A lower longitudinal reinforcement index yields less constraint. Thus, concrete may have a tendency to be subjected to a higher tensile stress and behave in a more brittle manner.

In this case, a lower structural factor of plasticity shall be used to reflect this fact. In contrast, a higher longitudinal reinforcement index may cause the constraint of deformation, forming a larger hydrostatic pressure. As a result, the concrete behaves in a more ductile manner. Higher ductility means higher effective strength. In this research, the structural factor of plasticity for torsional member is found to be

$$\nu_s = 0.94 - 0.16\Psi_{sl} \qquad 5.8$$

where Ψ_{sl} is the index of longitudinal reinforcement.

Figures 5.4.2 and 5.4.3 show the comparison of the observed and predicted ultimate torques with and without considering the structural factor of plasticity ν_s. Details of the specimens and the computation are listed in the Tables 5.4.1 and 5.4.2 in Appendix A.

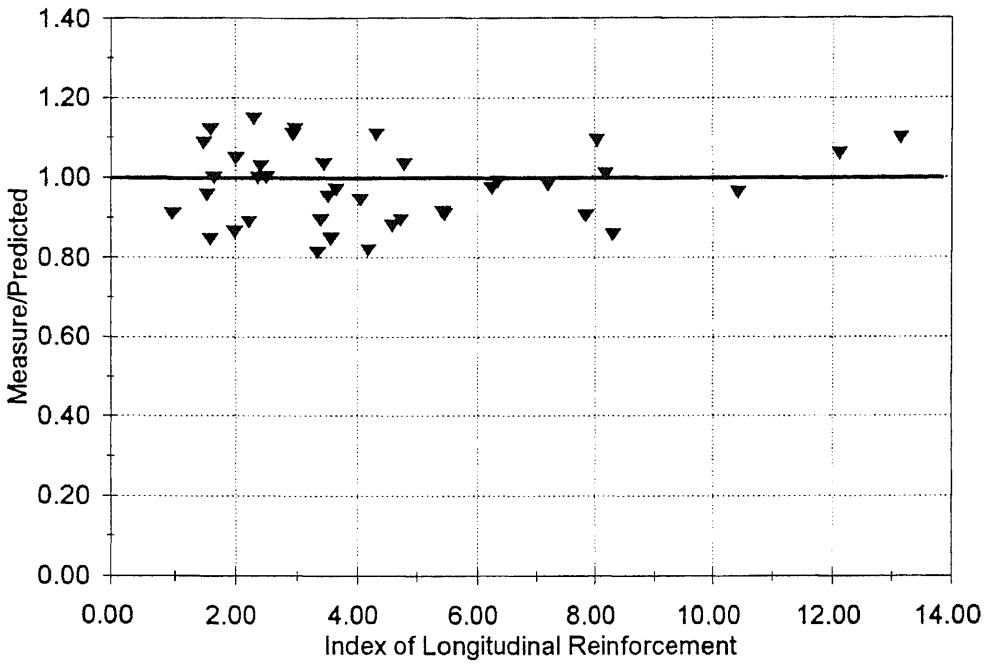

Figure 5.4.3 Comparison of Measured and Predicted Torsional Strengths of Reinforced Concrete (With ν_s)

PART II

CHAPTER 6

THE J INTEGRAL FOR NONLINEAR ELASTIC-PLASTIC MATERIAL

Part One of this dissertation discussed the failure of reinforced concrete shear elements using the theory of plasticity. The basic concept is based on the ductile failure of reinforced concrete structures under normal service conditions in bridges and buildings. However, due to the development of new materials and design methods, the usage of reinforced and/or prestressed concrete floating marine structures, storage tanks, nuclear vessel containments and other special structures have become increasingly common. Because these structures are subjected to the hazardous environment and high stress levels that traditional reinforced structures may never experience, increasing attention has been paid to studying new structural and material properties.

Similar to the evolving of analyses and design methods of metallic structures, the effect of having unstable local failure on global behavior of reinforced concrete structures became a major issue in the past decade. In the 40's of this century, the application of high strength steels initiated various structural

failures. These failure were caused by the nonhomogeneity of the material and the damage caused by local yielding and/or crack. These local failures may cause sudden release of the energy stored in the rest part of the highly stressed structures. As the energy-release rate exceeds the value that a newly developed damage area can dissipate, a sudden failure will occur in the structure. Studies of this type of failure develope a new are in research, and it is known as fracture mechanics.

The development of fracture mechanics makes the applications of new high strength materials possible. Profound understanding of the nature of fracture in existing materials has provides guide lines for developing new high performance materials.

Since the 70's, the concept of fracture mechanics has been introduced to the study of concrete structures. Special fracture properties such as size effect, softening, micro-cracks, and reinforcement etc. have distinguished concrete materials from metals.

Part II of this dissertation is devoted to the study of the fracture and fatigue crack propagation properties of general engineering materials, including metals and concrete.

Chapter Six gives a brief review of linear and nonlinear fracture mechanics. The plastic and elastic components of the J integral are proposed in this

chapter, which enables the use of the J integral for solving the fatigue crack propagation problem.

In Chapter Seven, a generalized process zone theory is proposed for nonlinear materials. This generalized process zone theory is used to study the so-called size effect on softening materials. A brittleness index is postulated in this chapter to characterize the ductility of the structures. The size effect can thus be explictly defined in terms of this brittleness factor.

An energy based damage accumulation theory is proposed in Chapter Eight. This damage accumulation theory may be used to solve the fatigue crack propagation problems for general engineering materials.

In Chapter Nine, both the fatigue crack initiation and propagation are studied using the proposed damage accumulation theory. The predicted fatigue crack propagation rate agrees well with the measured experimental data. The threshold stress intensity factor in fatigue crack propagation is obtained using notch analysis.

Fatigue crack initiation and propagation of concrete materials is also presented in Chapter Ten. The proposed generalized process zone and the damage accumulation theory are used to obtain the fatigue crack propagation rates for concrete materials. They agree well with the test data.

6.1 Introduction and Brief Review of Fracture Mechanics

6.1.1 Linear Elastic Fracture Mechanics

There are two important concepts reviewed in this section. One is the stress intensity factor, and the other is the energy-release rate. These two concepts are fundamental in fracture mechanics and they will be used intensively in the following chapters throughout this dissertation.

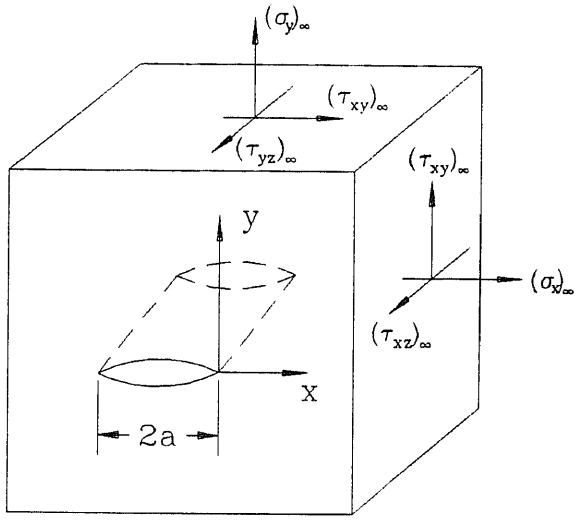

Figure 6.1.1 Stress Field Near a Crack Tip

The stress intensity factor represents the degree of stress concentration near a crack tip in a linear elastic solid. It shows the properties of the stress localization in a cracked solid. Considering a cracked infinite solid as shown in Figure 6.1.1, its stress field near the crack tip may be found as (Tada, et al, 1973)

$$\sigma_{ij} = \frac{K_I}{\sqrt{2\pi r}} \tilde{\sigma}_{ij}(\theta) + O\left(r^{1/2}\right) \qquad 6.1$$

where

$$\sigma_{ij}(\theta) = \cos\frac{\theta}{2}\begin{bmatrix} 1 - \sin\frac{\theta}{2}\sin\frac{3\theta}{2} \\ 1 + \sin\frac{\theta}{2}\sin\frac{3\theta}{2} \\ \sin\frac{\theta}{2}\cos\frac{3\theta}{2} \end{bmatrix} \qquad 6.2$$

and K_I is the stress intensity factor for mode I fracture problem, σ_{ij} is the stress field, θ and r are the absisscæ of the position in question in a polar coordinate system, and O is the estimated error. Fracture problems may be classified as three different modes. They are shown in Figure 6.1.2.

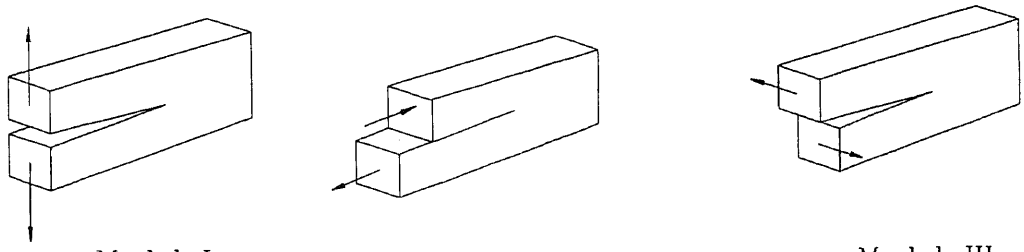

Figure 6.1.2 Basic Model of Crack Tip Deformations

Equations 6.2 and 6.4 imply the following important properties of the near-crack-tip stress field.

1. The stress field near a sharp crack has singularity at the crack tip, and it follows the $1/\sqrt{r}$ rule.

2. The approximate solutions of different elements with varying geometry setups have the same form as shown in Equations 6.2 and 6.4.

Different specimens have different stress intensity factors. The so-called stress intensity factor, K, may be defined as

$$K = \lim_{x \to a^+} \sqrt{2\pi(x-a)}\sigma_y(x,0) \qquad 6.3$$

or

$$K = \lim_{r \to 0^+} \sqrt{2\pi r}\sigma_y(r,0) \qquad 6.4$$

The above solutions are valid if the crack is sharp in a mathematical sense and the stress field in question is very close to the crack tip. However, these assumptions are hard to satisfied in engineering practice.

Materials used in engineering practice have certain strengths. As the stress near a sharp crack tip increases , the nearby material yields at the instant when the load is applied. The yielded material forms a blunt crack tip which reduces the stress. Therefore, from the point of view of engineering practice, the formulation for the stress field near a blunt crack tip may be found to be useful.

A simple and elegant solution for a deep notch in a linear elastic solid was given by Creager (Tada, et al, 1973). His solution shows that the stress intensity

factor near a notch tip is a superposition of a ρ related term and Equation 6.2 (see Figure 6.1.3)

$$\sigma_{ij} = \frac{K_I}{\sqrt{2\pi r}} \frac{\rho}{2r} \tilde{\sigma}_{ij}^{(\rho)}(\theta) + \frac{K_I}{\sqrt{2\pi r}} \tilde{\sigma}_{ij}(\theta) + O(r^{1/2}) \qquad 6.5$$

where

$$\tilde{\sigma}_{ij}^{(\rho)}(\theta) = \begin{bmatrix} -\cos\frac{3\theta}{2} \\ \cos\frac{3\theta}{2} \\ \sin\frac{3\theta}{2} \end{bmatrix}, \qquad 6.6$$

ρ is the radius of curvature of the notch tip, and the $O(r^{1/2})$ is the estimated error.

Equation 6.5 may fall back to Equation 6.2 in case of $r \gg \rho$. However, the singularity of the stress field disappears when $r \geq \rho > 0$.

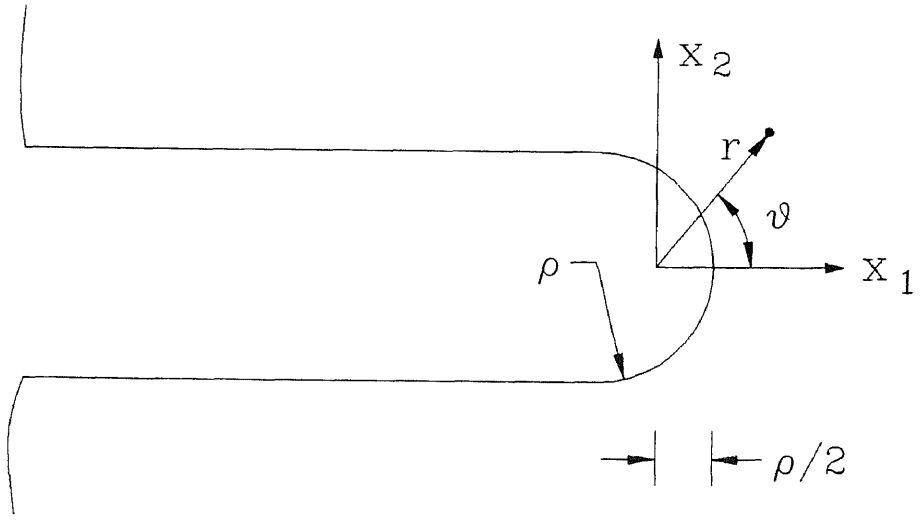

Figure 6.1.3 Coordinate System for North Analysis

6.1.2 Energy-Release Rate for Linear Elastic System

The energy-release rate for a linear elastic system is defined as the released energy from the system when the crack propagates a unit area under the applied load. Considering a system as shown in Figure 6.1.4, the load deflection curve changes as the crack length increases. The increasing crack length increases the compliance of the system. Thus the energy in the system must be released in a certain form. The released energy is absorbed by the newly cracked surface in linear elastic systems if the system undergoes stable crack propagation. The energy-release rate, therefore, may be written as

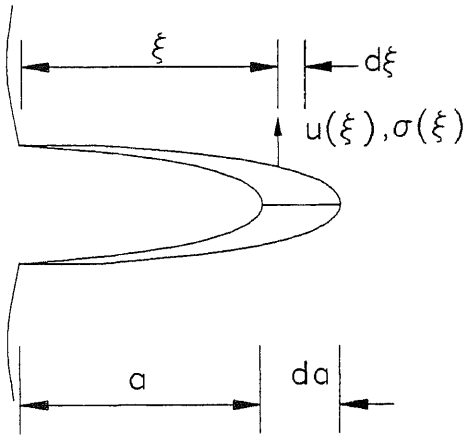

Figure 6.1.4 Derivation of K vs. G Relationship

$$G = \frac{\partial W}{\partial a} \qquad 6.7$$

for two-dimensional fracture problems, where a is the crack length, and W is the total enery of the system.

For the problem of centrally cracked linear elastic solid, the total energy of the system is

$$W = 2\int_0^a \sigma_{yy}^{(x,0)} v(x,0)dx \qquad 6.8$$

where 2a is the crack length, and v(x,0) is the displacement along the crack.

This is a symmetrical problem, thus, the fracture energy-release rate is given by

$$G = \frac{1}{2}\frac{\partial W}{\partial a} \qquad 6.9$$

The displacement, v(x,0), near a crack tip is found as

$$v(\xi)_{\theta=\pm\pi} = \pm\frac{æ+1}{2\mu}K_I(a+da)\sqrt{\frac{a+da-\xi}{2\pi}} \qquad 6.10$$

where æ and μ are elastic constants. The stress near a crack tip according to Equation 6.2 is

$$\sigma_y(\xi) = \frac{K_I(a)}{\sqrt{2\pi\xi}} \qquad 6.11$$

Thus, the total energy change in the system shown in Figure 6.1.4 is

$$dW = 2\int_0^{da}\frac{1}{2}v(\xi)\sigma_y(\xi)Bd\xi$$

or

$$dW = \frac{æ+1}{8\mu}K_I(a)K_I(a+da)Bda \qquad 6.12$$

where B is the width of the specimen. According to the definition, the energy-release rate G may be found as follows

$$\frac{dW}{da} = \frac{æ+1}{8\mu} K_I^2(a) \qquad 6.13$$

or

$$G_I = \begin{cases} \dfrac{K_I^2}{E} & \text{for plane stress} \\ \dfrac{K_I^2}{E}(1-\nu^2) & \text{for plane strain} \end{cases} \qquad 6.14$$

where E is the modulus of elasticity and ν is the Poisson ratio.

In conclusion, the energy-release rate and the stress intensity factor are equivalent in linear fracture mechanics.

6.1.3 Nonlinear Fracture Mechanics and the J Integral

For nonlinear fracture problems, Rice proposed a so called J integral to study the energy-release rate for cracked nonlinear elastic solids(Rice, 1965). This J integral has been shown to be path-independent, and it is identical to the energy-release rate in linear elastic solids.

The J integral has a form of

$$J = \int_\Gamma \left(W dx_2 - T_i \frac{\partial u_i}{\partial x} ds \right) \qquad 6.15$$

where Γ is an integral path which surrounds the tip. T_i is the traction normal the integral path, u_i is the

displacement, and **ds** is the differential integral path. It begins on the lower flat notch surface and ends on the upper flat notch surface as shown in Figure 6.1.5. **W** is the strain energy density, and is given by

$$W = \int_0^{\varepsilon_{ij}} \sigma_{kl} d\varepsilon_{kl} \qquad 6.16$$

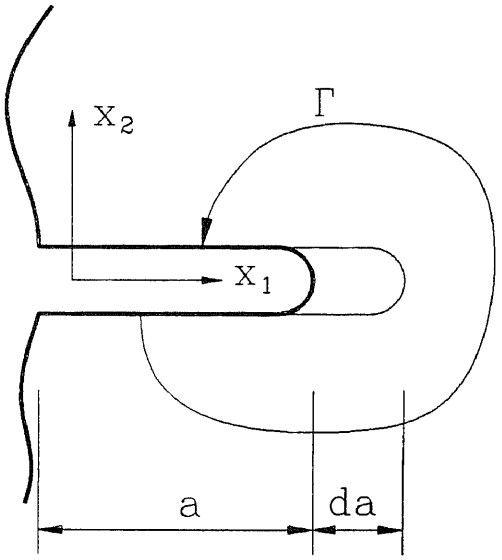

Figure 6.1.5 Flat Surface Notch in Two Dimensional Deformation Field(Rice, 1968)

The J integral is valid only when the material is nonlinear elastic and/or the system undergoes proportional loading for nonlinear elastic plastic materials.

Applying the J integral concept to the so-called process zone theory (Dugdale, 1960), it yields several

crucial results that are well-known in the field of fracture mechanics.

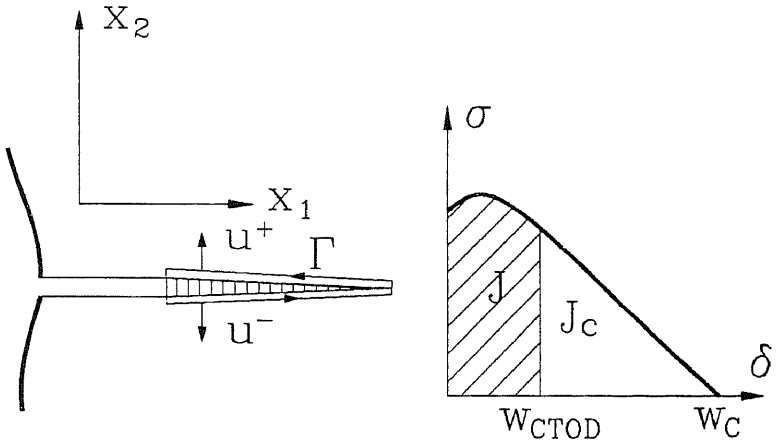

Figure 6.1.6 Process zone theory by J integral

Considering a strip yield zone, namely, process zone, ahead of a crack tip, the stress σ in this process zone is found to be a function of the separation w, or $\sigma = f(w)$. If the integral path surrounds the crack tip and it does not pass through the process zone as illustrated in Figure 6.1.6, the J integral may be found as

$$J = -\int_{\Gamma} T_i \frac{\partial u_i}{\partial x} ds = -\int_{p.z} \sigma_{yy} \frac{\partial}{\partial x}\left(u^+ - u^-\right) dx = -\int_{p.z} \sigma \frac{\partial w}{\partial x} dx$$

The separation w is solely dependent upon the position of x in the process zone, therefore, $\frac{\partial w}{\partial x}dx = dw$. Thus, the above integral becomes(Rice, 1968)

$$J = -\int_{w_{CTOD}}^{0} \sigma(w)dw = \int_{0}^{w_{CTOD}} \sigma(w)dw \qquad 6.17$$

where w_{CTOD} is the crack tip opening displacement.

Equation 6.17 shows that the J integral of a cracked specimen is equal to the area under a stress-separation curve (See Figure 6.1.6).

In the case of a constant cohesion σ_y, the J integral may be presented as

$$J = \sigma_y w_{CTOD} \qquad 6.18$$

In case the of small scale yielding (Rice, 1968),

$$J \approx G = \frac{K^2}{E'} \qquad 6.19$$

Where $E'=E$ for plane stress condition, and $E'=E/(1-\nu^2)$ for plane strain conditions.

6.2 Elastic-Plastic J Integral

The J integral has been commonly used to study the elastic-plastic fracture mechanics problems since the concept was proposed by Rice in 60's. The J integral is based on the non-linear elastic theory, as mentioned by Rice. Strictly speaking, the J integral is completely valid only under the following two circumstances: (1) the material is perfectly nonlinear elastic, and/or (2)

the structure undergoes a monotonically proportional loading if the material is elastic-plastic. The monotonically proportional loading requires that stresses in the whole specimen must increase proportionally and simultaneously. Therefore, the fatigue crack growth rate problem of an engineering material can not be treated with the J integral theory without proper modification. Hereof, an analysis model is proposed to estimate the elastic and plastic parts of the J integral in order to predict the fatigue crack growth rate of a specimen made of engineering materials.

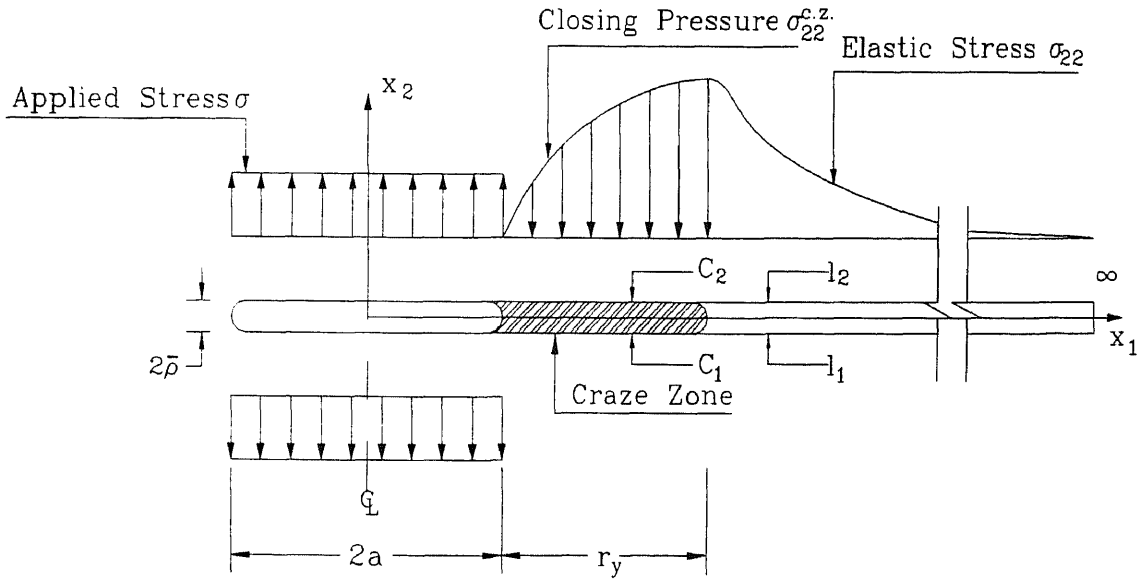

Figure 6.2.1 The J Integral of a Blunt Crack in an Elastic-Plastic Body

Since a fatigue crack in a specimen made of engineering materials always becomes blunt as the crack propagates, a blunt crack shall be analyzed instead of an ideal sharp crack. When the specimen is subjected to loads, a process zone may be developed if the maximum stress in front of the crack tip exceeds the maximum local strength of the material. In such cases, the stress distribution in front of the crack tip can be illustrated as in Figure 6.2.1

Consider a blunt crack with a width of $2\bar{\rho}$, a length of 2a, and a craze zone length r_y. If the integral path is chosen such that it starts from the bottom of the crack tip and extends horizontally to the point $(\infty,-\bar{\rho})$, then goes up to $(\infty,+\bar{\rho})$, and then goes back to $(a,+\bar{\rho})$, the J integral is(Rice, 1968),

$$J=\int_{\Gamma} w(x_1,x_2)dx_2-T_i\frac{\partial u_i}{\partial x_1}ds \qquad 6.20$$

or in the following form (Equation 12):

$$J=0-\left\{\int_{c_1}\sigma_{22}^{c.z}\frac{\partial u_2^-}{\partial x_1}dx_1+\int_{c_2}\sigma_{22}^{c.z}\frac{\partial u_2^+}{\partial x_1}dx_1+\int_{l_1}\sigma_{22}^{c.z}\frac{\partial u_2^-}{\partial x_1}dx_1+\int_{l_2}\sigma_{22}^{c.z}\frac{\partial u_2^+}{\partial x_1}dx_1\right\} \qquad 6.21$$

where c_1, c_2 are the lower and upper boundaries of the process zone. Also they are parts of the integral curve in the plastic zone; l_1, l_2 are the lower and upper parts of integral curve in the elastic field;$\sigma_{22}^{p.z}$ is the vertical stress in the process zone, which is known as the closing pressure;σ_{22} is the vertical stress in the

elastic stress field; and u_2^+, u_2^- are the displacements of the points on the upper and lower parts of integral curve.

The first part of the J integral $\int_\Gamma w(x_1,x_2)dx_2$ is equal to zero since the strain energy $w(x_1,x_2)$ is equal to zero when $x_1 \to \infty$. The second part of the J integral can be expressed as the sum of the plastic and the elastic components. The plastic part reads:

$$J_p = \int_0^{CTOD} \sigma(\delta)d\delta \qquad 6.22$$

Here δ is equal to $u_2^+ - u_2^-$, and is known as the crack opening displacement in the process zone. If the crack opening displacement in the process zone is approximately equal to the width of the process zone times the average strain in the process zone $\varepsilon_{p.z.}$, the plastic part of J integral can also be expressed as:

$$J_p = 2\bar{\rho}\int_0^{\bar{\varepsilon}_{c.z.}^{tip}} \sigma d\varepsilon \qquad 6.23$$

where

$2\bar{\rho}$ is the width of the process zone;

$\bar{\varepsilon}_{c.z.}^{tip}$ is the average crack tip strain value.

The elastic component of the J integral can be estimated by using stress intensity factor K_I' of the system. Here K_I' is the stress intensity factor of the specimen subjected to both external loads and the closing pressure on the process zone. The elastic component of the J integral reads:

$$J_e = \left(\int_{l_1} \sigma_{22} \frac{\partial u_2^-}{\partial x_1} dx_1 + \int_{l_2} \sigma_{22} \frac{\partial u_2^+}{\partial x_1} dx_1 \right) = \frac{\left[K_I'(\bar{\rho}, \sigma_{coh}, \sigma_{external}) \right]^2}{E'} \qquad 6.24$$

where $K_I'^2/E'$ is known as the elastic fracture energy-release rate of the system under external loads and closing pressure caused by the distributed cohesive force. It is a function of notch dimension, external load, and material properties such as the σ_{coh}–δ relationship in general.

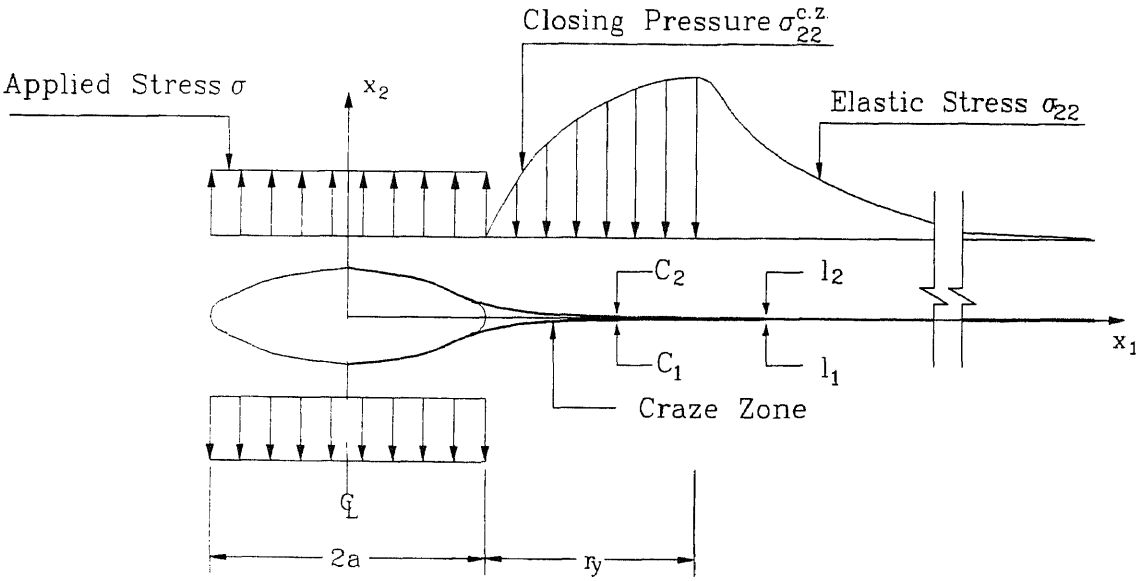

Figure 6.2.2 Classical Process Zone Theory and the J Integral

The elastic component of the J integral is negligible in ductile engineering materials because of the large distributed cohesive force in the process zone. According to the classical process zone theory,

this elastic component indeed is equal to zero since the relative displacement $u_2^+ - u_2^- = 0$ (See Figure 6.2.2).

Thus, the J integral is found to be the sum of elastic fracture energy-release rate and the plastic fracture energy dissipation rate for an elastic-plastic material, namely,

$$J = J_e + J_p = \frac{K_I'^2}{E'} + \int_0^{CTOD} \sigma(\delta) d\delta \qquad 6.25$$

When the system undergoes unloading, the elastic component J_e will be released. However, the plastic component J_p will be dissipated by the process zone and causes accumulative damages in the system.

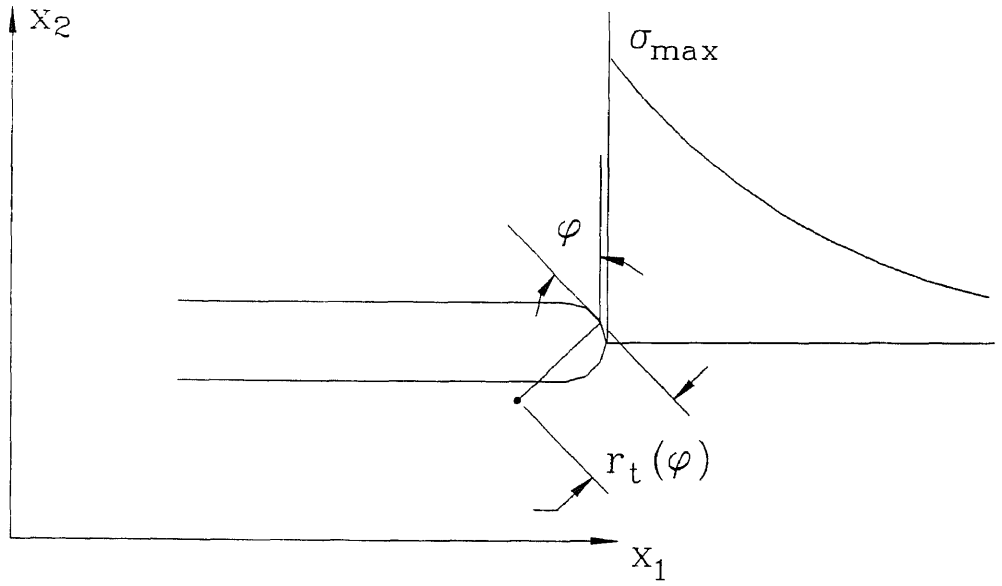

Figure 6.2.3 Stress field near a notch tip

A similar formula was achieved by Jenq and Shah (1985) for cementitious composites by considering the global energy balance. The critical value in the elastic part of the fracture energy-release rate is claimed to be a specimen size-independent parameter in their paper. The partition of the J integral into elastic and plastic components has been suggested for metals by Jones et al. (1974) and Weertman (1978). An equation similar to Equation 6.14 was proposed by Bazant(1985) for concrete structures based on crack band theory. When a system undergoes small scale yielding, the elastic component of the J integral may be estimated by means of notch analysis. For a given notch shown in Figure 6.2.3, its stress intensity value will be (Rice, 1968):

$$K_e = \sigma_{max}\sqrt{\frac{8}{15}r_t} \qquad 6.26$$

Equation 6.27 shows the case of a semicircular tip for which $r_t(\varphi) = r_t$, a constant. If the maximum stress σ_{max} is less than the yield strength of the material, the J integral contains only the elastic component and equals K^2/E or $(1-\nu^2)K^2/E$ in the plane stress and plane strain conditions, respectively.

If the maximum stress caused by the external load exceeds its local yield strength, a process zone will be developed as mentioned previously. The corresponding J integral will be the sum of both the elastic and plastic components. The maximum value of the elastic component

will be approximately equal to $\bar{\sigma}_y\sqrt{\frac{8}{15}r_t}$, where $\bar{\sigma}_y$ is the average local yielding stress in front of the crack tip, r_t is the radius at the noth tip. The average local strength of material is a function of mean grain size when the yield zone is relatively small and compatible to the mean grain size according to a number of the earlier works of 1950's and 60's. A comprehensive review of the works of that period was given by Bement et. al(1971). If a large scale yielding occurs, then the average yield strength of the material within the yielding zone will mainly depend upon the overall yield strength of the material, the size of process zone and loading condition simultaneously. An approximate method to estimate the average local strength during large scale yielding can be established by Weibull's risk theory (1939). Using Equation 6.26, the irreversible plastic part of the J integral can be stated as:

$$J_p = J - \frac{8}{15}\frac{\bar{\sigma}_y^2 r_t}{E'} \quad \text{if} \quad J > \frac{K_{th}'^2}{E'} \tag{6.27}$$

where J is the total fracture energy-release rate, and r_t is the radius at the notch tip.

This plastic component of the J integral will be used as a damage parameter to predict the fatigue crack growth rate in the following chapters of this dissertation.

CHAPTER 7

GENERALIZED PROCESS ZONE THEORY

7.1 Introduction

A highly stressed reversible process zone can be formed ahead of the crack tip for a specimen subjected to periodic loading. The size of this cyclic process zone may be estimated as if it were subjected to a monotonic loading assuming that the hardening of the material is isotropic. The equivalent strength used in the calculation should be $2\sigma_y$ instead of σ_y (Rice, 1966) (see Figure 7.1.1). According to the damage accumulation theory proposed in Chapter 8, the material in the cyclic process zone is crazed into two parts and forms a newly cracked area if the accumulative damage in the material reaches its critical condition. In case that the damage index in each cycle of loading can be determined in a certain manner, the prediction of crack propagation of the material may become possible by estimating the size of cyclic process zone.

For metallic structures the size of the process zone may be estimated by Irwin's[1968] effective crack length theory. His theory is based on the fact that most metallic materials are quite ductile and have a nearly constant yield strength when the stress in the material reaches its peak value. His process zone

formulation is based on the force balance near the crack tip and has a considerable accuracy in small scale yielding cases as compared with the Dugdale's striped yielding model. However, extension of this theory to cementitious material, such as motar and concrete may initiate technical problems due to the softening properties of the material.

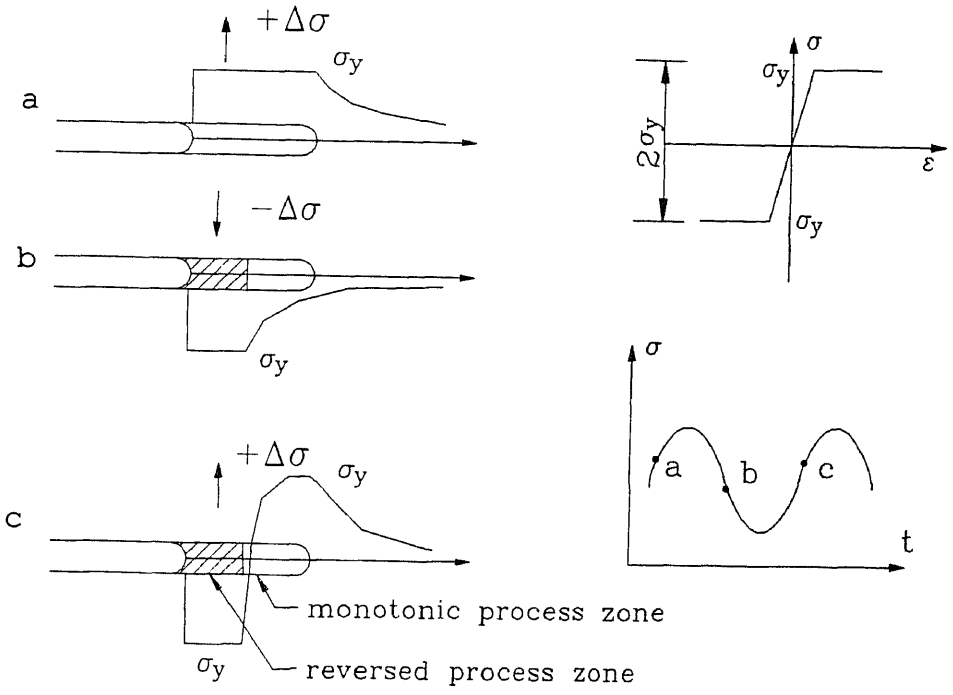

Figure 7.1.1 Cyclic Process Zone by Isotropic Hardening Rule (Rice, 1968)

Concrete and motar are known as softening materials and have a descending cohesive force. Previous researches showed difference in fracture properties between cementitious materials and metals (Capinteri, 1985) (Bazant, 1985) (Shah, 1984) (Sih, 1984). Several researches concluded that this descending cohesive force plays a key role in determining the fracture properties of the concrete structures, especially in the case of nonlinear fracture mechanics.

The so-called fictitious crack model proposed by Hillerborg (1985) has been widely accepted as an effective method in modeling the fracture properties of concrete and reinforced concrete structures. This model is based on the classical process zone theory by applying variable cohesive force to the process zone. This concept is not new to researchers in metallic materials. The use of variable cohesion in the process zone to model the hardening properties of different metals was proposed by Chen (1975). His idea, however, was not considered mathematically feasible in the 70's.

The development of digital computer technology and numerical methods, especially the finite element method, makes the fictitious crack model a reality. This model was originally proposed by Hillerborg at Lund Technical University and it showed a high potential for predicting the fracture properties of concrete structures. Numerous researches and technical papers have been

published in the literature on this topic since the 70's. However, most of these researches concentrated on the analysis methods and case studies.

An analytical method must be found to apply this process zone theory to the fatigue crack propagation problems of concrete structures. The key issues are: 1). prediction of the length of the process zone in a cementitious material, and 2). the crack opening displacement in the process zone.

These two problems are fundamental to the application of fracture mechanics to cementitious materials. In the following sections of this chapter, a generalized process zone theory is proposed based on the Paris' displacement formula. A closed form solution from the functional analysis is derived in this chapter. The theoretical results are then used to predict the fatigue crack propagation rate of concrete materials.

7.2 Generalized Process Zone Theory

Paris (1957) proposed a method to calculate certain displacements relevant to crack problems. His method was based on Castigliano's theorem and fracture mechanics. Assume the total strain energy of a cracked body is U under external load of P. The crack opening displacement Δ_F (Figure 7.2.1) was found as

$$\Delta_F = \frac{2}{E'}\int_{a_F}^{a_c} K_{IP}\frac{\partial K_{IF}}{\partial F}da \qquad 7.1$$

where K_{IF} is the stress intensity factor caused by a couple of virtual forces F on the position in question; K_{IP} is the stress intensity factor corresponding to the external load P; a is the integral variable; and a_c and a_F are the position of the crack tip and the position where the displacement is to be calculated.

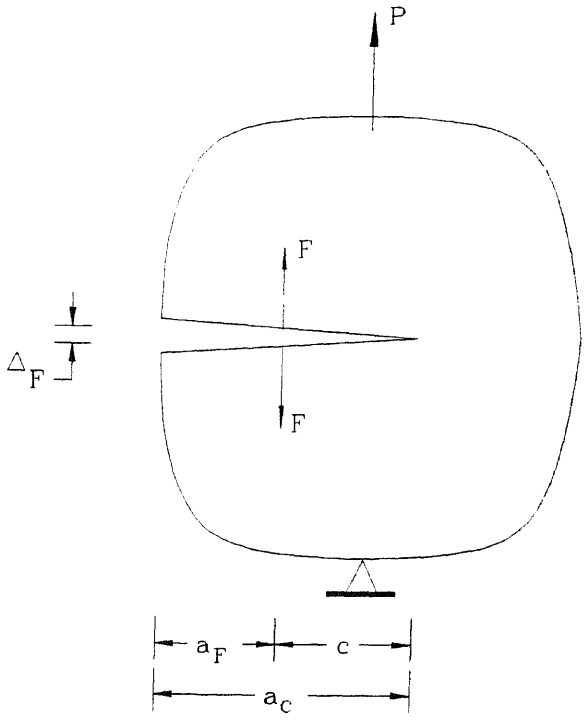

Figure 7.2.1 Crack Opening Displacement by Castigliano's Theorem

Using the principle of superposition, the Paris formula can be applied to the classical process zone theory and it yields a generalized approach to the

problem. Note that the stress intensity factor of a linear elastic cracked body is assumed to be a linear function of the load applied. Thus $\frac{\partial K_{IF}}{\partial F}$ in Paris' formula can be considered as the virtual strength intensity factor, $k^D(\xi,x)$, corresponding to a unit force **F**. The Paris' formula can be written as:

$$\delta(x) = \int_0^a K(\xi) k^D(\xi,x) d\xi \qquad 7.2$$

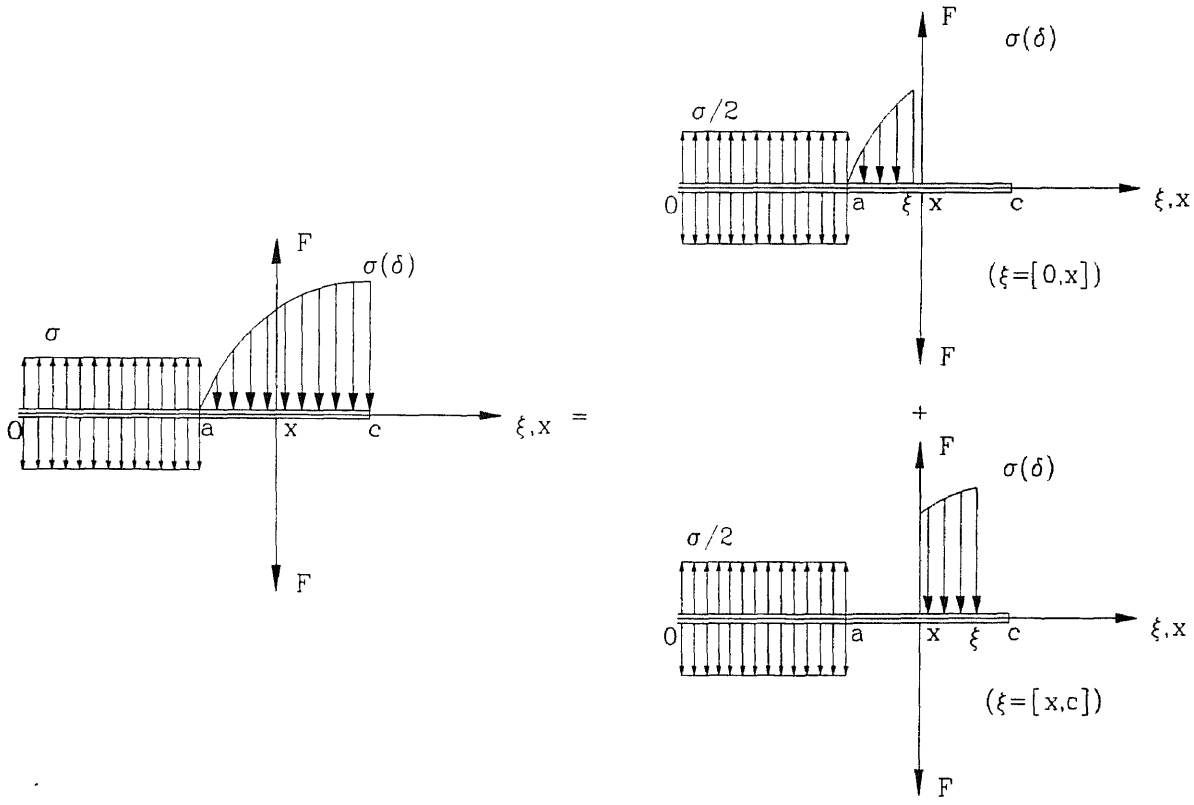

Figure 7.2.2 Generalized Process Zone Theory by Paris' Displacement Formula

where

a is the crack length (Figure 7.2.2),

K is the stress intensity factor, and

ξ is the moving coordinate along the crack length.

In case of existing a distributed cohesive force $\sigma(b)$ in the process zone $[a, c]$, a negative contribution by the distributed cohesive force to the total stress intensity factor shall be considered in computing the crack opening displacement in Equation 7.2. By using the principle of superposition, the crack opening displacement can be found as (Figure 7.2.2):

$$\delta(x) = \delta_1(x) + \delta_2(x) \tag{7.3}$$

where

$$\begin{aligned}\delta_1(x) &= \frac{2}{E'}\int_x^c \left(\frac{K(\xi)}{2} - \int_a^{\xi} K_c(\xi,\delta,b)db\right)k^D(\xi,x)d\xi \\ &= \frac{2}{E'}\int_x^c \frac{K(\xi)}{2}k^D(\xi,x)d\xi - \frac{2}{E'}\int_x^c \left(\int_a^{\xi} K_c(\xi,\delta,b)db\right)k^D(\xi,x)d\xi\end{aligned} \tag{7.4}$$

$$\delta_2(x) = \frac{2}{E'}\int_x^c \frac{K(\xi)}{2}k^D(\xi,x)d\xi - \frac{2}{E'}\int_x^c \left(\int_a^{\xi} K_c(\xi,\delta,b)db\right)k^D(\xi,x)d\xi \tag{7.5}$$

Equation 7.4 and 7.5 lead to a singular integral equation:

$$\delta(x) = \frac{2}{E'}\int_x^c K(\xi)k^D(\xi,x)d\xi - \frac{2}{E'}\int_x^c k^D(\xi,x)d\xi \int_a^{\xi} K_c(\xi,\delta,b)db \tag{7.6}$$

The smooth closure condition can be define the boundary condition needed to solve the problem. The physical meaning of the smooth closure condition is that the stress intensity factor at the tip of a process

zone is equal to zero, which indicates that the stress field has no singularity at this point, i.e.(Wang, et al., 1994), thus

$$K(c) - \int_a^c K_c(\xi, \delta, b)db = 0 \qquad 7.7$$

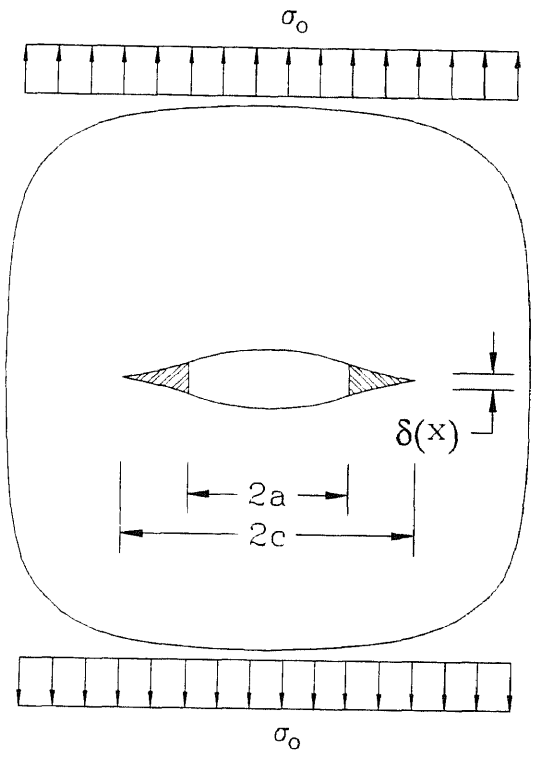

Figure 7.2.3 Centrally Cracked wide Plate Subjected to Distant Uniform Tensile Stress

As an example, the solution for a wide plate with a central crack problem (constant distributed cohesive force) is illustrated later in this section using the proposed method. In the case of variable distributed cohesive forces, Equation 7.6 becomes a singular integral equation with a free boundary condition as specified in Equation 7.7. Closed form solutions for the above equation do not exist in general.

However, in case that the material has a constant cohesion, the proposed equation becomes an integration of a given function. Thus, Equations 7.6 and 7.7 may have exact closed form solutions. In fact, most ductile metals can be considered to have a constant cohesion after yielding. Hence, the applications of Equations 7.6 and 7.7 to metallic structures have led to good results(Rice, 1968).

An exact solution for the problem of a wide plate with a central crack (see Figure 7.2.3) is derived herewith to illustrate the proposed generalized process zone theory.

The stress intensity factor of the specimen under a distant uniform stress of such a specimen is given below

$$\mathbf{K}(\xi) = \sqrt{\pi\xi}\sigma_0 \qquad 7.8$$

The virtual stress intensity factor is

$$\mathbf{k}^{D}(\xi, x) = \frac{2}{\sqrt{\pi\xi}} \frac{\xi}{\sqrt{\xi^2 - x^2}} \qquad 7.9$$

and the stress intensity factor by the cohesive force in a unit length is

$$K_c(\xi,\delta,b)=\frac{2}{\sqrt{\pi\xi}}\frac{\xi\sigma_y}{\sqrt{\xi^2-b^2}} \qquad 7.10$$

Thus the crack opening displacement $\delta(x)$ can be found by Equation 7.6

$$\delta(x)=\frac{4\sigma_0}{E'}\sqrt{c^2-x^2}-\frac{8}{\pi E'}\int_x^c\frac{\xi}{\sqrt{\xi^2-x^2}}d\xi\int_a^\xi\frac{\sigma_y}{\sqrt{\xi^2-b^2}}db \qquad 7.11$$

and the boundary condition reads:

$$\sqrt{\pi c}\sigma_0=\int_a^c\frac{2}{\sqrt{\pi c}}\frac{c\sigma_y}{\sqrt{c^2-b^2}}db \qquad 7.12$$

or

$$\frac{\pi\sigma_0}{2}=\int_a^c\frac{\sigma_y}{\sqrt{c^2-b^2}}db \qquad 7.13$$

A formula similar to Equation 7.11 was proposed by Chen (1975) by using the Paris' formula for this particular problem. However, the boundary condition used in Chen's research was derived from a vanishing integral Kernel of the equation. For the problem with constant cohesion, his research led to the same result listed hereafter.

Equations 7.10 and 7.13 lead to the following solutions:

$$\delta(x)=\frac{4}{E'}\sqrt{c^2-b^2}\left(\sigma_0-\frac{2\sigma_y}{\pi}\cos^{-1}\frac{a}{c}\right)+$$
$$\frac{4\sigma_y}{\pi E'}\left[a\ln\left(\frac{\sqrt{c^2-a^2}+\sqrt{c^2-x^2}}{\sqrt{c^2-a^2}-\sqrt{c^2-x^2}}\right)-x\ln\left(\frac{x\sqrt{c^2-a^2}+a\sqrt{c^2-x^2}}{x\sqrt{c^2-a^2}-a\sqrt{c^2-x^2}}\right)\right] \qquad 7.14$$

and

$$\sigma_0 = \frac{2\sigma_y}{\pi}\cos^{-1}\frac{a}{c} \qquad 7.15$$

Equation 7.14 can be simplified by using Equation 7.15,

$$\delta(x) = \frac{4\sigma_y}{\pi E'}\left[a\ln\left(\frac{\sqrt{c^2-a^2}+\sqrt{c^2-x^2}}{\sqrt{c^2-a^2}-\sqrt{c^2-x^2}}\right) - x\ln\left(\frac{x\sqrt{c^2-a^2}+a\sqrt{c^2-x^2}}{x\sqrt{c^2-a^2}-a\sqrt{c^2-x^2}}\right)\right] \qquad 7.16$$

The above solutions are identical to those obtained by using the Westgård stress function (Dugdale, 1960). This solution has been widely used to verify different approximations for nonlinear fracture mechanics.

7.3 Non-Linear Fracture Characteristics of Softening Materials

Equation 7.16 shows the crack opening displacement in the process zone of materials with perfectly plastic cohesion, which is a good approximation for metal structures. However, as mentioned in the previous sections, concrete is a typical softening material with a descending cohesive force. Thus, this solution is not applicable to the problems of this kind, instead, a cohesion shall be used. This variable cohesion is known as a function of crack opening displacement for cementitious material. Thus, Equation 7.6 becomes a singular integral equation with a free boundary problem. Its boundary condition is given by Equation 7.7.

General solutions for integral equations of this kind are not available. Numerical analysis methods may

be applicable to these problems, however, they do not yield closed form solution. And also, even for a simple problem like centrally crack plate under distant tensile stress, numerical method may require many computer hours to perform a complete analysis.

A detailed solution for a variable cohesive force is illustrated in the following section using an iterative functional analysis method. This method is expected to have fast convergence within the range of the practical problems (Wang, et. al., 1994). The crack length of the specimen is 2a, and the applied stress is $\sigma_{\circ}$. A linear cohesion vs. crack opening displacement relation is assumed in the analysis (see Figure 7.3.1)

As illustrated above, the proposed generalized process zone is easy to apply if there exists a constant distributed cohesive force. In case of varying cohesion $\sigma[\delta]$, the governing equation for a centrally cracked plate is

$$\delta(x)=\frac{4\sigma_0}{E'}\sqrt{c^2-x^2}-\frac{8}{\pi E'}\int_x^c\frac{\xi}{\sqrt{\xi^2-x^2}}d\xi\int_a^{\xi}\frac{\sigma[\delta(b)]}{\sqrt{\xi^2-b^2}}db \qquad 7.17$$

and the boundary condition is

$$\frac{\pi\sigma_0}{2}=\int_a^c\frac{\sigma[\delta(b)]}{\sqrt{c^2-b^2}}db \qquad 7.18$$

Equations 7.17 and 7.18 are similar to Equations 7.11 and 7.13. However, the constant cohesion is replaced by a function of $\sigma[\delta(x)]$. Thus, Equation 7.17 becomes a Freaholm integral equation. The general

solution of the integral equations of this kind is not available.

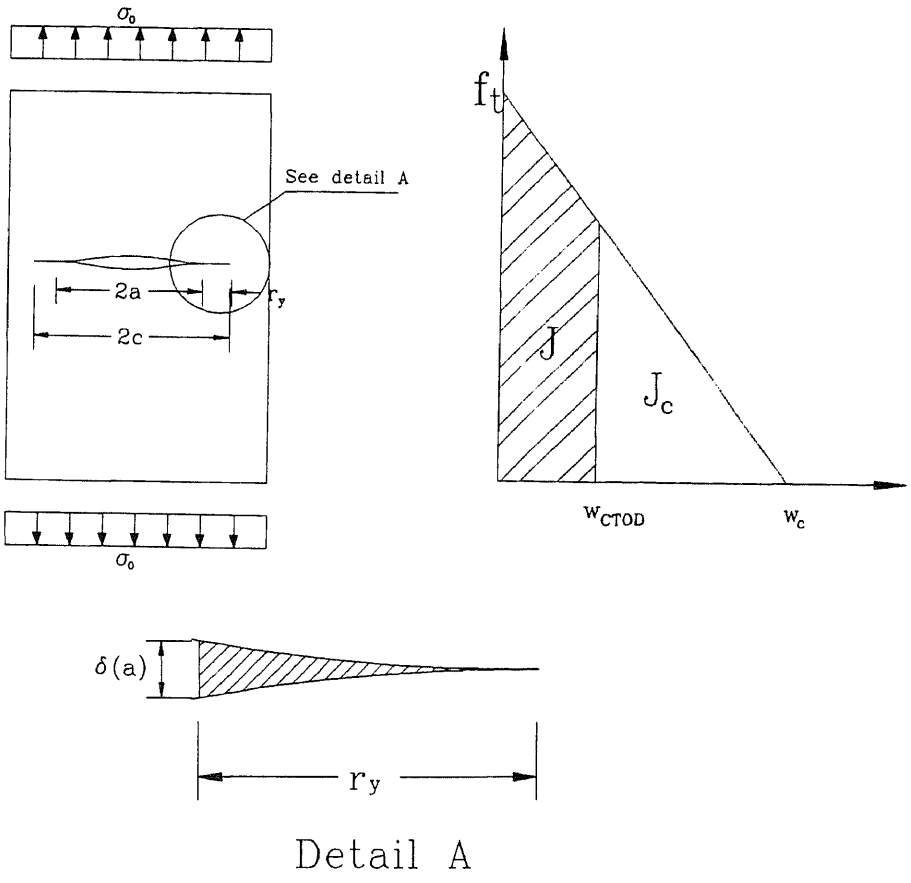

Figure 7.3.1 Centrally Cracked Wide Plate Subjected to Distant Tensile Stress.

An iterative functional analysis methods is used herewith to find an approximate closed form solution of this integral equation. Suppose an integral equation has a form of

$$Tf(x) = g(x) + \lambda \int_B K(x,s)Gf(s)dx \qquad 7.19$$

where f(x) is the desired solution, K and g are given functions, T and G are given operators.

By assuming an initial function f_1, the given operator Tf_1 leads to a new function of f_2, or in general,

$$f_{n+1} = Tf_n \tag{7.20}$$

This iteration method is expected to converge rapidly. The error caused in the interation may be estimated by the following equation

$$\|f_n - f\| \le a^n \tag{7.21}$$

where f is the true solution, f_n is the estimation after the n^{th} iteration, and a is a positive number much smaller than 1. $\|f_n - f\|$ denotes the maximum type norm on a suitable space of functions containing the functional sequence $\{f_n\}$ (Wang, et. al, 1994).

In the following analysis, a linearly descending cohesion vs. crack opening displacement relation is used to simulate the softening properties of the concrete material. The cohesion vs. crack opening displacement relation reads

$$\frac{\sigma}{f_t} = 1 - \frac{\delta}{w_c} \tag{7.22}$$

in which, σ is the cohesion in accordance with the crack opening displacement δ in the process zone, w_c is the critical crack opening displacement of the concrete, and f_t is the tensile stress of the concrete.

In the case that the crack opening displacement in the process zone is given by a function of the abscissa, or $\delta(b)$, the local cohesion can be uniquely determined using Equation 7.22. However, the crack opening displacement $\delta(b)$ is unknown and shall be determined by the governing equation.

In order to find the approximate closed form solution, the iterative method may be performed by assuming an initial deformed shape of the process zone. For simplicity, a linear function is assumed for the first iteration. Thus the cohesion in the process zone may be found as follows

$$\frac{\sigma}{f_t} = 1 - \frac{\delta(a)}{w_c}\frac{c-b}{c-a} \qquad 7.23$$

where, a is the initial crack length, b is the integral variable, and c is the sum of the initial crack length and the size of the process zone respectively. $\delta(a)$ is the crack tip opening displacement.

By doing so, the integral equation becomes an integration of a given function, which leads to

$$\delta(s) = \frac{4\sigma_\infty}{E} c\sqrt{1^2 - s^2} - \frac{8 f_t c}{\pi E}\int_s^1 \frac{\zeta d\zeta}{\sqrt{\zeta^2 - s^2}}\int_\alpha^\zeta \frac{1 - k^*(1-\tau)}{\sqrt{\zeta^2 - \tau^2}} d\tau \qquad 7.24$$

where, $\alpha=a/c$, $s=x/c$, $z=\xi/c$, $\tau=b/c$ and $k^*=\delta(a)/w_c(1-\alpha)$ are dimensionless parameters.

Equation 7.24 leads to the following formula for crack opening displacement:

$$\delta(s)=\sqrt{1-s^2}\left[(1-k^*)\left(\frac{\pi}{2}-\arcsin\alpha\right)+k^*\sqrt{1-\alpha^2}\right]+\alpha(1-k^*)\int_s^1\sqrt{\frac{\zeta^2-s^2}{\zeta^2-\alpha^2}}\frac{1}{\zeta}d\zeta$$
$$-\frac{k^*}{2}\sqrt{1-\alpha^2}\sqrt{1-s^2}+\frac{k^*}{2}\left\{\frac{s^2-\alpha^2}{2}\ln\left[\frac{\sqrt{1-s^2}-\sqrt{1-\alpha^2}}{s^2-\alpha^2}\right]\right\} \qquad 7.25$$

and the boundary condition yields

$$(1-k^*)\left(\frac{\pi}{2}-\arcsin\alpha\right)+k^*\sqrt{1-\alpha^2}=\frac{\pi}{2}\frac{\sigma_\infty}{f_t} \qquad 7.26$$

Thus, the solution may be simplified as follows

$$\delta(s)=\frac{\pi}{2}\frac{\sigma_\infty}{f_t}\sqrt{1-s^2}+\alpha(1-k^*)\int_s^1\sqrt{\frac{\zeta^2-s^2}{\zeta^2-\alpha^2}}\frac{1}{\zeta}d\zeta-\frac{k^*}{2}\sqrt{1-\alpha^2}\sqrt{1-s^2}$$
$$+\frac{k^*}{2}\left\{\frac{s^2-\alpha^2}{2}\ln\left[\frac{\sqrt{1-s^2}-\sqrt{1-\alpha^2}}{s^2-\alpha^2}\right]\right\} \qquad 7.27$$

The crack tip opening displacement may be found by letting $s\to\alpha$, and it reads

$$\frac{\delta(\alpha)}{w_c}=\frac{8f_t}{\pi E}\frac{c}{w_c}\left(\frac{\pi}{2}\frac{\sigma}{f_t}\sqrt{1-\alpha^2}-\frac{k^*}{2}(1-\alpha^2)\right)=\frac{\Psi}{\alpha}\left(\frac{\pi}{2}\frac{\sigma}{f_t}\sqrt{1-\alpha^2}-\frac{k^*}{2}(1-\alpha^2)\right) \qquad 7.28$$

where

$$\Psi=\frac{8f_t a}{w_c\pi E} \qquad 7.29$$

and

$$k^*=\frac{\ln(1/\alpha)}{\frac{1-\alpha}{\Psi}+\ln(1/\alpha)+\frac{1-\alpha^2}{\alpha}} \qquad 7.30$$

This functional iterative method is expected to have very fast convergence. With a properly chosen initial deformed shape, the first iteration may give a very good approximation of the true solution.

For instance, a concrete mixture has a tensile strength of 2.9 MPa, critical crack opening displacement of 120μm, modulus of elasticity of 29.6 GPa. For a centrally cracked plate, an unstable crack progress occurs when the crack tip opening displacement reaches the critical value of w_c under the applied stress σ_0. The maximum normalized tensile strength, σ_0/f_t of the specimens with different crack lengths predicted by the above equations are listed in Table 7.3.1. As the crack length increases from 0 to 10 meters, the predicted tensile strength of the specimen drops from $1.0f_t$ to $0.151f_t$.

Table 7.3.1 Size Effect Predicted by Generalized Process Zone Theory

a(m)	σ_o/ft	Ψ	ψ	a/c	K(N/m$^{2/3}$)	K_{eff}(N/m$^{2/3}$)	K/K_{IC}	K_{eff}/K_{IC}
0.001	0.995	0.002	0.005	0.003	1.618E+05	2.322E+06	0.071	1.023
0.025	0.929	0.052	0.128	0.074	7.547E+05	2.312E+06	0.333	1.019
0.050	0.881	0.104	0.257	0.137	1.012E+06	2.311E+06	0.446	1.019
0.100	0.809	0.208	0.513	0.241	1.315E+06	2.316E+06	0.580	1.021
0.200	0.711	0.416	1.026	0.391	1.635E+06	2.334E+06	0.721	1.029
0.300	0.644	0.624	1.540	0.494	1.813E+06	2.352E+06	0.799	1.037
0.400	0.593	0.832	2.053	0.568	1.928E+06	2.367E+06	0.850	1.043
0.500	0.553	1.040	2.566	0.623	2.008E+06	2.379E+06	0.885	1.048
0.600	0.520	1.247	3.077	0.666	2.069E+06	2.390E+06	0.912	1.053
0.700	0.492	1.455	3.590	0.700	2.115E+06	2.398E+06	0.932	1.057
0.800	0.468	1.663	4.103	0.728	2.152E+06	2.405E+06	0.948	1.060
0.900	0.448	1.871	4.617	0.751	2.183E+06	2.412E+06	0.962	1.063
1.000	0.430	2.079	5.130	0.771	2.208E+06	2.417E+06	0.973	1.065
5.000	0.211	10.395	25.649	0.945	2.422E+06	2.468E+06	1.067	1.088
10.000	0.151	20.791	51.300	0.972	2.453E+06	2.477E+06	1.081	1.092

By the classical process zone theory, the critical J integral value is $1/2w_cf_t$, or 174 N/m for the material chosen. In case of small scale yielding, the critical

stress intensity factor shall be equal to $\sqrt{J_c E}$, or 2.269×10^6 $Nm^{2/3}$.

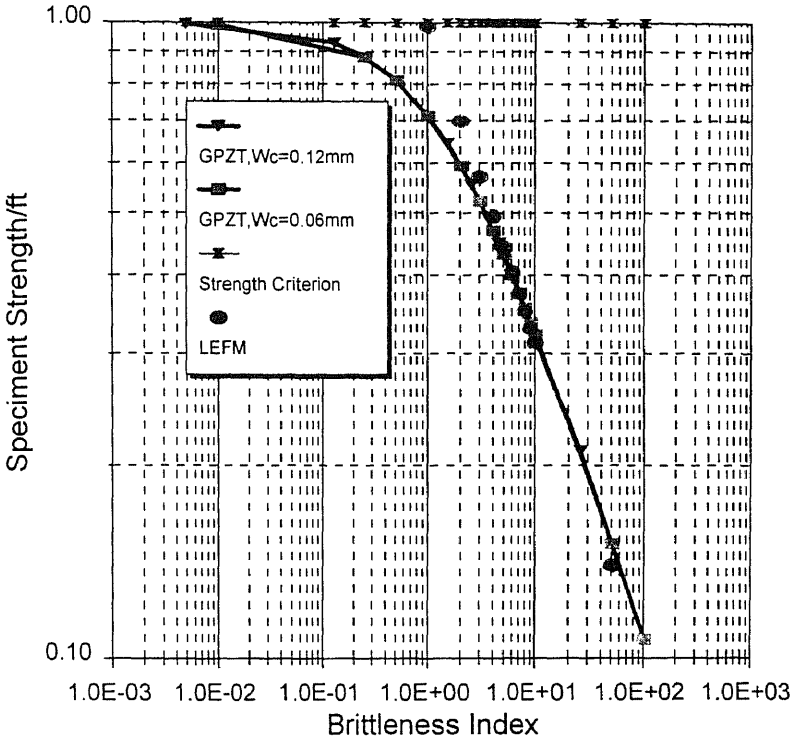

Figure 7.3.2 Size effect for Cenmentitious Material by the Generalized Process Zone Theoty

The result from the proposed generalized process zone theory is listed in Table 7.3.1. The numerical result plotted in a logarithm scale graph is shown in

Figure 7.3.2. The graph shows the famous 1:2 slope in the linear elastic range. It also shows the smooth transition from the strength failure criterion to the stress intensity factor criterion of the material. Therefore, Figure 7.3.2 clearly demonstrates the effectiveness and theoretical significance of the proposed generalized process zone theory. This result also reflects the fast convergence of the iterative method used in this analysis.

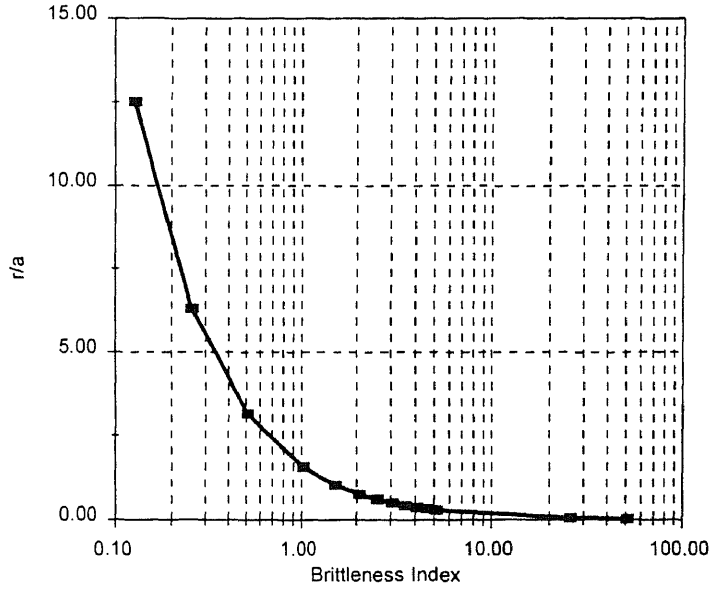

Figure 7.3.3 Normalized Maximum Process Zone Size at the Time of Failure (of normal scale)

Equation 7.29 may be written in the form of stress intensity factor and J_c as follows

$$\Psi = \frac{4\pi a f_t^2}{\frac{1}{2} w_c f_t \pi^2 E} = \frac{4K_{nf}^2}{\pi^2 J_c E} = 0.4\frac{K_{nf}^2}{J_c E} \qquad 7.31$$

Defineing a brittleness index ψ,

$$\psi = \frac{K_{nf}^2}{J_c E} \qquad 7.32$$

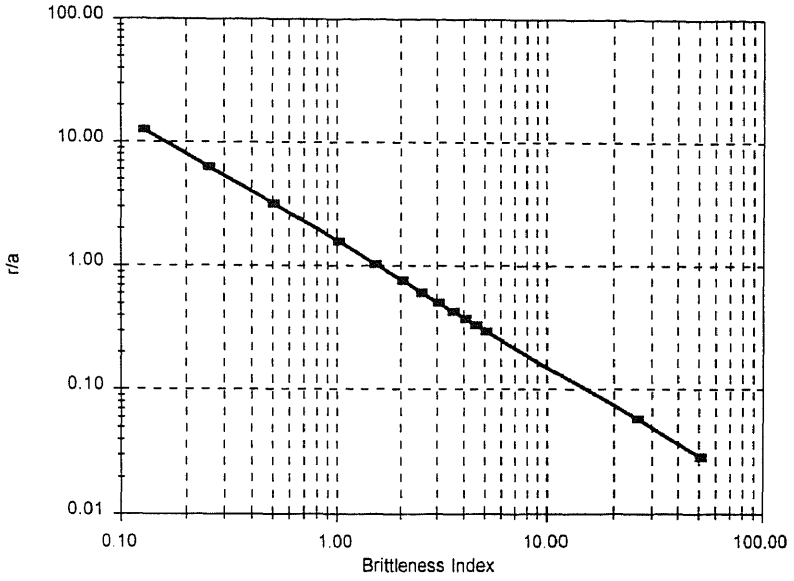

Figure 7.3.4 Normalized Maximum Process Zone Size at the Time of Failure (in logarithm scale)

Figure 7.3.2 shows the graph of the normalized strength of the specimen at the time of failure vs. brittleness index. It clearly shows the size effect in term of this brittleness index. The structures with smaller brittleness index have higher ductility, and they may be analyzed using the theory of plasticity. These structures shall have a brittleness index less than 0.05 as indicated in Figure 7.3.2.

The structures with a brittleness index greater than 5 may be classified as brittle structures. They may be analyzed by linear elastic fracture mechanics with higher accuracy. The failure criterion in this case is $K \leq K_{IC}$.

However, for the structures with a brittleness index less than 5 and greater than 0.05, neither the traditional theory of plasticity nor the linear fracture mechanics prevails. In such cases, the structures shall be analyzed by the nonlinear fracture mechanics.

Table 7.3.1 implies the above statements. In the case of a small brittleness index, the strength of structure may be overestimated if the linear fracture mechanics is used. However, the effective crack length method proposed by Irwin has led to a good approximation (Irwin, 1965). The effective stress intensity factor predicted by Irwin's method is close to the K_{IC} at the time of failure for the structures with any brittleness indexes. Thus, $K_{eff} \geq K_{IC}$ may be used as a unified failure criterion within acceptable accuracy.

The maximum sizes of process zones at the time of failure is listed in Table 7.3.1 and they are illustrated in Figures 7.3.3 and 7.3.4. Figure 7.3.4 shows a linear relationship between the maximum size of the process zone and the brittleness index in a logarithm scale.

The proposed brittleness index ψ has a straight forward physical meaning. It is the ratio between the applied fracture energy-release rate and the fracture energy toughness (J_c) at the time of failure of an ideal plastic-yielding-brittle-fracture material. Definition of an ideal plastic-yielding-brittle-fracture material is the material that will fail either due to plastic flow or unstable crack propagation. Thus, if ψ is less than 1, a structure will fail due to plastic flow, or brittle fracture, i.e.

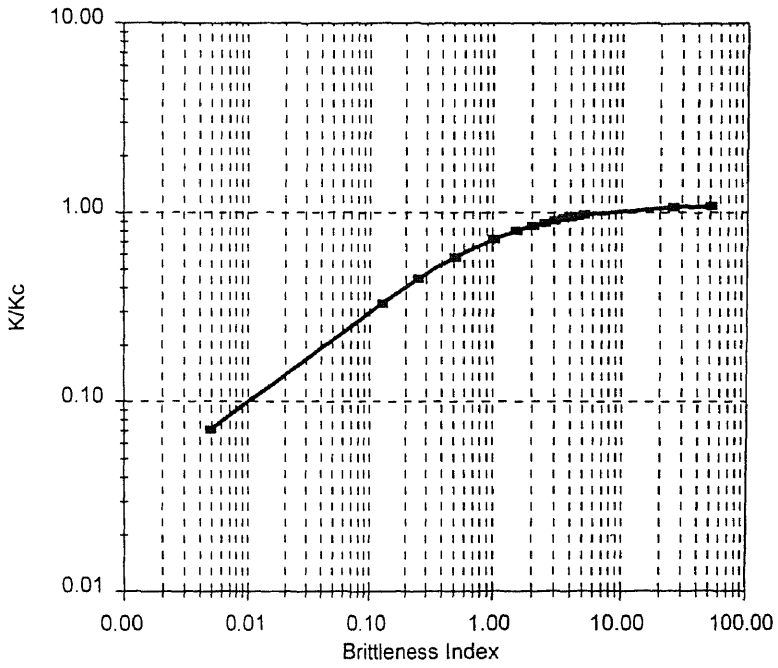

Figure 7.3.5 Maximum Stress Intensity Factor at the Time of Failure

$\sigma = \sigma_y$ for $\psi < 1$

$K = K_{IC}$ for $\psi \geq 1$

These two criteria are straight lines in a logarithm scaled coordinate system as shown in Figure 7.3.2. The line indicates the fracture criterion has a slope of 1:2 as expected. Engineering materials must converge to these lines in extreme cases when $\psi << 1$ and $\psi >> 1$. Theoretically, the theory of plasticity may only apply to the structures with $\psi = 0$. And also, the principle of linear fracture mechanics is true only when $\psi = \infty$. However, in engineering practice, the theory of plasticity and linear fracture mechanics may apply to the structures of certain ψ value with considerable accuracy.

Results from the analysis of another material with a smaller critical crack opening displacement of 0.06mm is also shown in Figure 7.3.2. The results from these two analyses are almost identical as illustrated in Figure 7.3.2, even though their critical crack tip opening displacements differ from one another by 100 percent. This fact may prove that the proposed brittleness index is objective and independent of the material and structural properties. Thus, it may be used to identify the ductility and failure mode of a structure.

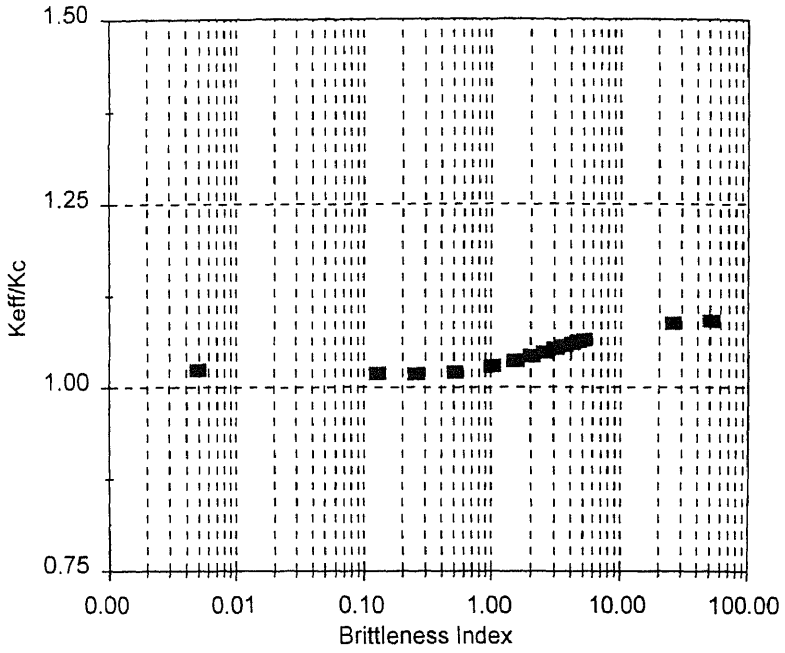

Figure 7.3.6 Maximum Effective Stress Intensity Factor at the Time of Failure

CHAPTER 8

DAMAGE ACCUMULATION THEORIES

8.1 Damage of Materials

The strength of materials will constantly decrease under unfavorable mechanical and environmental conditions. The constant decrease in strength and overall performance of materials is caused by micro-structural changes in the materials. Unfavorable microstructural changes may be defined as *damage* to materials. The constant decrease in the strength of materials shall be considered as a damage accumulation process in general. Several types of damage in the material, such as creep, ductile plastic flow, environmental and chemical damages, etc., have been examined closely in previous research.

A damage parameter ϕ can be defined with some material entities to characterize damages in the material. ϕ is defined to be equal to **0** for a virgin (undamaged), and **1** for a fully damaged material material. This damage parameter shall be considered as a vector in general (Vakulenko and Kachanov, 1971, and Murakami and Ohno, 1981). However, the damage parameter may be defined as a scalar in the simplest case. For instance, the damage parameter may be obtained by counting the ratio between the damaged (lost) area A and

the undamaged (initial) area A_0 for materials having isotropic damage (Kachanov, 1986), namely,

$$\phi = \frac{A}{A_0} \qquad 8.1$$

A more comprehensive consideration can be made from the point of view of thermodynamics. According to the theory of thermodynamics, changes to the material structures can be defined as reversible and irreversible processes. Irreversible processes may cause damage and finally lead to failure of the material.

The specific entropy s shall be considered to analyze an irreversible thermodynamic process. A straight forward definition of failure is to assume that the specific entropy of the material reaches the critical value s* (Chudnovsky, 1973). The critical entropy density s* is considered as a "stable" material property that depends mainly on the type of failure. Let ε_{kk} be the strain tensor, $T\text{-}T_0$ be the increase in temperature , then the *specific entropy* reads (Kovalenko, 1969):

$$s = (3\lambda + 2\mu)\alpha_T \varepsilon_{kk} + c_\varepsilon \ln \frac{T}{T_0} \qquad 8.2$$

where λ and μ are the Lamé constants, α_T is the coefficient of thermal expansion, and c_ε is the specific heat at constant strain. For an irreversible process,

$$ds>0 \qquad 8.3$$

Equation 8.3 clearly shows an accumulative damage process if specific entropy is used as a damage parameter. As the material is exposed to unfavorable conditions constantly, its specific entropy will keep increasing as a result of an irreversible process. The failure of material is defined as the specific entropy has reached its critical value.

The critical entropy concept shall be considered as a universal failure criterion. It is well-known that the degree of freedom of particles in the material shall increase as the specific entropy increases. On the contrary, the minimum entropy may be reached if the system is well "organized", or *crystallized* in terms of material science.

A "perfect" material has the minimum specific entropy, and shall have the best mechanical performance. Normal engineering materials are far away from being "perfect" and their specific entropies are much greater than the minimum value. Therefore, the strength of an engineering material is much less than its ideal strength. However, an "undamaged" engineering material shall have a very stable specific entropy. Here, the word "undamaged" does not mean that the material is perfect in a crystal structural sense, but represents an average condition of "natural" materials of its kind.

As shown in Equation 8.2, the specific entropy is a function of strain tensor and temperature. It may be

simplified as an explicit function of strain tensor only if the temperature is constant. The strain tensor is known as a strain energy and stress related quantity in a constant temperature process. The specific entropy can also be considered as a strain energy and stress tensor related parameter. The increase of specific entropy can be interpreted as a damage accumulation process as the plastic strain tensor increases. Thus the damage accumulation can be considered as an energy dissipation process in terms of engineering mechanics.

The critical specific entropy may be reached if the dissipated specific energy equals the toughness of the material under the corresponding loading condition. In most cases, if the strain tensor is in the elastic range, the strain energy may be released when unloading. Thus, an elastic loading process may be considered as a reversible thermodynamic process, and therefore it is a damage-free process. However, as plastic deformation occurs, the material undergoes an accumulative damage process as its entropy increases. The proposed damage accumulation theory is based on this concept.

8.2 Overall Behavior of Fatigue Crack Growth

Fatigue failure was considered as a result from the strength degradation of materials initially under cyclic loading. Tremendous amounts of research were conducted to study the strength degradation behavior of metals in England, France and Germany during the 1850's to 1900's (Timoshenko, 1953). These researches yielded the well-known concept of S-N (strength degradation vs. number of cycles) curve. The S-N curve has been well used in engineering practice for more than half century before the development of fracture mechanics.

In the mid 40's, industrial uses of high strength steels caused numerous fatal structural failures. Most of these structures were analyzed in accordance with design codes based on the concept of the S-N curve prior to that time. The reasons for these sudden structural failures were not well explained before the establishment and the application of fracture mechanics. New failure criteria such as fracture toughness, critical fracture energy-release rate and the critical J integral lead destructive mechanics to a new age. Fatigue crack propagation has been considered as the most important behavior in fatigue related failures since then.

Initiated in metal structural design, the fatigue crack propagation concept is now widely used in structural designs. From reinforced concrete to high performance composite material structures, this concept

gives engineers and researchers a much deeper understanding in mechanical behavior of engineering materials.

Paris (1962, 1963) proposed the first fatigue crack growth rate formula which was based on the concept of fracture mechanics. His empirical formula, well-known as Paris' power law, predicts that the fatigue crack propagation rate is proportional to the m^{th} power of ΔK, namely,

$$\frac{da}{dN} = c(\Delta K)^m \qquad 8.4$$

where ΔK is the amplitude of the applied stress intensity factor K, c and m are empirical parameters which are considered as material constants.

For a variety of metals m is roughly equal to 4. Therefore, this relationship is also called Paris' fourth power law occasionally. Since then the fatigue test data based on the stress intensity concept has been widely reported (Frost, et al, 1974), which provided the basic behavior of fatigue crack propagation under cyclic loading. A typical da/dN vs. ΔK curve can be divided into three different stages as illustrated in Figure 8.2.1.

Stage one concerns the early development of fatigue crack propagation. At this stage the fatigue crack propagation rate is mainly influenced by micro-structural features of the material including the grain

size and the crush strength of the grain. Researches on the properties of fatigue crack growth rate at this stage focus on the threshold stress intensity factor K_{th}. K_{th} is the minimum value required to initiate the fatigue crack propagation.

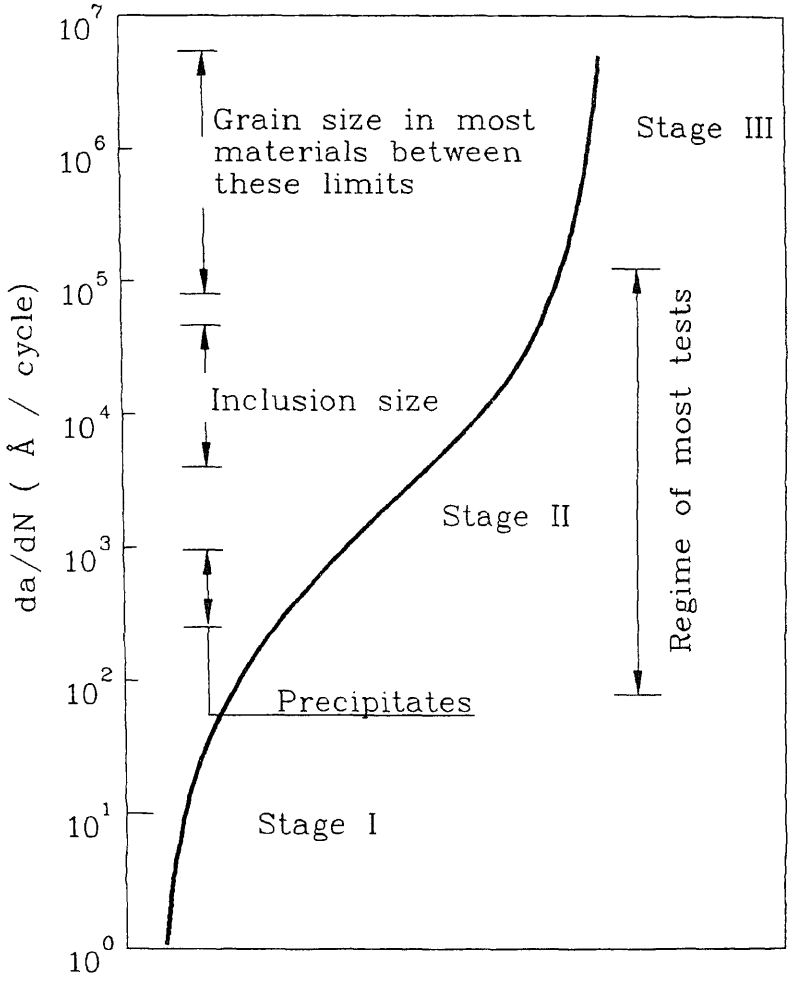

Figure 8.2.1 Overall behavior of fatigue crack propagation

At stage two the size of the plastic zone ahead of the crack tip is long enough when compared with the mean grain size, but is much smaller than the crack length. Hence, use of linear elastic fracture mechanics (LEFM) may be acceptable. As shown in Figure 8.2.1, the crack propagation is stable and the rate is the m^{th} power of the amplitude of the applied stress intensity factor in this stage. The formulation of fatigue crack propagation rate using linear fracture mechanics may lead to the famous Paris' power crack propagation law (Rice, 1966). Such a power function is a straight line in a logarithmic coordinates system.

At stage three, the high stress level causes a large plastic zone near the crack tip as compared with the specimen geometrically. Errors caused by the large scale yielding of the material can not be neglected. Hence, the influence of non-linear properties of material should also be taken into account. Therefore the nonlinear fracture mechanics must be applied to this stage. As shown in Figure 8.2.1, when the stress intensity factor reaches a certain value, say K_C, the fatigue crack propagation will become unstable and lead to a brittle fracture failure of the specimen. In some empirical studies the value of K_C was used as a fitting parameter to characterize the onset of instability (Miller & Gallagher, 1981). Here, K_C should not be confused with the fracture toughness K_{IC} of the

material. It is a material strength and specimen geometry related quantity.

8.3 A Brief Review On Energy Approach

The classical energy approach was found to be effective in the previous study of fatigue crack propagation rates. As mentioned in section 8.2, the accumulative damage in a system can be quantified by a damage parameter. The dissipated energy is directly related to the damage of the material. Thus, use of the energy method and the concept of linear fracture mechanics may reveal some of the fundamental properties of fatigue crack propagation.

Rice (1966,1967,1968) proposed an energy method to analyze the fatigue problem based on the fracture energy concept, which gave a similar power law as the one proposed by Paris (1962, 1963). His analysis was based on the plastic model of a discrete surface of tensile yielding or slip ahead of a crack tip.

Rice traced the deformation history of a particular point ahead of the crack tip in an elastic-perfectly plastic solid from the time when it was reached by the plastic zone to the time when it was reached by the crack tip. It is assumed that the separation occurs when the total absorbed hysteresis energy U in a newly created surface is equal to a postulated critical value U_c. Let $\Delta u_y(x,0)$ be the plastic displacement of the

discrete surface of tensile yielding per load reversal when the crack tip is at x=0 (see Figure 8.3.1), and the growth rate is assumed to be a constant while crossing a zone w of reversed deformation. Rice derived the following formula for fatigue crack growth rate:

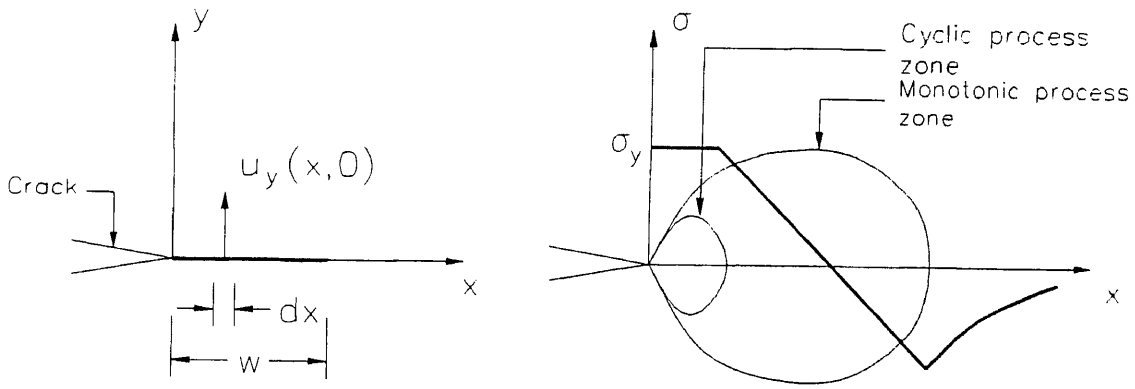

Figure 8.3.1 Discrete Surface Model and Cyclic Process Zone of an Elastic-Perfectly Plastic Solid

$$\frac{da}{dN} = \frac{4\sigma_y}{U_c}\int_0^w \Delta u_y(x,0)dx \qquad 8.5$$

This formula can be simplified as

$$\frac{da}{dN} = \frac{5\pi(1-v^2)}{96EU_c\sigma_y^2}\Delta k^4 \qquad 8.6$$

where σ_y is the yield stress , E is the elastic modulus, and ν is the Poisson ratio.

This energy approach yields the same result as Paris' empirical formula. Its logarithm da/dN vs. ΔK curve is a straight line. This analysis successfully leads to the power low of fatigue crack propagation rate. However, like all the other power laws, it faces a challenge. Tests show that different materials have different power values, rather than a constant of 4.

To solve this problem and obtain a reasonable modified version of the power law, Fine and Davidson (1983) suggested that the U_c's value, or the energy associated with a moving fatigue crack varies according to the stress-intensity factor K. A formula based on the theory of thermodynamics was proposed in their paper. By establishing an equation of energy balance, a simple formula was obtained in their study,

$$\frac{da}{dN} = A\frac{\Delta K^4}{\mu U_c \sigma_y^2} \qquad 8.7$$

where

A is a dimensionless constant; $U_c = 2\Gamma$, or twice the surface energy, and μ is the shear modulus.

To change the power, Fine and Davidson assumed that U_c is a function of ΔK, namely,

$U_c = B(\Delta K)^n$, with B = empirical constant, 8.8

which leads to

$$\frac{da}{dN} = A\frac{\Delta K^4}{\mu\sigma_y^2 B(\Delta K)^n} = M\Delta K^m \qquad 8.9$$

where $m = 4 - n$. If $n = 0$ and the value of U_c is a constant with respect to ΔK, then m becomes 4. In many cases m is not equal to 4 , or in other words, n is not always equal to 0.

This variable U_C concept leaves room to justify the difference between the analytical and experimental results. However, the empirical study on this thermodynamics based theory did not show a very encouraging result (Fine and Davidson, 1983, and Davidson and Lankford, 1983). Some significant errors were found between the test result and the analytical result. Despite this shortcoming, their variable U_C concept initiated a useful approach to the problem. Their variable specific fracture energy concept was later used by Nielsen (1990).

Nielsen assumed the cyclic fracture toughness as a function of the applied stress intensity factor K_I . The cyclic fracture toughness was said to be a constant $K_{IC\ Basic}$ if the applied one was less than a so called "transition" stress intensity factor $K_{I\ Trans}$. Beyond $K_{I\ Trans}$, the cyclic fracture toughness was defined as a power function of the applied stress intensity factor. His formula reads (Figure 8.3.2):

$$K_{IC} = \begin{cases} K_{ICBasic} & \text{if } K_I \le K_{ITrans} \\ M' K_I^{n'} & \text{if } K_I > K_{ITrans} \end{cases} \qquad 8.10$$

where M′ and n′ are material constants. For some high strength steels, M′≈1 and n′≈1 (Nielsen, 1990).

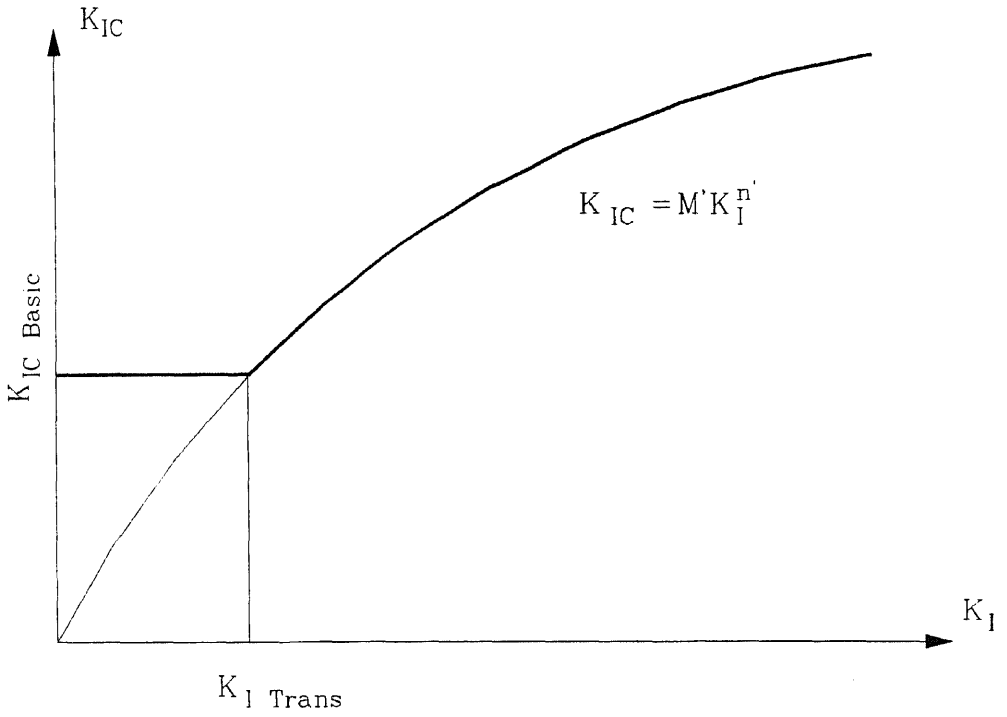

Figure 8.3.2 Cyclic Fracture Toughness as Function of Applied Stress Intensity Factor (Nielsen, 1990)

Although both Rice and Fine's theories had a problem in fitting some experimental results, they did point out an important phenomenon that the fatigue crack propagation is a damage accumulating process involving irreversible plastic deformation, or plastic energy dissipation during cyclic loading. However, their formulas are only applicable to the second stage, namely the Paris' power regime. To apply the energy method to

stage one and stage three, the following aspects shall be considered:

1. Elastic component of fracture energy

Both Rice and Fine used an energy related parameter to characterize the fracture properties of the material. Known as J_{IC}, this parameter can be interpreted as the energy required to create a newly cracked unit area. In small scale yielding condition, the J integral is approximately equal to K^2/E', where E' is an elastic constant which depends on the stress states. A straight forward consideration is to assume that 100 percent of the fracture energy is used to create a newly cracked area.

It is well known that the total energy supplied by the external loading will be stored in a system in the forms of elastic and plastic strain energies. The elastic energy will be released during unloading rather than be dissipated by the material to cause the damage. Only the plastic part will cause the accumulative damage to extend the crack in the ductile fracture case. Thus, the previous energy formula should be modified by substituting $K^2-K_e^2$ where K_e^2 indicates the elastic part of the supplied energy, and will be discussed later in details. If the supplied work done is less than the elastic threshold, the fatigue crack shall not extend. Hence, K_e^2 can be considered as the threshold stress intensity factor in the fatigue problem.

Indeed, most of the strain energy in the system at stage I is elastic, and is released during unloading. Only a small portion of the total strain energy is of plasticity and shall increase the accumulative damage in a system. Thus the observed fatigue crack propagation rate will be significantly smaller than the predicted value by Paris' power law at this stage (see Figure 8.2.1).

At stage III of fatigue crack propagation, a large portion of the specimen undergoes plasticity. A large yielding zone will be found as compared with the geometry of the specimen. Elastic fracture mechanics always underestimates the size of the process zone (Irwin, 1960) in this case. A smaller process zone implies less plastic fracture energy, and/or minor damage in the system. Consequently, the predicted fatigue crack growth rate by the elastic fracture mechanics will always come short of the measured ones in stage III.

To offset this inaccuracy, nonlinear elastic-plastic fracture mechanics shall be applied to estimate the size of the process zone. Though explicit solutions for some special specimens with constant cohesive force are now available (Dugadle, 1960, Tada, Paris and Irwin, 1973), it is difficult in general to obtain complete closed form solutions for nonlinear behavior of fracture process zones near fatigue crack tips. However, the

exact solutions show little disagreement with the results predicted by linear fracture mechanics for small scale yielding problems in metallic structures. Indeed some simple modifications, such as the effective crack length method proposed by Irwin (1960), have proved to be effective in considering the effects caused by plasticity in the material.

Because of the above two major aspects, linear fracture mechanics can not be applied to the stage I and III without proper modifications.

8.4 Damage Accumulation Theory

Damages can be characterized by using specific entropy of the materials in general as discussed in the first section of this chapter. However, this universal principle may prove difficult in solving practical engineering problems. An energy based damage accumulation theory may be more suitable for practical mechanical damage problems. However the specific entropy criterion may be ideal in solving chemical and other environmentally related damage problems.

The proposed damage accumulation theory is based upon the energy analysis method. Failure of most engineering materials is caused by the accumulation of the plastic deformation, or the plastic strain energy dissipated by the material. Since the plastic deformation is irreversible, the plastic strain energy

may be accumulated step by step in each cycle if the external load exceeds its elastic limit for an elastic-plastic material. Whenever the structure is unloaded, the elastic energy is released. In many cases, the elastic limit may change in each cycle of loading due to the accumulative damage in the material, but the envelope of stress-strain curve of the material under cyclic loading will be approximately identical to its monotonic stress-strain curve. This phenomenon is well-known and has been used to obtain the descending part of the stress-strain curve for a strain softening material such as concrete.

According to this phenomenon, it is reasonable to assume that only the accumulative plastic strain energy causes damage which finally leads to the failure of materials. The elastic part of strain energy will not cause any damage in the material and will be released after unloading. Therefore, it is postulated that the following two assumptions are the basic principles of the proposed damage accumulation theory:

1. The total plastic specific strain energy which can be dissipated by the material before it reaches its ultimate state shall be considered as a material constant. This constant is constitutional and can be determined experimentally.

2. The specific elastic strain energy which is stored in the material shall not cause any damage, and

it shall be released when the structure undergoes unloading.

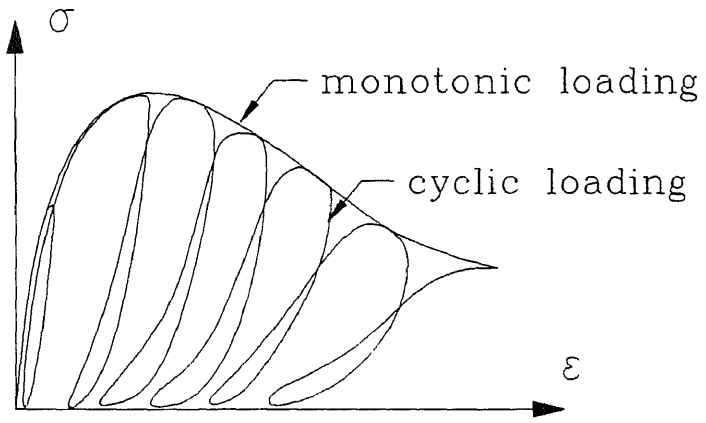

Figure 8.4.1 Cyclic Stress-Strain Relationship for Concrete

The above principles can be considered as the energy version of the entropy criteria mentioned previously. When irreversible damage develops, the specific entropy of the system increases. In other words, the increasing accumulative plastic strain causes the damage and finally leads to the failure of materials.

When the above principles are applied to the fatigue problem, it can be postulated in the following statement: after each cycle of loading, the process zone

near the crack tip will accumulate plastic energy. The elastic part of the energy will be released during unloading. When the accumulative plastic fracture energy dissipation rate in the process zone exceeds its ultimate value, say

$$J_c = \int_0^{\delta} \sigma d\delta \qquad 8.11$$

then the total damage has occurred and the crack will extend throughout the entire process zone. As a result, the crack will propagate by the length of the cyclic process zone r_p^{cyc}. More precisely, a damage index can be defined as follows:

$$\phi = \frac{J_p^{accu}}{J_c} \qquad 8.12$$

in which

J_c is the critical value of the J integral, and

J_p^{accu} is the accumulative plastic component of the J integral.

If the crack tip has a smooth notch and the external load is small enough so that the total J integral does not exceed its elastic limit, then there will be no plastic deformation at all. Consequently no damage shall be accumulated in the structure and the crack shall cease to extend in this case. In terms of the damage accumulation index, ϕ is equal to zero. The stress intensity factor corresponding to the above limit is therefore defined as the threshold value of fatigue

crack propagation. On the other hand, if the external load is so large that the accumulative damage exceeds its limit within only one step of loading, the process zone will become a newly developed crack area in this single loading cycle. This can be considered as monotonic loading case, and the corresponding damage index is equal to one.

This damage accumulation theory can be expressed more precisely in terms of thermoelasticity as mentioned in the previous sections of this chapter. From Equations 8.2 and 6.15, the J integral can be related to the entropy for a constant temperature process. Thus the entropy criteria in damage accumulation theory can be considered compatible with the critical J integral criterion in this case.

This J integral based damage accumulation theory will be used to predict the fatigue crack propagation formula in the next chapter.

CHAPTER 9

FATIGUE CRACK PROPAGATION OF METAL STRUCTURES

9.1 Effective Stress Intensity Factor and Size of Cyclic Plastic Zone

The J integral represents the fracture energy release rate for a nonlinear elastic specimen. It is equal to K^2/E' if the material is linear elastic (Rice, 1968). For an elastic-plastic specimen, this relation may still be true if the system undergoes a small-scale yielding. A more precise formulation is given below:

$$J = \frac{K_{eff}^2}{E'} \qquad 9.1$$

Here K_{eff} is the effective stress intensity factor (Irwin, 1960). The accuracy of this formula is also illustrated in section 3 of Chapter Eight for softening materials.

According to Irwin, the compliance of the specimen increases due to the yielding of the material ahead of the crack tip. This effect can be taken into account by using an enlarged effective crack length instead of the real one. In other words, the stress intensity value will increase due to the yielding of the material. By considering the force balance in the specimen, an enlarging factor η can be found to account for the effects caused by the small scale yielding in the

specimen. This enlarging factor η depends on the stress intensity factor, the yield strength and the geometry of the specimen (Irwin, 1960) simultaneously:

$$\eta = \frac{1}{\sqrt{1 - \frac{K^2}{K_{nf}^2}}} \qquad 9.2$$

and

$$K_{nf} = \eta K \qquad 9.3$$

$$K_{nf} = K \frac{\sigma_y}{\sigma} \qquad 9.4$$

where σ_y = local yield strength, and σ = the applied stress.

K_{nf} can be considered as a nominal ultimate stress intensity factor. It is the stress intensity factor of the specimen under an ultimate load as predicted by the theory of plasticity. In the case of the wide plate problem, K_{nf} is equal to $\sigma_y\sqrt{\pi a}$.

Under cyclic loading, the size of the reversal plastic zone or the highly strained cyclical process zone is *not* a function of K, but ΔK according to Rice (1966). Indeed, the formulation proposed in section 4 may be used to calculate the size of a cyclic process zone. The corresponding stress and strength used in the computation shall be equal to $\Delta\sigma$ and $2\sigma_y$, respectively, for an isotropic hardening material (Figure 9.1.1).

Some experimental results (Loye and Bathias, 1983), show that in a plane strain condition, r_p^c or the size of

a highly strained cyclical process zone can be expressed as:

$$r_p^c = 0.007\frac{\Delta K^2}{\sigma_y^2} \qquad 9.5$$

or in general,

$$r_p^c = \alpha\frac{\Delta K^2}{\sigma_y^2} \qquad 9.6$$

where α is a constant which can be determined according to the material and the loading condition.

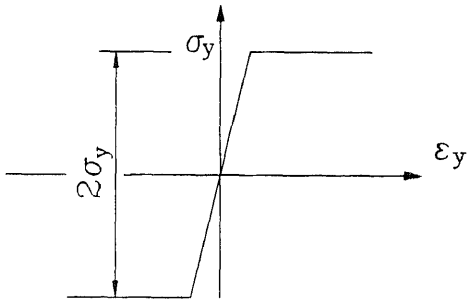

Figure 9.1.1 Isotropic and Perfectly Elastic-Plastic Material

The above analysis provides a good approximation in many cases. Exact solutions are difficult to obtain for most practical engineering problems though a generalized process zone theory proposed in Chapter seven provides possibilities for finding closed form solutions. The exact solutions are not that important in engineering practice, however, exact solutions may serve as references to examine the above approximate solutions used in daily engineering practice.

9.2 Near-Threshold Properties of Fatigue Crack Propagation

For a long crack problem, the crack tip dimension is compatible to the mean grain size of the material after the fatigue-crack initiation. Grains near a sharp crack tip will be crashed under external loading. The crashed grains form a blunt crack tip and reduce the stress intensity factor as well as the stress near the crack tip. If the stress ahead of the blunt crack tip is lower than the average local yield strength $\bar{\sigma}_y$, the fatigue crack will stop propagating. According to Rice(1965), the maximum stress ahead of the blunt crack tip can be approximately written as:

$$\sigma_{max} = \frac{K}{\sqrt{\frac{8}{15}\bar{\rho}}} \qquad 9.7$$

where K is the applied stress intensity factor, and $\bar{\rho}$ is the mean grain size of the materials.

When σ_{max} is less than the yield strength, the whole specimen undergoes elastic deformation. The structure shall not accumulate any plastic strain, and no material can be further damaged except the grain near the crack tip. This stress intensity factor is said to be the *threshold value*, namely K_{th}. A true stress-strain curve may be found as

$$\sigma = C\varepsilon^n \qquad 9.8$$

where

σ = true stress,

ε = true strain,

n = strain hardening coefficient, and

C = material constant, defined as the true stress at a true strain of 1.0.

The stress at the onset of the localized necking may be used as a characterized strength to find the threshold stress intensity factor. Thus

$$\bar{\sigma}_y = Cn^n \tag{9.9}$$

Here the true plastic strain at neck instability is equal to n (Hertzberg, 1976). Thus, the threshold stress intensity factor for such materials can be found as:

$$K_{th} = Cn^n\sqrt{\frac{8}{15}\bar{\rho}} \tag{9.10}$$

In the case of perfectly plastic materials, the hardening coefficient is zero, and above equation reads:

$$K_{th} = \bar{\sigma}_y\sqrt{\frac{8}{15}\bar{\rho}} = C\sqrt{\frac{8}{15}\bar{\rho}} \tag{9.11}$$

Empirical formulas similar to Equations 9.10 and 9.11 have been found for different groups of materials (Stark and William, 1984) (Barson and McNicol, 1974). Their formulas have the form of

$$\frac{K_{th}}{\sigma_y\sqrt{\bar{\rho}}} = c_{th} \tag{9.12}$$

where c_{th} may be referred as a material constant. The similarity of Equations 9.11 and 9.12 may show the validity of the above analysis for some metals.

As mentioned in Chapter Seven, the elastic component of the J integral can be estimated by:

$$J_e = \frac{K_{th}^2}{E'} \qquad 9.13$$

The error of this estimation is expected to be minor in most cases since the majority of the system undergoes elastic deformation if the applied stress intensity factor is close to the threshold value.

9.3 Fatigue Crack Growth Rate

Consider a cracked specimen with a given value of the J integral under the external load. As mentioned previously, the total J value can be divided into two components, namely J_e and J_p, or the elastic and plastic components of the J integral. When the fracture energy dissipation rate of the system changes from J_{min} to J_{max}, the increment of $J_{max} - J_{min}$ indicates the accumulative damage of the system if J_{min} exceeds its elastic limits as mentioned previously. This is because the elastic parts in both J_{max} and J_{min} are assumed to be of $J_{min} > J_{th}$ according to the proposed damage theory. If J_{min} is less than its elastic l: total difference in plastic components of J_m will be equal to J^p_{max}, or $J_{max} - J_e$. In general,

accumulative plastic fracture energy dissipation rate within the process zone in one cycle of loading will be:

$$J_p^{accu} = \begin{cases} J_{max} - J_{min}, & \text{when} \quad J_{min} \geq \dfrac{K_{th}^2}{E} \\ J_{max} - J_{th}, & \text{when} \quad J_{min} < \dfrac{K_{th}^2}{E} \end{cases} \qquad 9.14$$

Recall Equation 3.12, the damage index in each cycle of loading ϕ can be found as

$$\phi = \begin{cases} \dfrac{J_{max} - J_{min}}{J_c}, & \text{when } J_{min} \geq \dfrac{K_{th}^2}{E'} \\ \dfrac{J_{max} - \dfrac{K_{th}^2}{E'}}{J_c}, & \text{when } J_{min} M < \dfrac{K_{th}^2}{E'} \end{cases} \qquad 9.15$$

The total number N of cycles needed to accumulate a complete damage in the process zone will be equal to $1/\phi$. From a physical point of view, N is the total number of cycles needed to break the cyclic process zone into two free surfaces, or newly created crack. By applying the effective stress intensity factor, the J integral can be expressed as K_{eff}^2 / E'. Consequently, N can be expressed in terms of the effective stress intensity factor as follows:

$$N = \frac{1}{\phi} = \frac{J_c}{J_p^{accu}} \begin{cases} \dfrac{K_{IC}^2}{K_{eff}^{max\,2} - K_{eff}^{min\,2}}, & \text{when} \quad K_{eff}^{min} \geq K_{th} \\ \dfrac{K_{IC}^2}{K_{eff}^{max\,2} - K_{th}^2}, & \text{when} \quad K_{eff}^{min} < K_{th} \end{cases} \qquad 9.16$$

where

$$K_{eff}^{max} = \eta K_{max}$$

$$K_{eff}^{min} = \eta K_{min}$$

K_{IC} = the critical stress intensity value

$\bar{\sigma}_y$ = the average local yield strength.

As mentioned above, the whole process zone will be broken into a newly developed crack area if the accumulative damage exceeds the material limit. Therefore, the average crack propagation rate with respect to the number of cycles can be found as r_p^c/N. If expressed in a derivative form, the fatigue propagation rate reads

$$\frac{da}{dN} = r_p^c \begin{cases} \dfrac{K_{eff}^{max\,2} - K_{eff}^{min\,2}}{K_{IC}^2}, & \text{when } K_{eff}^{min} \geq K_{th} \\ \dfrac{K_{eff}^{max\,2} - K_{th}^2}{K_{IC}^2}, & \text{when } K_{eff}^{min} \geq K_{th} \end{cases} \qquad 9.17$$

If R is used to denote the ratio of the stress intensity factor, or

$$R = \frac{K_{min}}{K_{max}} \qquad 9.18$$

r_p^c in Equation 9.17 can be expressed as a function of the maximum stress intensity value and the stress ratio since $r_p^c = \alpha \dfrac{\Delta K^2}{\bar{\sigma}_y^{\,2}}$ (see Equation 9.6):

$$\frac{da}{dN} = \alpha \frac{K_{max}^4}{\bar{\sigma}_y^{\,2}} \left[\frac{1}{1-\varsigma^2} - \frac{1}{1-(R\varsigma)^2} - \right] \cdot \left[\frac{1}{\sqrt{1-\varsigma^2}} - \frac{1}{\sqrt{1-(R\varsigma)^2}} - \right] \qquad 9.19$$

where

$$\varsigma^2 = \frac{K_{max}^2}{2K_{nf}^2} \qquad 9.20$$

Equation 9.17 presents the average crack growth rate of a long crack under cyclic loading. In practice, a crack will not propagate in a constant speed. Some experiments show that the crack growth rate will have a big jump after several cycles of loading. However, Equation 9.17 shows an average rate over a certain number of loading cycles.

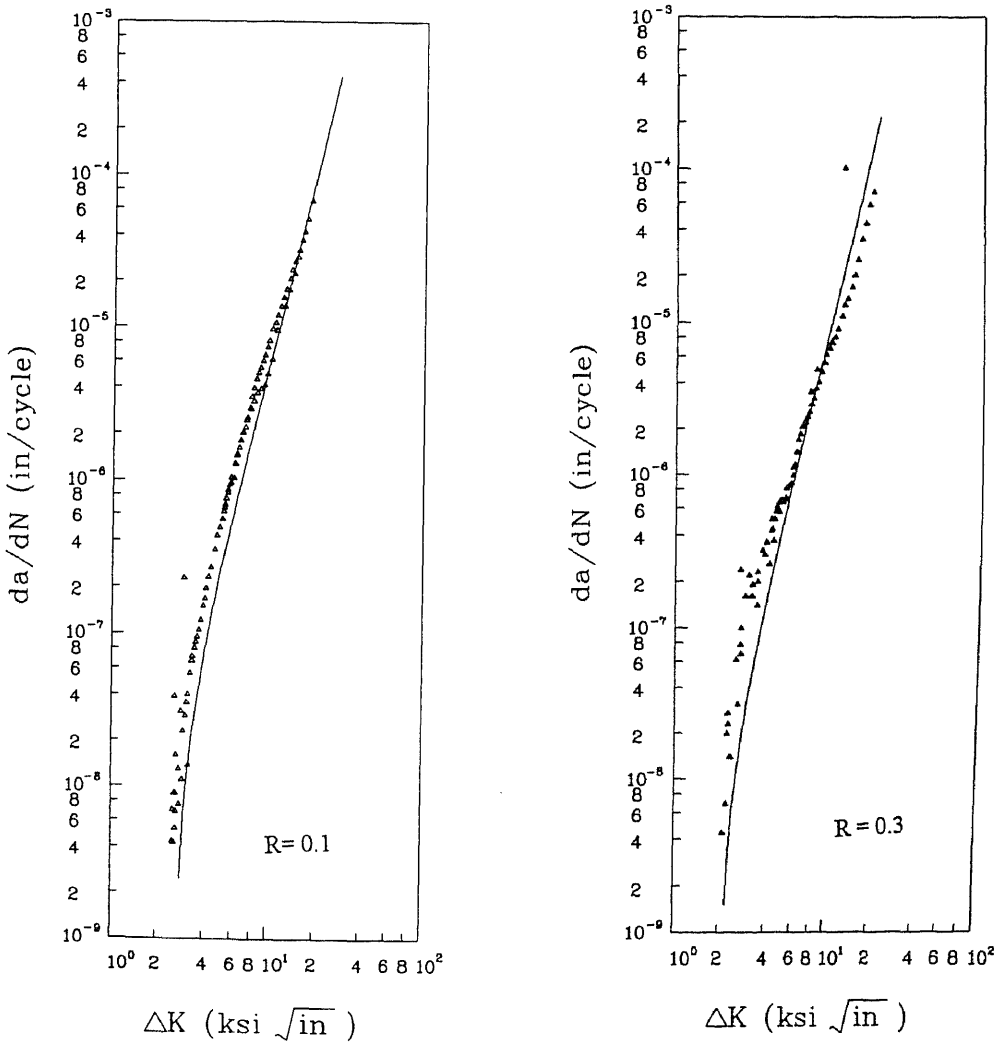

Figure 9.3.1 Comparison Between Predicted and Measured Data (R=0.1 and 0.3)

The exact solution for a classical Dugdale problem is available (Chapter 7). Therefore, a more precise formulation can be obtained for this ideal case.

Based on strip yield model, Dugdale(1960) found the exact solution for a wide plate with a central crack:

$$\delta = \frac{8\bar{\sigma}_y a}{\pi E} \ln \frac{c}{a} \qquad 9.21$$

$$\frac{c}{a} = \sec\left(\frac{\pi a}{2\bar{\sigma}_y}\right) \qquad 9.22$$

where δ is the crack tip opening displacement, a is half of the crack length, σ is the applied stress, $\bar{\sigma}_y$ is the average local yield strength, and c is half of the total length of crack and process zone ahead of the crack tip.

According to the solution, the size of the process zone under monotonic loading can be written as

$$r_y = c - a = a\left(\sec\frac{\pi\sigma}{2\bar{\sigma}_y} - 1\right) \qquad 9.23$$

Since the material is assumed to be perfectly elastic-plastic, the J integral can be found as the product of the crack opening displacement δ and the yield strength $\bar{\sigma}_y$

$$J = \bar{\sigma}_y \delta \qquad 9.24$$

so that

$$J = \frac{8\bar{\sigma}_y^2 a}{\pi E'} \ln\left(\sec\frac{\pi\sigma}{2\bar{\sigma}_y}\right) \qquad 9.25$$

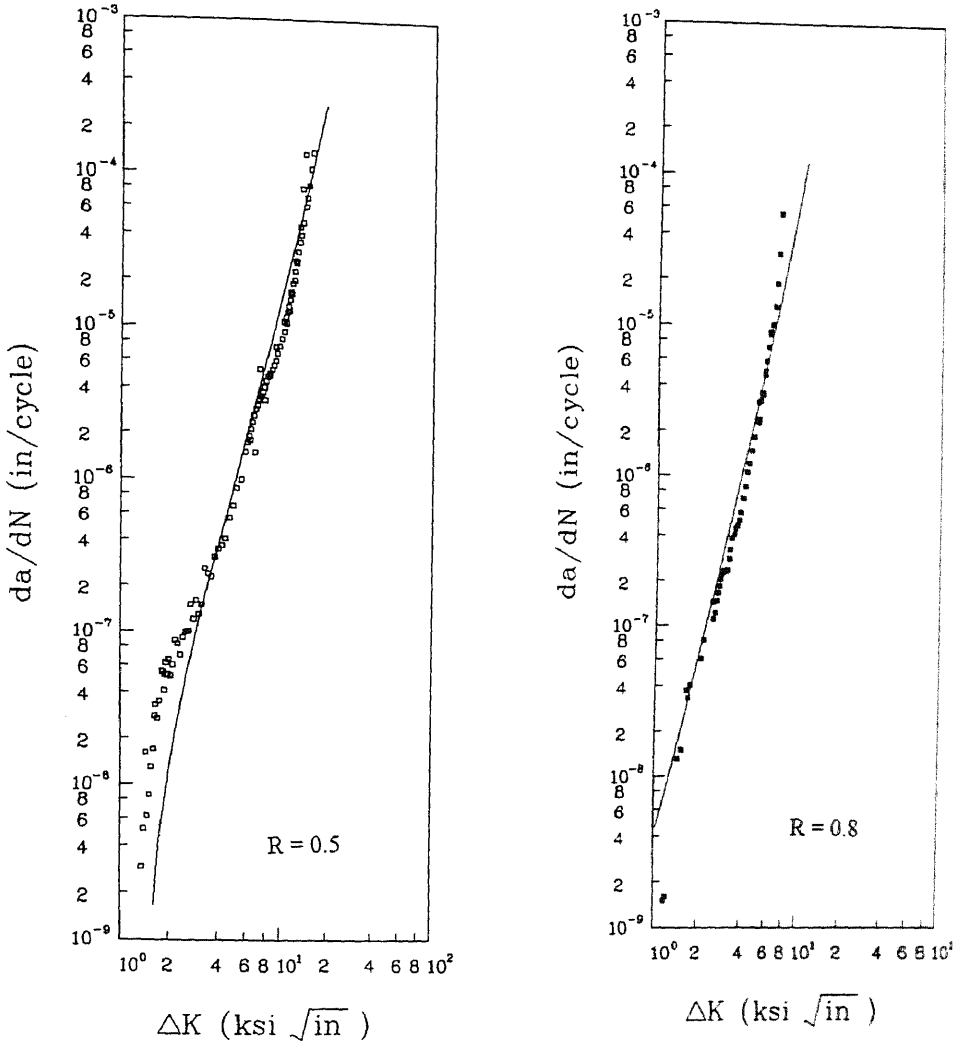

Figure 9.3.2 Comparison Between Predicted and Measured Data (R=0.5 and 0.8)

Thus the effective stress intensity factor is,

$$K_{eff} = \sqrt{\frac{8a}{\pi}\ln\left(\sec\frac{\pi\sigma}{2\bar{\sigma}_y}\right)}\,\bar{\sigma}_y \qquad 9.26$$

No significant difference is found by comparing Equation 9.26 with Equation 9.2 provided that the applied stress $\sigma_0 < 0.6\sigma_y$. However, Equation 9.2 is derived based on the concept of force balance near the crack tip, therefore, it may be also applicable to cases beyond the wide plate with central crack problem.

The fatigue crack growth rate formulas for this typical Dugdale's problem can be found as

$$\frac{da}{dN} = \frac{8\bar{\sigma}_Y^2}{\pi K_c^2}\left(\sec\frac{\pi\Delta\sigma}{2\bar{\sigma}_y} - 1\right)\ln\frac{\cos\frac{\pi\sigma_{min}}{2\bar{\sigma}_y}}{\cos\frac{\pi\sigma_{max}}{2\bar{\sigma}_y}} \quad \text{when } K_{eff}^{min} > K_{th} \quad \text{and} \qquad 9.27$$

$$\frac{da}{dN} = \frac{8\bar{\sigma}_Y^2 a^2}{\pi K_c^2}\left(\sec\frac{\pi\Delta\sigma}{2\bar{\sigma}_y} - 1\right)\left(\ln\sec\frac{\pi\sigma_{min}}{2\bar{\sigma}_y} - K_{th}^2\right) \quad \text{when } K_{eff}^{min} < K_{th} \qquad 9.28$$

where $\sigma_y' = \bar{2}\bar{\sigma}_y$ and are $\Delta\sigma = \sigma_{max} - \sigma_{min}$ in case of cyclic loading (Rice, 1968).

9.4 Experimental Verification of Proposed Formulas

To verify the proposed formulas, the test results published in the ASTM STP 738 (Miller and Gallagher,1981) are analyzed. The reported test data vary from 10^{-9} in/cycle to 10^{-3} in/cycle, which cover almost all the three regions of fatigue crack growth.

The specimens are made of Al2219-T851, its 0.2% yield strength is 370 MPa and K_c is $38.5\text{Mpa}\sqrt{\text{m}}$, and the mean grain size varies from 30 to 60μm. The R values are

0.1, 0.3, 0.5, and 0.8, respectively. Figures 9.3.1 to 9.3.2 show that the predicted fatigue crack propagation rate agree well with the measured data in a wide range both in terms of amplitude of stress intensity factor and R value. In these figures, the separated symbols indicate the measured test data, and the continuous curve represents the predicted fatigue crack growth rate by Equation 9.17.

9.5 Discussions of Proposed Formulas

9.5.1 On Fatigue Crack Propagation Rate

1. Crack Size Effect

The proposed formulas show that the crack length has a significant influence on the da/dN value. This is because the size of process zone is strongly affected by the geometry of the specimen. The analysis in this research shows that in small scale yielding condition, the predicted da/dN curve shall convert to the Paris power law.

Figure 9.5.1 illustrates influence of the crack length on the da/dN curve. This influence becomes more significant in stage III. Therefore, the Paris power law is applicable to a long crack with small scale yielding and shall not be excessively used. Figure 9.5.1 also indicates that the variation of power value in the Paris' formula may be caused by the different yield strength and the geometry of the specimens.

2. R ratio

As in Equation 9.16, the fatigue crack propagation is found to be a function of the amplitude of the J integral and stress intensity factor. Thus the R ratio shall not have a significant influence on a da/dN vs. ΔJ curves as the da/dN vs. ΔK curves. This finding has been proved by several experimental results.

3. The average local yield strength

The mean value of maximum local yield strength in a statistical sense is a function of mean grain size and process zone size. The smaller the mean grain size is, the larger is the ratio of the local strength and uniaxial tensile strength. For example, when the mean grain size is 30μm, the ratio is about 1.6. This ratio becomes 1.8 to 1.9 if the mean grain size is 14μm. It is important to find a practical method to predict this ratio. Before the method can be established, the mean value of maximum local yield strength of the material must be identified by using the experimental K_{th} value and Equation 9.11. This has been proved acceptable for some metals such as Ti-6Al-4V, Ti-8.6Al, and Al2219-T851 etc.

The average local yield strength is also a function of process zone size. The normal yield strength shall be used if the specimen undergoes large scale yielding. This phenomenon was explained by Weibull's risk-of-rupture criterion (Weibull, 1939), and a solution was

illustrated by Carpinteri (1984). At stage three, the process zone size is of the order of specimen, therefore, the mean grain strength can not be used at this stage. The local strength will decrease as the size of process zone increases. The yield strength of the material shall be considered as the minimum and the mean grain strength as the maximum. A continuous function may be used to predict the mean local strength which varies from the minimum yield strength to the maximum mean grain strength of the material. The Weibull's risk theory is used herein to find the function as mentioned previously.

It is well known in Weibull's theory that the material is assumed to be homogenous. However in a large scale yielding condition, the non-homogeneous properties of the material may be smoothed out in a large process zone. As an extreme case, if the size of process zone is of the order of the specimen size, the material in the process zone can definitely be considered as homogeneous.

4. Properties near the threshold

As mentioned previously, da/dN is determined by $K_{max}-K_{th}$ instead of $K_{max}-K_{min}$, if K_{min} is less than K_{th}. Since K_{th} is considered as a material constant, the K_{max} value will dominate the near threshold properties of the fatigue crack propagation, or the da/dN value at stage I. This phenomenon was first mentioned by Cooke and Beever

(1974) when they discussed their experimental results on fatigue crack propagation in Pearlite Steels. Since most of the structures are designed to work in a near threshold loading environment, this finding is very important and may simplify analyses in the design of such structures.

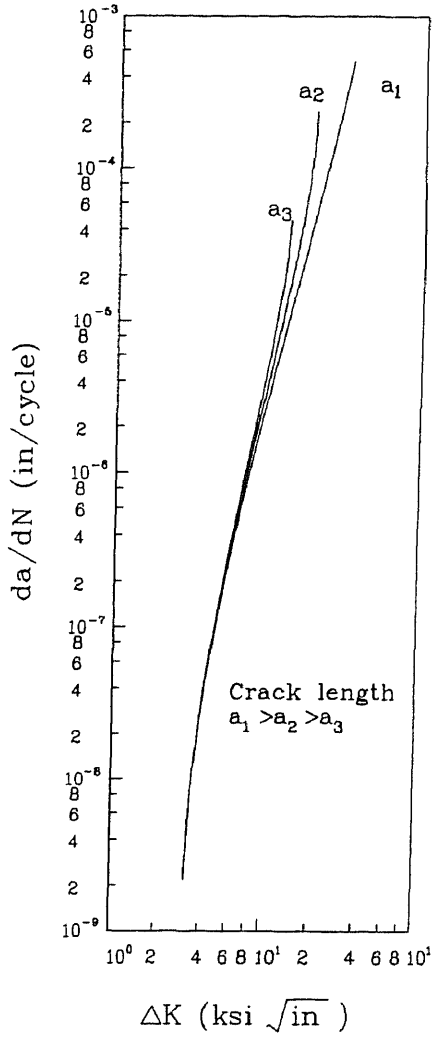

Figure 9.5.1 Predicted Fatigue Crack Growth Rate of Specimens with Different Crack Length

5. Smooth transition from stage II to stage III

A transition from stage II to stage III is achieved by using the concept of effective stress intensity factor. As mentioned previously if the process zone size is large enough, the material within the process zone may be considered as homogeneous, and its strength will decrease as the size of process zone increases. On the other hand, the effective stress intensity factor predicted by Irwin's theory also increases as the size of the process zone increases. These two major effects together allow a smooth transition of the da/dN curve from stage II to stage III as long as the size of process zone continues to increase.

Chapter 10

Fatigue Crack Propagation of Concrete Structures

Fatigue crack propagation in concrete structures is a new research area. Very few researches have been conducted in this area. Theoretical analyses are not available in general. Most of the empirical studies on fatigue problems in concrete structures are limited to repeating the S-N curve measurements.

In the following sections of this chapter, several critical problems of fatigue crack propagation are studied by the proposed generalized process zone theory and damage accumulation theory.

Section 10.1 studies the fatigue crack initiation condition and the threshold value for concrete materials. Also, the estimated size of process zone under cyclic loading is presented to determine the fatigue crack propagation rate for concrete structures.

In section 10.2, the damage accumulation theory proposed in Chapter 8 and the fatigue propagation rate formula are used again for the concrete structures. Test results by others are used here to verify the validity of the proposed formula.

10.1 Fatigue Crack Initiation in Concrete Structures

Concrete materials are similar to metals in a micro-structural sense. The micro-structures of metal are made of randomly distributed grains. They are grouped together with cohesive force between grains. These grains usually have much higher strength than the global strength of the metal because of imperfections in metals.

Fatigue cracks are usually initiated between grains. As the crack grows, the stress intensity factor begins building up. As the stress ahead of the crack tip reaches a level higher enough to crush the grains near the crack tip, a blunt crack tip is formed. As a result, the stress intensity factor drops down. In case that the applied load is not strong enough to raise the stress intensity factor to a certain level to crush the new grains near the crack tip, the crack will stop propagating. This stress intensity factor needed for fatigue crack propagation is called the threshold value. Section two of Chapter nine presents an analytical method to determine this threshold stress intensity for metals.

For concrete structures, this threshold value has similar physical characteristics, and may be derived using the same analytical approach. However, minor changes are made to reflect the properties of concrete materials.

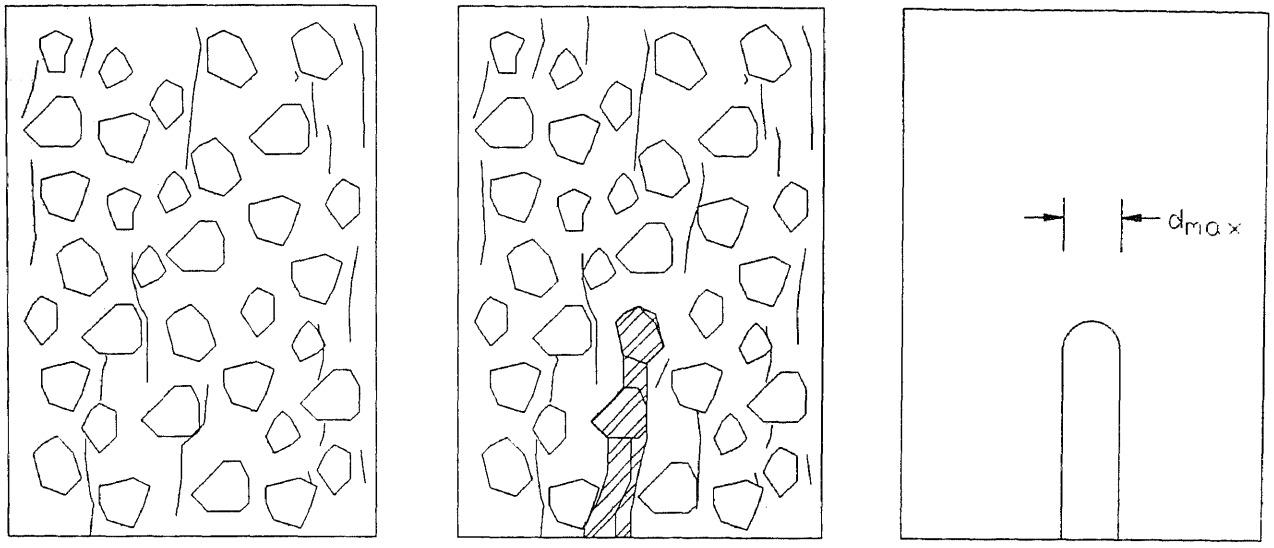

Figure 10.1.1 Fatigue Crack Initiation in Concrete Structures

Firstly, concrete is made of fine and coarse aggregates. The bond stress provided by the cement acts as the cohesive force in metals. Micro-cracks caused by shrinkage provide an initial imperfection in material. As the external loads increases, micro-cracks in the structure will start propagating around the coarse aggregates (see Figure 10.1.1). The propagation of the micro-cracks isolates the coarse aggregates and forms a blunt crack tip to prevent further propagation of the fatigue crack. In case the applied loads are not strong

enough to raise the stress level ahead of the blunt crack tip to cause further damage to the material, this crack will NOT propagate further. Thus, the damage in the material is local rather than global in the structural system. In this case, based on the damage accumulation theory proposed in the previous chapter, the structure undergoes elasticity rather than plasticity. Thus, the damage index of the structure is 0.

According to the notch analysis presented in Chapter nine, the fatigue crack propagation threshold value of concrete may be given by,

$$K_{th} = f_t \sqrt{\frac{8}{15}\bar{d}} \qquad 10.1$$

where f_t is the tensile strength of concrete, and $\bar{d}$ is the size of the coarse aggregate.

In contrast to metals, the bond strength in concrete material is provided by the cohesive strength of cement. As a strain softening and low tensile strength material, tensile failure of concrete material is mainly due to stress concentration and localization. Thus, the global tensile strength of concrete material can be considered the same as the local strength. Different sizes of aggregates may affect the tensile strength as well. However, since the sizes of the cement molecules are much smaller than those of coarse aggregates used in concrete mixture, the effect of

aggregate size on local tensile strength shall be ignored.

Similar to metals, the maximum elastic component of the J integral may be estimated in accordance with the threshold stress intensity value,

$$J_e = \frac{K_{th}^2}{E'} \qquad 10.2$$

The error of this estimation is negligible since the majority of the material undergoes elasticity.

This threshold stress intensity factor formula will be used to predict the fatigue crack propagation of concrete material in the next section of this chapter.

10.2 Cyclic Process Zone in Concrete

Concrete materials have different strengths under different loading conditions. Its compressive strength is about 8-12 times of its tensile strength. In the case that the material undergoes isotropic hardening, the effective strength of concrete used to predict the size of cyclic process zone is

$$f_{eff} = f_t + f_c' \qquad 10.3$$

which is shown in Figure 10.2.1.

The above equation is based on the fact that the material ahead of a crack tip is highly stressed. Any loads corresponding to stress intensity factor higher than the threshold value may create a yielding (process)

zone. A process zone may occur under this loading, and the plastic deformation may remain at the crack tip.

As the system undergoes unloading, a reversed plastic (process) zone is formed in accordance with an equivalent strength of f_t+f_c'. Therefore, to predict the size of a reversed process zone, the effective strength of f_t+f_c' must be used instead of f_t as in monotonic loading case.

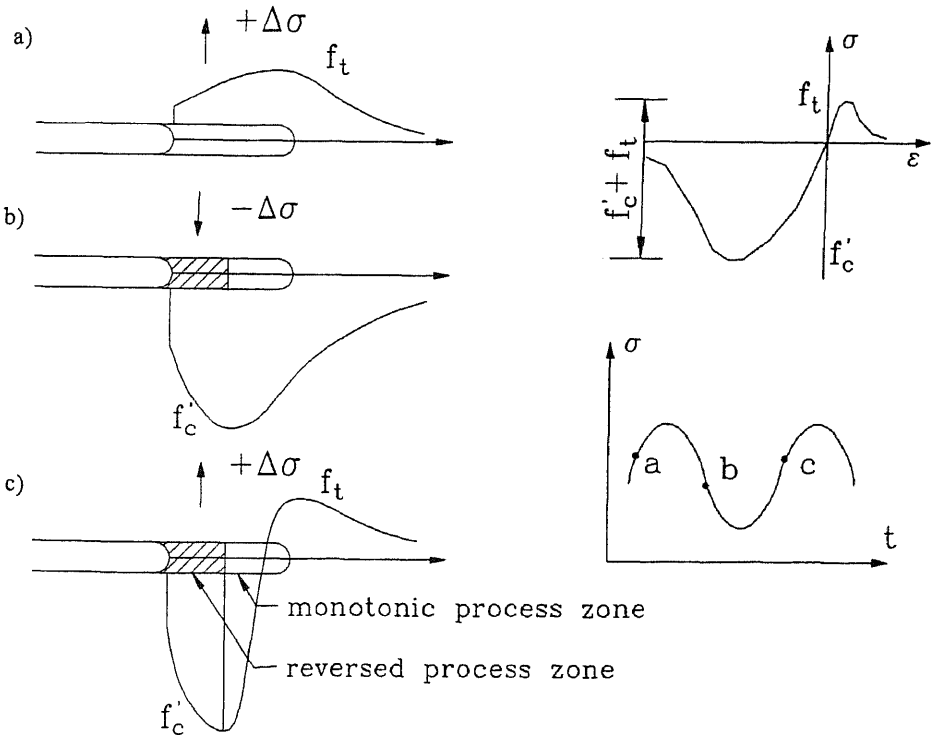

Figure 10.2.1 Cyclic Process Zone in Cementitious Materials

This concept was proposed by Rice to predict the size of the cyclic process zone for metals (1966). The effective strength used in his research was $2\sigma_y$, or twice the yield strength, which is based on the fact that metals have similar tensile and compressive strengths.

The size of the process zone in metallic structures can be predicted in terms of the amplitude of the applied stress intensity factor as illustrated in Chapter nine. The same concept is used here for concrete structures. As mentioned previously, the size of the process zone under monotonic loading of softening material is larger than that in a perfectly-plastic material. Under cyclic loading, however, the loading level is comparatively low, and the reversed plastic flow literally increases the strength of the material as explained by the isotropic hardening rule. Thus, the size of the cyclic process zone in concrete structure may be predicted by a method similiar to that used in metallic structure.

For a concrete specimen with a tensile strength of f_t and a compressive strength of f_c' subjected to cyclic loading, the size of cyclic process zone is

$$r_{cyc} = \frac{(1-2\nu)^2}{2\pi}\frac{\Delta K^2}{(f_t + f_c')^2} \qquad 10.4$$

where, ΔK is the amplitude of the applied stress intensity factor, ν is the Poisson ratio of concrete.

The term $(1-2\nu)^2$ is used in plane strain condition (Irwin, 1960).

For most fatigue crack propagation tests, the stress condition near the crack tip is of plane strain rather than plane stress when the process zone is very small in comparison to the width of the specimen. However, as the load increases, the size of process zone becomes compatible with the width. Therefore, the stress profile is converted from plane strain condition to plane stress condition. In a plane stress condition, the cyclic process zone may be estimated as follows

$$r_{cyc} = \frac{1}{2\pi}\frac{\Delta K^2}{(f_t + f_c')^2} \qquad 10.5$$

Thus a longer process zone can be formed in the material which leads to a faster rate in fatigue crack propagation. Also, a higher stress intensity factor level can cause a larger scale yielding, which increases the value of the J integral. The larger value of the J integral usually causes a rapid damage accumulation. These two aspects may be responsible for a rapid increase of fatigue crack propagation at a higher stress level.

The so-called size effect is always a major concern in the fracture related research of concrete structures. In Chapter 7, the size effect predicted by generalized process zone theory clearly illustrates that the critical value of J integral J_C is a constant. However,

the critical stress intensity factor is a size dependent parameter for softening materials. Strictly speaking, the stress intensity factor shall not be used to predict the fracture characteristics of structures made of softening materials. Nevertheless, the effective stress intensity factor by Irwin's effective crack length may provide a good approximation as indicated in Chapter Six. This effective stress intensity factor concept is utilized again to predict the fatigue crack propagation rate using the proposed damage accumulation theory.

10.3 Fatigue crack propagation rate of concrete structures

Chapter Nine presents the application of the proposed damage accumulation theory to predict the fatigue crack propagation in metallic structures. The formulation of fatigue crack propagation rate consists of two parts, namely, the size of the cyclic process zone and the damage index.

The size of the cyclic process zone in concrete structures r_{cyc} is given in Equation 10.5. Just as for as metals, the damage index may be defined as the ratio between the accumulative plastic component of the J integral per cycle and the critical value. Thus, the fatigue crack propagation may be predicted as

$$\frac{da}{dN} = r_{cyc} \cdot \phi \qquad 10.6$$

or

$$\frac{da}{dN} = \frac{(1-2\nu)^2}{2\pi} \frac{\Delta K^2}{(f_t + f_c')^2} \frac{(K_{max}^{eff\ 2} - K_{min}^{eff\ 2})}{K_{IC}^2} \qquad 10.7$$

Where

$K_{IC} = \sqrt{J_c E'}$ is the critical stress intensity factor for structures with very high brittleness index. K_{eff}^{max} and K_{eff}^{min} are the maximum and minimum stress effective intensity factors under cyclic loading according to Irwin's effective crack length theory. As indicated in chapter Six, the results from the generalized process zone theory show that the potential size effect caused by nonlinear property of the material may be eliminated by using the effective strength intensity factor.

A few empirical studies have been conducted on the fatigue crack propagation. The experimental data on fatigue crack propagation rate of concrete structures are very limited in comparison to metals. Thus, the proposed formula can only be compared with limited experimental results presently available in the literature.

A complete test result was given by Baluch et. al (1987). The mix design of the concrete used in their investigation is (by Weight):Coarse Aggregate 45%, Fine Aggregate 27%, Type I Cement 18.5%, and Water 9.5%. Grading of coarse and fine aggregates is given in Table 10.3.1.

The compressive strength obtained from testing of 76.6mm by 152.4mm cylinders was 27.6 MPa.

The specimen used in the test was a three point bending specimen with dimensions of 51mm x 152mm x 1360 mm (Width x depth x Span). A saw cut notch of 3mm width with various notch depth was used in the test to initiate the fatigue crack.

Fatigue crack length was computed by comparing the compliance between the fatigue specimen and the pre-tested calibration specimen in order to avoid the measurement of fatigue crack length physically.

Table 10.3.1 Gradation of Coarse and fine aggregates

Coarse Aggregate		Fine Aggregate	
Sieve Size (mm)	% Passing	Sieve Size (mm)	% Passing
12.7	100	2.36	100
9.5	60	1.18	63
4.75	40	0.6	45
2.36	20	0.3	20
1.18	5		

The tensile strength of the concrete used in theoretical analysis may be predicted by (Hilsdorf and Bramshuber, 1991)

$$f_t = 0.3 f_c'^{2/3} (\text{MPa}) \qquad 10.8$$

The modulus of elasticity of concrete, E_c may be estimated as

$$E_c = 10^4 \cdot f_c'^{1/3} \qquad 10.9$$

and the critical energy release rate is

$$G_f = a_d (f_c' + 8)^{0.7} (\text{Nm/m}^2) \qquad 10.10$$

Here G_f is the critical energy release rate for structures with infinite brittleness index, or, K_c^2/E, as illustrated in Chapter seven. a_d is an empirical parameter determined by the maximum coarse aggregate size given in Table 10.3.2. (Hilsdorf and Bramshuber, 1991)

Table 10.3.2 Coefficient a_d vs. maximum aggregate size d

d[mm]	a_d
8	4
16	6
32	10

For the concrete mixture used in their investigation, the tensile strength is about 2.7MPa, and the K_C is equal to $1.4MNm^{-3/2}$.

The test result shows that the fatigue crack propagation rate of concrete varies from 1.5×10^{-7} m/cycle to 6×10^{-6} m/cycle in accordance with different amplitude of the stress intensity factor. Here, R is defined as the maximum to minimum ratio of stress intensity factor, which is 0.3 in this test.

The comparison of measured and predicted fatigue crack propagation rate by the proposed formula is shown in Figure 10.3.1. The comparison shows that the results predicted by the proposed formula have an acceptable accuracy in prediction the fatigue crack propagation of concrete structures. However, the experimental work on

this subject is limited in scope. Thus further experimental studies are needed to fully understand the behavior of fatigue crack propagation in concrete structures.

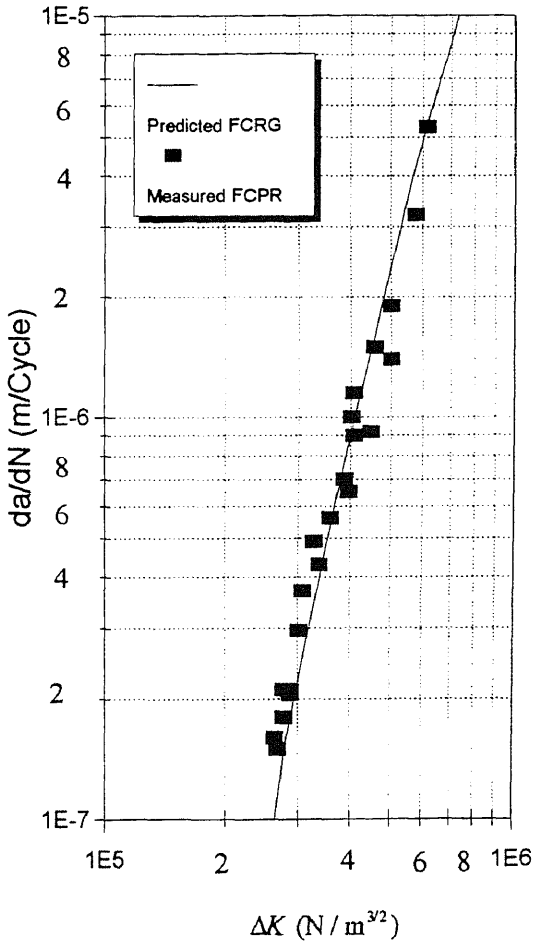

Figure 10.3.1 Comparison of Measured and Predicted Fatigue Crack Propagation Rates in Concrete Structures

Chapter 11

CONCLUSIONS

11.1 Conclusion of Part I

The limit analysis method is used here to predict the ultimate shear strength of different reinforced concrete structural elements. These elements are: push-off shear transfer, brackets, deep beams. In addition to these two-dimensional problems, the torsional strength of rectangular reinforced concrete beams is analyzed with the same method. Solutions by the limit analysis method are verified with over two hundred specimens tested around the world. This research yields the following conclusions:

1. The limit analysis method may be used to predict the shear strength of plain and/or reinforced concrete structures;
2. A generalized energy dissipation rate is proposed in this research. It may be used in the limit analysis of reinforced concrete structures subjected to multi-stress conditions.
3. The results from the limit analysis method show clear physical meanings. The simplicity and the accuracy of the proposed method show that it may be used as an

alternative approach to the shear strength design of reinforced concrete structures.

4. The ductility of the plain and/or reinforced concrete structures is studied using two coefficients, ν_c and ν_s, respectively. Known as the material and structural coefficients of plasticity, respectively, ν_c and ν_s are defined in accordance with the material and structural properties.
5. A unified definition of over-reinforcing is proposed in terms of reinforcement index. The maximum reinforcement ration $\Psi_{max}=m/2$, where $m=f_t'/f_t$.

11.2 Conclusion of Part II

The research in Part II of this dissertation can be concluded in the following:

1. The J integral contains both elastic and plastic components for nonlinear elastic-plastic materials. The elastic component of the J integral is found to be a function of the stress intensity factor under combined external loads and the cohesion in the process zone.
2. The fracture damage level in engineering materials may be defined by the accumulative plastic component of the J integral. Fracture occurs when the accumulative plastic component of the J integral reaches its critical value.

3. A generalized process zone theory is proposed for nonlinear engineering materials. This generalized process zone theory is able to predict the nonlinear fracture properties for both hardening and softening materials.
4. A brittleness index is proposed here based on the results from the generalized process zone theory. This brittleness index may be used as objective indicator to determine the ductility of the structures. The classical theory of plasticity may be used for structures with a brittleness index less than 0.05. In the case that this index is larger than 5, they linear elastic fracture mechanics becomes applicable. However, for structures with a brittleness index between 0.05 and 5, it must be analyzed using nonlinear fracture mechanics.
5. Fatigue crack propagation rates of metallic and concrete structures are found to be a function of the size of the cyclic process zone and the damage index. A damage index is defined as the ratio between the accumulative plastic component of the J integral and the critical J value.
6. Near threshold fatigue crack propagation properties are found to be independent of the amplitude of the stress intensity factor. These properties are mainly determined by the maximum stress intensity factor.

7. The effective stress intensity may be used to predict the nonlinear fracture properties with acceptable accuracy.

APPENDIX A

Table 5.2.1 Comparison of Measured and Predicted Shear Strength of Push-off Shear Transfer Specimens

t	Sources	f_c' (MPa)	f_t (MPa)	ν	ρ	fy (MPa)	ψ	$\tau_{cal.}$	τ_{test}	$\frac{\tau_{test}}{\tau_{cal}}$
D0-1	Wang	15.73	2.047	0.649	0.000	N/A	0.000	2.587	2.606	1.007
D0-2	Wang	15.73	2.047	0.649	0.000	N/A	0.000	2.587	2.736	1.057
D0-3	Wang	15.73	2.047	0.649	0.000	N/A	0.000	2.587	2.753	1.064
D0-4	Wang	15.73	2.047	0.649	0.000	N/A	0.000	2.587	2.794	1.080
D4-1	Wang	15.73	2.047	0.660	0.002	484.1	0.738	3.467	3.121	0.900
D4-2	Wang	15.73	2.047	0.660	0.002	485.1	0.733	3.461	3.232	0.934
D4-3	Wang	15.73	2.047	0.660	0.002	486.1	0.749	3.478	3.251	0.935
D6-1	Wang	15.73	2.047	0.662	0.006	220.6	0.903	3.640	3.427	0.941
D6-2	Wang	15.73	2.047	0.662	0.006	220.6	0.909	3.646	3.146	0.863
D6-3	Wang	16.78	2.137	0.657	0.006	220.6	0.893	3.817	3.787	0.992
D8-1	Wang	15.73	2.047	0.668	0.008	231.7	1.312	4.049	3.381	0.835
D8-2	Wang	15.73	2.047	0.668	0.008	231.7	1.312	4.049	3.772	0.931
D8-3	Wang	15.73	2.047	0.668	0.008	231.7	1.284	4.022	3.755	0.934
1.1A	Hsu	27.38	2.962	0.607	0.004	349.5	0.855	5.390	5.171	0.959
1.1B	Hsu	30.31	3.170	0.593	0.004	331.0	0.775	5.631	5.819	1.033
1.2A	Hsu	26.82	2.921	0.620	0.009	349.6	1.698	6.521	6.895	1.057
1.2B	Hsu	29.20	3.092	0.607	0.009	331.0	1.552	6.691	6.757	1.010
1.3A	Hsu	26.82	2.921	0.631	0.013	349.6	2.504	7.535	7.585	1.007
1.3B	Hsu	27.38	2.962	0.626	0.013	331.0	2.356	7.471	7.378	0.988
1.4A	Hsu	31.50	3.252	0.615	0.018	349.6	3.078	9.016	9.377	1.040
1.4B	Hsu	26.93	2.929	0.639	0.018	331.0	3.114	8.138	8.826	1.085
1.5A	Hsu	31.50	3.252	0.624	0.022	349.6	3.791	9.591	9.653	1.006
1.5B	Hsu	28.39	3.034	0.640	0.022	331.0	3.752	8.900	9.543	1.072
1.6A	Hsu	30.11	3.156	0.641	0.026	349.6	4.559	9.648	9.874	1.023
1.6B	Hsu	28.29	3.027	0.650	0.026	331.0	4.443	9.179	9.791	1.067
6.1	Hsu	27.66	2.982	0.605	0.004	331.0	0.807	5.351	5.516	1.031
6.2	Hsu	27.45	2.967	0.645	0.022	331.0	3.803	8.715	8.155	0.936
M1	Hsu	28.82	3.065	0.600	0.004	351.0	0.839	5.552	5.240	0.944
M2	Hsu	26.89	2.926	0.621	0.009	369.4	1.788	6.653	6.757	1.016
M3	Hsu	27.55	2.974	0.628	0.013	360.7	2.549	7.725	7.653	0.991
M4	Hsu	38.61	3.725	0.576	0.018	351.0	2.877	9.966	7.860	0.789
M5	Hsu	27.13	2.944	0.652	0.022	363.4	4.165	8.804	8.826	1.003
M6	Hsu	28.41	3.036	0.655	0.026	363.7	4.832	9.298	9.101	0.979
									$\bar{x}$	0.985
									STD	0.070

Table 5.2.2 Section and Material Properties for Bracket Specimens

No	Specimen	b	h_o	c/h_o	l_c/h_o	f'_c (kg/cm^2)	f'_c (psi)	f_y (kg/cm^2)	f_y (psi)	ρ_{st} (%)	ρ'_{st} (%)
1	a12	0.200	0.565	0.530	0.265	323.2	4607	4300	61.3	1.74	0.00
2	A12	0.200	0.565	0.530	0.265	323.2	4607	4150	59.2	1.74	0.00
3	A22	0.200	0.565	0.530	0.265	323.2	4607	4210	60.0	1.74	0.00
4	A21	0.200	0.565	0.530	0.265	323.2	4607	4220	60.2	1.74	0.00
5	A31	0.200	0.565	0.530	0.265	296.0	4219	4135	58.9	1.74	0.00
6	A32	0.200	0.565	0.530	0.265	216.0	3079	4165	59.4	1.74	0.00
7	B11	0.200	0.565	0.266	0.265	313.6	4470	4270	60.9	1.74	0.00
8	B12	0.200	0.565	0.266	0.265	297.6	4242	7270	103.6	1.74	0.00
9	B21	0.200	0.565	0.795	0.265	313.6	4470	4240	60.4	1.74	0.00
10	B22	0.200	0.565	0.795	0.265	297.6	4242	4220	60.2	1.74	0.00
11	C11	0.200	0.565	0.530	0.177	323.2	4607	4165	59.4	1.74	0.00
12	C12	0.200	0.565	0.530	0.177	297.6	4242	4310	61.4	1.74	0.00
13	C21	0.200	0.565	0.530	0.354	296.0	4219	4340	61.9	1.74	0.00
14	C22	0.200	0.565	0.500	0.354	296.0	4219	4295	61.2	1.74	0.00
15	C31	0.200	0.565	0.530	0.422	296.0	4219	4005	57.1	1.74	0.00
16	C32	0.200	0.565	0.530	0.422	296.0	4219	4040	57.6	1.74	0.00
17	D11	0.200	0.365	0.411	0.411	323.2	4607	4350	62.0	2.70	0.00
18	D12	0.200	0.365	0.411	0.411	313.6	4470	4460	63.6	2.70	0.00
19	D21	0.200	0.765	0.588	0.196	313.6	4470	4260	60.7	1.28	0.00
20	D22	0.200	0.765	0.588	0.196	323.2	4607	4280	61.0	1.28	0.00
21	F11	0.200	0.565	0.530	0.265	297.6	4242	4150	59.2	1.74	0.00
22	F12	0.200	0.565	0.530	0.265	313.6	4470	4060	57.9	1.74	0.00
23	IB1	0.200	0.565	0.530	0.265	264.0	3763	4230	60.3	0.85	0.00
24	IB2	0.200	0.565	0.560	0.265	264.0	3763	4230	60.3	0.85	0.00
25	II1	0.200	0.565	0.530	0.265	264.0	3763	4230	60.3	0.85	0.00
26	II4	0.200	0.565	0.530	0.265	224.0	3193	4230	60.3	0.85	0.00
27	IIB2	0.200	0.265	0.565	0.265	264.0	3763	3450	49.2	1.12	0.00
28	A1	0.200	0.365	0.900	0.411	162.4	2315	3973	56.6	0.83	0.00
29	A2	0.200	0.365	0.650	0.411	148.8	2121	3980	56.7	0.83	0.00
30	A3	0.200	0.365	0.350	0.411	177.6	2532	4030	57.4	0.83	0.00
31	A4	0.200	0.365	0.250	0.411	240.0	3421	3890	55.5	0.55	0.00
32	A5	0.200	0.365	0.205	0.411	206.4	2942	3511	50.0	0.47	0.00
33	C2	0.200	0.365	0.580	0.411	206.4	2942	4487	64.0	0.83	0.23
34	J11	0.200	0.365	0.500	0.411	202.4	2885	4060	57.9	0.83	0.00
35	J12	0.200	0.365	0.500	0.411	173.6	2475	4060	57.9	0.83	0.00
36	J13	0.200	0.365	0.500	0.411	173.6	2475	3973	56.6	0.83	0.00
37	4	0.203	0.400	0.171	0.185	224.0	3193	3070	43.8	0.93	0.00
38	5	0.203	0.410	0.171	0.185	206.4	2942	3050	43.5	1.86	0.00
39	8	0.203	0.510	0.138	0.124	264.0	3763	3230	46.0	1.49	0.00
40	9	0.203	0.510	0.138	0.124	412.0	5873	3170	45.2	1.49	0.00
41	10	0.203	0.612	0.144	0.185	304.8	4345	3310	47.2	1.24	0.00
42	11	0.406	0.307	0.330	0.148	248.0	3535	3360	47.9	1.24	0.00
43	17	0.203	0.411	0.370	0.185	253.6	3615	6730	95.9	0.48	0.00
44	18	0.203	0.411	0.370	0.124	269.6	3843	3340	47.6	0.48	0.00
45	22	0.203	0.615	0.248	0.124	238.4	3398	6730	95.9	0.32	0.00

Table 5.2.2 Section and Material Properties (Continued)

No	Specimen	b	h_o	c/h_o	l_c/h_o	f'_c (kg/cm^2)	f'_c (psi)	f_y (kg/cm^2)	f_y (psi)	ρ_{st} (%)	ρ'_{st} (%)
46	23	0.203	0.615	0.248	0.150	250.4	3569	3170	45.2	0.32	0.00
47	24	0.203	0.410	0.372	0.125	270.4	3854	3340	47.6	0.93	0.00
48	20	0.203	0.513	0.297	0.125	226.4	3227	6730	95.9	0.38	0.00
49	26	0.203	0.410	0.372	0.185	272.0	3877	3760	53.6	0.93	0.00
50	28	0.203	0.615	0.249	0.185	211.2	3011	3340	47.6	0.62	0.00
51	29	0.203	0.615	0.249	0.124	237.6	3387	3350	47.8	0.62	0.00
52	30	0.203	0.508	0.300	0.150	272.0	3877	3210	45.8	0.99	0.00
53	31	0.203	0.610	0.250	0.125	257.6	3672	3290	46.9	0.82	0.00
54	32	0.203	0.610	0.250	0.125	277.6	3957	3210	45.8	0.82	0.00
55	33	0.203	0.410	0.372	0.185	244.0	3478	3340	47.6	1.86	0.00
56	34	0.203	0.410	0.372	0.185	259.2	3695	3760	53.6	1.86	0.00
57	37	0.203	0.615	0.249	0.124	239.2	3410	3620	51.6	1.24	0.00
58	41	0.203	0.410	0.590	0.310	267.2	3809	3120	44.5	0.93	0.00
59	43	0.203	0.615	0.394	0.207	264.0	3763	3230	46.0	0.62	0.00
60	44	0.203	0.613	0.394	0.207	244.8	3490	3190	45.5	0.62	0.00
61	46	0.203	0.410	0.590	0.310	244.8	3490	3120	44.5	1.86	0.00
62	47	0.203	0.410	0.590	0.310	259.2	3695	3120	44.5	1.86	0.00
63	60	0.203	0.410	0.621	0.185	241.6	3444	3120	44.5	0.93	0.00
64	61	0.203	0.410	0.621	0.185	260.8	3718	3820	54.5	0.93	0.00
65	69	0.203	0.410	0.621	0.185	233.6	3330	3120	44.5	1.86	0.00
66	70	0.203	0.410	0.621	0.185	249.6	3558	3750	53.5	1.86	0.00
67	75	0.203	1.060	0.300	0.072	260.8	3718	3200	45.6	0.95	0.00
68	76	0.203	1.060	0.300	0.072	259.2	3695	3290	46.9	0.95	0.00
69	77	0.203	0.616	0.144	0.207	140.0	1996	3190	45.5	0.48	0.00
70	78	0.203	0.616	0.154	0.207	139.2	1984	3120	44.5	0.93	0.00
71	80	0.203	0.512	0.297	0.248	154.4	2201	3060	43.6	0.49	0.00
72	81	0.203	0.510	0.298	0.249	163.2	2326	3150	44.9	0.94	0.00
73	82	0.203	0.405	0.297	0.314	133.6	1904	3180	45.3	1.23	0.00
74	84	0.203	0.408	0.528	0.311	144.8	2064	3320	47.3	0.93	0.00
75	87	0.203	0.613	0.145	0.207	245.6	3501	3120	44.5	0.93	0.00
76	88	0.203	0.613	0.145	0.207	241.6	3444	2250	32.1	1.24	0.00
77	89	0.203	0.513	0.297	0.248	253.6	3615	3150	44.9	0.49	0.00
78	90	0.203	0.510	0.298	0.249	268.8	3832	3270	46.6	0.93	0.00
79	91	0.203	0.405	0.297	0.314	257.6	3672	3290	46.9	1.23	0.00
80	93	0.203	0.410	0.528	0.310	252.0	3592	3350	47.8	0.93	0.00
81	94	0.203	0.405	0.531	0.314	249.6	3558	3290	46.9	1.23	0.00
82	96	0.203	0.613	0.145	0.207	407.2	5804	3270	46.6	0.93	0.00
83	97	0.203	0.510	0.298	0.249	416.0	5930	3270	46.6	0.94	0.00
84	99	0.203	0.510	0.298	0.249	416.0	5930	3270	46.6	0.94	0.00
85	100	0.203	0.405	0.297	0.314	407.2	5804	3350	47.8	1.23	0.00.
86	130	0.203	0.405	0.531	0.314	417.6	5953	3350	47.8	1.23	0.00
87	2E	0.203	0.612	0.249	0.208	283.2	4037	3160	45.0	0.62	0.00
88	3E	0.203	0.612	0.249	0.208	253.6	3615	3030	43.2	0.62	0.00
89	4E	0.203	0.612	0.249	0.208	267.2	3809	3160	45.0	0.62	0.00
90	6E	0.203	0.408	0.370	0.186	257.6	3672	3390	48.3	0.48	0.00

Table 5.2.2 Section and Material Properties (Continued)

No	Specimen	b	h_o	c/h_o	l_c/h_o	f'_c (kg/cm^2)	f'_c (psi)	f_y (kg/cm^2)	f_y (psi)	ρ_{st} (%)	ρ'_{st} (%)
91	1S	0.203	0.394	0.590	0.322	283.2	4037	3100	44.2	0.93	0.34
92	2S	0.203	0.394	0.590	0.322	293.6	4185	3100	44.2	0.93	0.62
93	3S	0.203	0.394	0.590	0.322	283.2	4037	3170	45.2	0.93	0.93
94	4S	0.203	0.394	0.372	0.322	276.8	3946	3120	44.5	0.93	0.34
95	5S	0.203	0.394	0.372	0.322	286.4	4083	3120	44.5	0.93	0.93
96	7S	0.203	0.594	0.394	0.215	263.2	3752	3170	45.2	0.93	0.34
97	8S	0.203	0.594	0.394	0.215	274.4	3911	3530	50.3	0.93	0.62
98	9S	0.203	0.594	0.394	0.215	270.4	3854	3630	51.7	0.93	0.93
99	10S	0.203	0.394	0.295	0.322	266.4	3797	3470	49.5	0.93	0.62

Table 5.2.3 Comparison Between Measured and Predicted Shear Strengths of Brackets

No	Specimen	Ψ_s	λ	$\frac{P_u}{f_t^* A}$	P_u (Measured) ($\times 10^3$kgf)	P_u (Predicted) ($\times 10^3$kgf)	$\frac{P_u(\text{Measured})}{P_u(\text{Predicted})}$
1	a12	3.940	0.265	3.704	76.5	79.5	0.962
2	A12	3.802	0.265	3.665	76.5	78.6	0.973
3	A22	3.857	0.265	3.681	62.5	79.0	0.791
4	A21	3.867	0.265	3.683	67.5	79.0	0.854
5	A31	3.936	0.265	3.625	70.0	74.9	0.935
6	A32	4.615	0.265	3.501	73.9	62.1	1.190
7	B11	3.785	0.001	4.000	75.0	88.7	0.845
8	B12	6.593	0.001	4.000	85.0	86.7	0.980
9	B22	4.130	0.530	2.879	49.5	58.1	0.852
10	B21	4.206	0.530	2.842	67.2	56.1	1.198
11	B22	3.877	0.353	3.367	55.0	71.1	0.773
12	C11	4.158	0.353	3.354	55.5	68.4	0.812
13	C12	4.066	0.176	4.000	80.0	83.9	0.953
14	C22	4.003	0.146	4.000	77.5	84.4	0.918
15	C21	3.708	0.108	4.000	81.0	84.9	0.954
16	C31	3.741	0.108	4.000	82.5	84.9	0.971
17	C32	5.906	0.000	4.000	80.0	58.1	1.378
18	D11	6.133	0.000	4.000	62.5	57.3	1.090
19	D12	2.976	0.392	3.021	80.0	84.7	0.945
20	D21	2.952	0.392	3.036	63.5	86.2	0.736
21	D22	3.940	0.265	3.631	63.5	75.2	0.845
22	F11	3.768	0.265	3.629	73.4	76.9	0.955
23	F12	2.073	0.265	2.932	47.3	57.5	0.823
24	IB1	2.084	0.295	2.864	60.0	55.8	1.075
25	IB2	2.073	0.265	2.932	58.0	57.5	1.009
26	II1	2.247	0.265	2.892	47.5	52.3	0.909
27	II4	2.242	0.300	2.909	39.8	26.6	1.498
28	IIIB2	2.549	0.489	2.318	20.0	21.9	0.914
29	A1	2.563	0.239	2.792	27.5	26.3	1.047
30	A2	2.256	0.000	3.894	39.5	42.1	0.937
31	A3	1.234	0.000	3.885	40.0	49.2	0.813
32	A4	1.016	0.000	3.773	37.0	44.2	0.836
33	A5	3.049	0.169	3.417	30.0	38.9	0.771
34	J11	2.152	0.089	3.315	35.0	37.9	0.924
35	J12	2.337	0.089	3.290	34.0	34.6	0.982
36	J13	2.287	0.089	3.267	37.5	34.4	1.090
37	A13	1.704	0.000	3.526	45.4	48.0	0.946
38	A14	3.532	0.000	4.000	63.5	53.5	1.187
39	B14	2.656	0.014	4.000	79.5	75.0	1.059
40	C13	2.172	0.014	4.000	119.0	90.0	1.322
41	C14	2.116	0.000	4.000	78.5	96.4	0.815
42	D12	2.439	0.182	3.276	83.0	69.7	1.190
43	D13	1.872	0.185	3.031	38.8	43.6	0.889
44	D14	0.912	0.246	2.430	36.7	35.6	1.030
45	4	1.273	0.124	2.842	47.0	60.0	0.783

Table 5.2.3 Comparison Between Measured and Predicted Shear Strengths (Continued)

No	Specimen	Ψ_s	λ	$\frac{P_u}{f_t^* A}$	P_u (Measured) ($\times 10^3$kgf)	P_u (Predicted) ($\times 10^3$kgf)	$\frac{P_u(\text{Measured})}{P_u(\text{Predicted})}$
46	5	0.583	0.098	2.468	39.8	53.7	0.742
47	8	1.765	0.247	2.862	40.2	41.9	0.959
48	9	1.564	0.172	2.845	39.0	48.4	0.805
49	10	1.961	0.187	3.114	49.6	46.2	1.073
50	11	1.288	0.064	2.945	56.6	59.1	0.957
51	17	1.230	0.125	2.811	56.3	59.3	0.950
52	18	1.770	0.150	3.129	61.5	57.9	1.062
53	22	1.535	0.125	3.040	67.0	66.1	1.013
54	23	1.446	0.125	3.036	63.2	68.4	0.924
55	24	3.670	0.187	3.696	51.5	52.1	0.989
56	20	4.012	0.187	3.860	55.5	56.0	0.991
57	26	2.649	0.125	3.542	70.5	74.9	0.941
58	28	1.668	0.280	2.738	35.0	39.6	0.883
59	29	1.139	0.187	2.668	54.5	58.6	0.931
60	30	1.166	0.187	2.642	51.0	55.8	0.915
61	31	3.479	0.280	3.288	47.1	45.6	1.032
62	32	3.384	0.280	3.308	47.5	47.2	1.006
63	33	1.801	0.436	2.458	36.0	33.0	1.092
64	34	2.125	0.436	2.592	34.0	36.1	0.943
65	37	3.663	0.436	2.825	39.0	37.2	1.047
66	41	4.261	0.436	2.953	36.4	40.2	0.905
67	43	1.751	0.228	2.880	97.0	107.6	0.902
68	44	1.806	0.228	2.901	113.0	108.0	1.046
69	46	1.180	0.000	3.009	41.6	48.8	0.852
70	47	2.243	0.000	3.645	48.0	59.0	0.814
71	60	1.102	0.049	2.679	37.5	37.9	0.990
72	61	2.110	0.049	3.281	48.8	47.7	1.024
73	69	3.096	0.000	3.891	38.5	40.4	0.953
74	70	2.423	0.217	2.792	31.7	29.5	1.076
75	75	1.654	0.000	3.772	71.0	82.3	0.862
76	76	1.603	0.000	3.721	68.2	80.6	0.846
77	77	0.874	0.049	2.820	49.5	51.9	0.954
78	78	1.674	0.049	3.402	70.0	64.0	1.094
79	80	2.254	0.000	4.000	56.0	59.0	0.949
80	81	1.822	0.218	2.915	40.0	41.5	0.964
81	82	2.377	0.217	3.146	52.0	44.0	1.181
82	84	1.401	0.000	4.000	114.0	108.1	1.055
83	87	1.418	0.049	3.554	85.0	79.8	1.065
84	88	1.418	0.049	3.554	85.0	79.8	1.065
85	89	1.898	0.000	4.000	77.5	71.4	1.085
86	90	1.954	0.217	3.313	54.0	57.4	0.940
87	91	1.051	0.041	3.045	65.8	70.5	0.933
88	93	1.062	0.041	2.981	56.0	65.5	0.855
89	94	1.080	0.041	3.028	66.0	68.2	0.967
90	96	0.936	0.184	2.540	28.8	36.6	0.787

Table 5.2.3 Comparison Between Measured and Predicted Shear Strength (Continued)

No	Specimen	Ψ_s	λ	$\frac{P_u}{f_t^* A}$	P_u (Measured) ($\times 10^3$kgf)	P_u (Predicted) ($\times 10^3$kgf)	$\frac{P_u(\text{Measured})}{P_u(\text{Predicted})}$
91	97	2.198	0.268	3.019	41.6	43.2	0.962
92	99	2.639	0.268	3.207	47.6	46.7	1.019
93	100	3.292	0.268	3.393	47.8	48.6	0.983
94	130	2.152	0.050	3.706	52.6	54.6	0.964
95	2E	3.103	0.050	4.000	65.5	59.8	1.095
96	3E	2.289	0.179	3.265	69.5	69.2	1.004
97	4E	3.051	0.179	3.609	79.2	78.0	1.015
98	6E	3.791	0.179	3.863	77.2	83.0	0.931
99		2.949	0.000	4.000	68.3	58.4	1.170
						Average	0.973
						STD	0.130

Table 5.3.1 Material Properties and Dimensions of Deep Beams

Number	Specimen	ρh (%)	ρv (%)	fhy psi	fhy Mpa	fvy psi	fvy Mpa	Es ksi	Es Gpa	f_c' psi	f_c' MPa	a in	a m	h in	h m	b in	b m	d in	d m
(1)	(2)	(3)	(4)	(5)	(6)	(7)	(8)	(9)	(10)	(11)	(12)	(13)	(14)	(16)	(17)	(18)	(19)	(20)	(21)
1	1A1-10	2.15	0.28	62500	430.94	63430	437.35	27000	186.17	2710	18.685	12.0	0.305	14.0	0.343	4.0	0.098	11.00	0.270
2	1A3-11	2.36	0.28	62500	430.94	63430	437.35	27000	186.17	2615	18.030	12.0	0.305	14.0	0.343	4.0	0.098	11.00	0.270
3	1A4-12	2.46	0.28	62500	430.94	63430	437.35	27000	186.17	2330	16.065	12.0	0.305	14.0	0.343	4.0	0.098	11.00	0.270
4	1A4-51	2.46	0.28	62500	430.94	63430	437.35	27000	186.17	2980	20.547	12.0	0.305	14.0	0.343	4.0	0.098	11.00	0.270
5	1A6-37	2.67	0.28	62500	430.94	63430	437.35	27000	186.17	3050	21.030	12.0	0.305	14.0	0.343	4.0	0.098	11.00	0.270
6	2A1-38	2.15	0.63	62500	430.94	63430	437.35	27000	186.17	3145	21.685	12.0	0.305	14.0	0.343	4.0	0.098	11.00	0.270
7	2A3-39	2.36	0.63	62500	430.94	63430	437.35	27000	186.17	2865	19.754	12.0	0.305	14.0	0.343	4.0	0.098	11.00	0.270
8	2A4-40	2.46	0.63	62500	430.94	63430	437.35	27000	186.17	2950	20.340	12.0	0.305	14.0	0.343	4.0	0.098	11.00	0.270
9	2A6-41	2.67	0.63	62500	430.94	63430	437.35	27000	186.17	2775	19.134	12.0	0.305	14.0	0.343	4.0	0.098	11.00	0.270
10	3A1-42	2.15	1.25	62500	430.94	63430	437.35	27000	186.17	2670	18.410	12.0	0.305	14.0	0.343	4.0	0.098	11.00	0.270
11	3A3-43	2.36	1.25	62500	430.94	63430	437.35	27000	186.17	2790	19.237	12.0	0.305	14.0	0.343	4.0	0.098	11.00	0.270
12BT	3A4-45	2.46	1.25	62500	430.94	63430	437.35	27000	186.17	3020	20.823	12.0	0.305	14.0	0.343	4.0	0.098	11.00	0.270
13	3A6-46	2.67	1.25	62500	430.94	63430	437.35	27000	186.17	2890	19.927	12.0	0.305	14.0	0.343	4.0	0.098	11.00	0.270
14	1B1-04	2.15	0.24	62500	430.94	63430	437.35	27000	186.17	3200	22.064	14.5	0.368	14.0	0.343	4.0	0.098	11.00	0.270
15	1B3-29	2.36	0.24	62500	430.94	63430	437.35	27000	186.17	2915	20.099	14.5	0.368	14.0	0.343	4.0	0.098	11.00	0.270
16	1B4-40	2.46	0.24	62500	430.94	63430	437.35	27000	186.17	3020	20.823	14.5	0.368	14.0	0.343	4.0	0.098	11.00	0.270
17	1B6-31	2.67	0.24	62500	430.94	63430	437.35	27000	186.17	2830	19.513	14.5	0.368	14.0	0.343	4.0	0.098	11.00	0.270
18	2B1-05	2.15	0.42	62500	430.94	63430	437.35	27000	186.17	2780	19.168	14.5	0.368	14.0	0.343	4.0	0.098	11.00	0.270
20	2B4-07	2.46	0.42	62500	430.94	63430	437.35	27000	186.17	2790	19.237	14.5	0.368	14.0	0.343	4.0	0.098	11.00	0.270
21	2B4-52	2.46	0.42	62500	430.94	63430	437.35	27000	186.17	3160	21.788	14.5	0.368	14.0	0.343	4.0	0.098	11.00	0.270
22	2B6-32	2.67	0.42	62500	430.94	63430	437.35	27000	186.17	2865	19.754	14.5	0.368	14.0	0.343	4.0	0.098	11.00	0.270
23	3B1-08	2.15	0.63	62500	430.94	63430	437.35	27000	186.17	2355	16.238	14.5	0.368	14.0	0.343	4.0	0.098	11.00	0.270
24	3B1-36	2.15	0.77	62500	430.94	63430	437.35	27000	186.17	2960	20.409	14.5	0.368	14.0	0.343	4.0	0.098	11.00	0.270
25	3B3-33	2.36	0.77	62500	430.94	63430	437.35	27000	186.17	2755	18.996	14.5	0.368	14.0	0.343	4.0	0.098	11.00	0.270
26	3B4-34	2.46	0.77	62500	430.94	63430	437.35	27000	186.17	2790	19.237	14.5	0.368	14.0	0.343	4.0	0.098	11.00	0.270
27	3B6-35	2.67	0.77	62500	430.94	63430	437.35	27000	186.17	2995	20.651	14.5	0.368	14.0	0.343	4.0	0.098	11.00	0.270
29	4B1-09	2.15	1.25	62500	430.94	63430	437.35	27000	186.17	2480	17.100	14.5	0.368	14.0	0.343	4.0	0.098	11.00	0.270
29	1C1-14	2.15	0.18	62500	430.94	63430	437.35	27000	186.17	2790	19.237	18.0	0.457	14.0	0.343	4.0	0.098	11.00	0.270
30	1C1-02	2.36	0.18	62500	430.94	63430	437.35	27000	186.17	3175	21.892	18.0	0.457	14.0	0.343	4.0	0.098	11.00	0.270
31	1C4-15	2.46	0.18	62500	430.94	63430	437.35	27000	186.17	3290	22.685	18.0	0.457	14.0	0.343	4.0	0.098	11.00	0.270
32	1C6-16	2.67	0.18	62500	430.94	63430	437.35	27000	186.17	3160	21.788	18.0	0.457	14.0	0.343	4.0	0.098	11.00	0.270
33	2C1-17	2.15	0.31	62500	430.94	63430	437.35	27000	186.17	2880	19.858	18.0	0.457	14.0	0.343	4.0	0.098	11.00	0.270
34	2C3-03	2.36	0.31	62500	430.94	63430	437.35	27000	186.17	2790	19.237	18.0	0.457	14.0	0.343	4.0	0.098	11.00	0.270
35	2C3-27	2.36	0.31	62500	430.94	63430	437.35	27000	186.17	2800	19.306	18.0	0.457	14.0	0.343	4.0	0.098	11.00	0.270
36	2C4-18	2.46	0.31	62500	430.94	63430	437.35	27000	186.17	2965	20.444	18.0	0.457	14.0	0.343	4.0	0.098	11.00	0.270
37	3C1-19	2.67	0.31	62500	430.94	63430	437.35	27000	186.17	3010	20.754	18.0	0.457	14.0	0.343	4.0	0.098	11.00	0.270

Table 5.3.1 Material Properties and Dimensions of Deep Beams (Continued)

Number	Specimen	ρ_h (%)	ρ_v (%)	f_{hy} psi	f_{hy} Mpa	f_{vy} psi	f_{vy} Mpa	E_s ksi	E_s Gpa	f_c' psi	f_c' MPa	a in	a m	h in	h m	b in	b m	d in	d m
(1)	(2)	(3)	(4)	(5)	(6)	(7)	(8)	(9)	(10)	(11)	(12)	(13)	(14)	(16)	(17)	(18)	(19)	(20)	(21)
38	3C1-20	2.15	0.56	62500	430.94	63430	437.35	27000	186.17	3050	21.030	18.0	0.457	14.0	0.343	4.0	0.098	11.00	0.270
39	3C3-21	2.36	0.56	62500	430.94	63430	437.35	27000	186.17	2400	16.548	18.0	0.457	14.0	0.343	4.0	0.098	11.00	0.270
40	3C4-22	2.46	0.56	62500	430.94	63430	437.35	27000	186.17	2650	18.272	18.0	0.457	14.0	0.343	4.0	0.098	11.00	0.270
41	3C6-23	2.67	0.56	62500	430.94	63430	437.35	27000	186.17	2755	18.996	18.0	0.457	14.0	0.343	4.0	0.098	11.00	0.270
42	4C1-24	2.15	0.77	62500	430.94	63430	437.35	27000	186.17	2840	19.582	18.0	0.457	14.0	0.343	4.0	0.098	11.00	0.270
43	4C3-04	2.36	0.63	62500	430.94	63430	437.35	27000	186.17	2690	18.548	18.0	0.457	14.0	0.343	4.0	0.098	11.00	0.270
44	4C3-28	2.36	0.77	62500	430.94	63430	437.35	27000	186.17	2790	19.237	18.0	0.457	14.0	0.343	4.0	0.098	11.00	0.270
45	4C4-25	2.46	0.77	62500	430.94	63430	437.35	27000	186.17	2685	18.513	18.0	0.457	14.0	0.343	4.0	0.098	11.00	0.270
46	4C6-26	2.67	0.77	62500	430.94	63430	437.35	27000	186.17	3080	21.237	18.0	0.457	14.0	0.343	4.0	0.098	11.00	0.270
47	4D1-13	2.67	0.42	62500	430.94	63430	437.35	27000	186.17	2330	16.065	25.0	0.635	14.0	0.343	4.0	0.098	11.00	0.270
48	1-30	0.52	2.45	41600	286.83	40600	279.94	29000	199.96	3120	21.512	10.0	0.254	30.0	0.735	3.0	0.0735	27.40	0.671
49	1-25	0.63	2.45	41600	286.83	40600	279.94	29000	199.96	3560	24.546	10.0	0.254	25.0	0.613	3.0	0.0735	22.50	0.551
50	1-20	0.80	2.45	41600	286.83	40600	279.94	29000	199.96	3080	21.237	10.0	0.254	20.0	0.490	3.0	0.0735	17.30	0.424
51	1-15	1.41	2.45	41600	286.83	40600	279.94	29000	199.96	3080	21.237	10.0	0.254	15.0	0.368	3.0	0.0735	12.30	0.301
52	1-10	1.73	2.45	41600	286.83	40600	279.94	29000	199.96	3140	21.650	10.0	0.254	10.0	0.245	3.0	0.0735	7.40	0.181
53	2-30	0.52	0.86	41600	286.83	44000	303.38	29000	199.96	3785	26.098	10.0	0.254	30.0	0.735	3.0	0.0735	27.20	0.666
54	2-25	0.63	0.86	41600	286.83	44000	303.38	29000	199.96	2700	18.617	10.0	0.254	25.0	0.613	3.0	0.0735	22.20	0.544
55	2-20	0.80	0.86	41600	286.83	44000	303.38	29000	199.96	2880	19.858	10.0	0.254	20.0	0.490	3.0	0.0735	17.30	0.424
56	2-15	1.09	0.86	41600	286.83	44000	303.38	29000	199.96	3300	22.754	10.0	0.254	15.0	0.368	3.0	0.0735	12.40	0.304
57	2-10	1.73	0.86	41600	286.83	44000	303.38	29000	199.96	2920	20.133	10.0	0.254	10.0	0.245	3.0	0.0735	7.30	0.179
58	5-30	1.14	0.61	40600	279.94	40600	279.94	29000	199.96	2690	18.548	10.0	0.254	30.0	0.735	3.0	0.0735	25.80	0.632
59	5-25	1.24	0.61	40600	279.94	40600	279.94	29000	199.96	2790	19.237	10.0	0.254	25.0	0.613	3.0	0.0735	20.90	0.512
60	5-20	1.41	0.61	40600	279.94	40600	279.94	29000	199.96	2920	20.133	10.0	0.254	20.0	0.490	3.0	0.0735	16.00	0.392
61	5-15	1.70	0.61	40600	279.94	40600	279.94	29000	199.96	3180	21.926	10.0	0.254	15.0	0.368	3.0	0.0735	11.20	0.274
62	5-10	2.34	0.61	40600	279.94	40600	279.94	29000	199.96	3270	22.547	10.0	0.254	10.0	0.245	3.0	0.0735	6.50	0.159
63	G339.1	2.59	1.09	47300	326.13	32000	220.64	29000	199.96	2890	19.927	8.0	0.203	9.0	0.221	3.0	0.0735	7.25	0.178
64	G339.3	3.41	1.09	44200	304.76	32000	220.64	29000	199.96	2910	20.064	8.0	0.203	9.0	0.221	3.0	0.0735	7.25	0.178

Table 5.3.2 Comparison of Measured and Predicted Ultimate Shear Strengths of Deep Beams "

Number (1)	f_c' psi (2)	f_c' MPa (3)	ψ_h (4)	ψ_v (5)	m (6)	K (7)	ν (8)	λ (9)	α (10)	β (11)	Measured lb (12)	Measured KN (13)	Predicted lb (14)	Predicted KN (15)	x* (16)
1	2710.00	18.685	5.559	0.735	8.199	1.033	0.707	0.860	37.830	37.830	36250	161.240	28481.40	126.685	1.273
2	2615.00	18.030	6.220	0.749	8.102	1.017	0.710	0.860	37.430	37.430	33350	148.341	27833.49	123.803	1.198
3	2330.00	16.065	6.906	0.798	7.796	0.966	0.720	0.860	36.210	36.210	31750	141.224	25820.30	114.849	1.230
4	2980.00	20.547	6.049	0.699	8.463	1.078	0.697	0.860	38.650	38.650	38430	170.937	30261.01	134.601	1.270
5	3050.00	21.030	6.487	0.690	8.528	1.089	0.695	0.860	38.650	38.650	41385	184.080	30708.35	136.591	1.348
6	3145.00	21.685	5.142	1.529	8.616	1.104	0.692	0.860	40.170	40.170	39230	174.495	37850.02	168.357	1.036
7	2865.00	19.754	5.924	1.605	8.352	1.059	0.701	0.860	38.000	38.000	38350	170.581	36051.35	160.356	1.064
8	2950.00	20.340	6.081	1.581	8.434	1.073	0.698	0.860	38.700	38.700	38650	171.915	36612.97	162.854	1.056
9	2775.00	19.134	6.816	1.632	8.264	1.044	0.704	0.860	37.230	37.230	36400	161.907	35440.86	157.641	1.027
10	2670.00	18.410	5.603	3.306	8.158	1.026	0.708	0.860	10.930	10.930	36200	161.018	42265.29	187.996	0.856
11	2790.00	19.237	6.008	3.229	8.279	1.047	0.704	0.860	12.700	12.700	38830	172.716	43623.40	194.037	0.890
12	3020.00	20.823	6.008	3.098	8.500	1.084	0.696	0.860	15.730	15.730	40140	178.543	46066.95	204.906	0.871
13	2890.00	19.927	6.672	3.170	8.377	1.063	0.700	0.860	14.070	14.070	37800	168.134	44710.18	198.871	0.845
14	3200.00	22.064	5.330	0.604	8.666	1.112	0.690	1.040	0.460	0.460	33150	147.451	29629.78	131.793	1.119
15	2915.00	20.099	6.236	0.634	8.401	1.067	0.700	1.040	0.460	0.460	32275	143.559	27920.25	124.189	1.156
16	3020.00	20.823	6.282	0.622	8.500	1.084	0.696	1.040	0.460	0.460	31550	140.334	28559.78	127.034	1.105
17	2830.00	19.513	7.053	0.643	8.318	1.053	0.702	1.040	0.460	0.460	34475	153.345	27392.38	121.841	1.259
18	2780.00	19.168	5.733	1.137	8.269	1.045	0.704	1.040	46.470	46.470	29000	128.992	29362.29	130.603	0.988
19	2755.00	18.996	6.324	1.142	8.244	1.041	0.705	1.040	46.300	46.300	29500	131.216	29229.57	130.013	1.009
20	2535.00	17.479	6.894	1.194	8.019	1.003	0.713	1.040	44.590	44.590	28350	126.101	28017.62	124.622	1.012
21	3160.00	21.788	6.137	1.063	8.630	1.106	0.691	1.040	48.900	48.900	33700	149.898	31267.16	139.076	1.078
22	2865.00	19.754	7.008	1.119	8.352	1.059	0.701	1.040	47.060	47.060	32650	145.227	29806.36	132.579	1.095
23	2355.00	16.238	6.274	1.866	7.824	0.971	0.719	1.040	31.540	31.540	29400	130.771	31422.59	139.768	0.936
24	2960.00	20.409	5.547	2.016	8.444	1.074	0.698	1.040	31.490	31.490	35735	158.949	38368.41	170.663	0.931
25	2755.00	18.996	6.324	2.094	8.244	1.041	0.705	1.040	29.470	29.470	35600	158.349	36829.62	163.818	0.967
26	2790.00	19.237	6.548	2.080	8.279	1.047	0.704	1.040	29.840	29.840	34850	155.013	37099.45	165.018	0.939
27	2995.00	20.651	6.847	2.004	8.477	1.080	0.697	1.040	31.810	31.810	37350	166.133	38621.49	171.788	0.967
28	2480.00	17.100	6.097	3.598	7.960	0.993	0.715	1.040	5.510	5.510	34500	153.456	38415.14	170.871	0.898
29	2790.00	19.237	6.107	0.519	8.279	1.047	0.704	1.290	0.520	0.520	26750	118.984	24415.41	108.600	1.096
30	3175.00	21.892	6.268	0.485	8.643	1.108	0.691	1.290	0.520	0.520	27750	123.432	26567.66	118.173	1.045
31	3290.00	22.685	6.417	0.477	8.746	1.126	0.687	1.290	0.520	0.520	29450	130.994	27182.56	120.908	1.083
32	3160.00	21.788	7.108	0.486	8.630	1.106	0.691	1.290	0.520	0.520	27500	122.320	26486.41	117.812	1.038
33	2800.00	19.306	6.095	0.892	8.289	1.048	0.703	1.290	0.520	0.520	27900	124.099	27322.81	121.532	1.021
34	2790.00	19.237	6.703	0.894	8.279	1.047	0.704	1.290	0.520	0.520	23300	103.638	27261.54	121.259	0.855
35	2800.00	19.306	6.690	0.892	8.289	1.048	0.703	1.290	0.520	0.520	25925	115.314	27322.81	121.532	0.949
36	2965.00	20.444	6.767	0.865	8.448	1.075	0.698	1.290	0.520	0.520	28000	124.544	28315.57	125.948	0.989
37	3010.00	20.754	7.288	0.859	8.491	1.082	0.696	1.290	0.520	0.520	27900	124.099	28581.71	127.131	0.976

x*= Measured/Predicted

Table 5.3.2 Comparison of Measured and Predicted Ultimate Shear Strengths of Deep Beams (Continued)

Number (1)	f_c' psi (2)	f_c' MPa (3)	ψ_h (4)	ψ_v (5)	m (6)	K (7)	ν (8)	λ (9)	α (10)	β (11)	Measured lb (12)	Measured KN (13)	Predicted lb (14)	Predicted KN (15)	x* (16)
38	3050.00	21.030	5.829	1.541	8.528	1.089	0.695	1.290	39.690	39.690	31650	140.779	33284.10	148.048	0.951
39	2400.00	16.548	7.272	1.782	7.874	0.979	0.717	1.290	33.180	33.180	28100	124.989	29407.47	130.804	0.956
40	2650.00	18.272	7.182	1.659	8.138	1.023	0.709	1.290	36.320	36.320	28700	127.658	30883.98	137.372	0.929
41	2755.00	18.996	7.635	1.625	8.244	1.041	0.705	1.290	37.280	37.280	30850	137.221	31542.51	140.301	0.978
42	2840.00	19.582	6.049	2.199	8.328	1.055	0.702	1.290	28.160	28.160	32950	146.562	35879.61	159.593	0.918
43	2690.00	18.548	6.835	1.852	8.179	1.030	0.707	1.290	33.180	33.180	28900	128.547	32502.00	144.569	0.889
44	2790.00	19.237	6.703	2.220	8.279	1.047	0.704	1.290	27.630	27.630	34250	152.344	35507.32	157.937	0.965
45	2685.00	18.513	7.131	2.265	8.174	1.029	0.707	1.290	26.470	26.470	34300	152.566	34705.43	154.370	0.988
46	3080.00	21.237	7.202	2.108	8.556	1.093	0.694	1.290	30.480	30.480	35850	159.461	37587.35	167.189	0.954
47	2330.00	16.065	9.651	1.541	7.796	0.966	0.720	1.780	37.210	37.210	19650	87.403	23618.80	105.056	0.832
48	3120.00	21.512	0.737	3.389	8.593	1.100	0.692	0.330	38.580	38.580	53700	238.858	66727.32	296.803	0.805
49	3560.00	24.546	0.849	3.221	8.979	1.165	0.677	0.400	38.530	38.530	50400	224.179	61191.79	272.181	0.824
50	3080.00	21.237	1.184	3.540	8.556	1.093	0.694	0.500	35.370	35.370	42600	189.485	45086.96	200.547	0.945
51	3080.00	21.237	1.677	3.679	8.556	1.093	0.694	0.670	32.680	32.680	36900	164.131	34116.27	151.749	1.082
52	3140.00	21.650	2.853	3.944	8.611	1.103	0.692	1.000	20.160	20.160	20100	89.405	22616.58	100.599	0.889
53	2785.00	19.203	0.782	1.368	8.274	1.046	0.704	0.330	37.520	37.520	56000	249.088	57421.34	255.410	0.975
54	2700.00	18.617	0.978	1.412	8.189	1.032	0.707	0.400	35.910	35.910	50400	224.179	47152.98	209.736	1.069
55	2880.00	19.858	1.226	1.395	8.367	1.061	0.701	0.500	34.710	34.710	48400	215.283	39082.89	173.841	1.238
56	3300.00	22.754	1.619	1.351	8.755	1.127	0.686	0.670	33.370	33.370	31400	139.667	30903.52	137.459	1.016
57	2920.00	20.133	2.962	1.558	8.405	1.068	0.699	1.000	17.620	17.620	22400	99.635	17398.66	77.389	1.287
58	2690.00	18.548	1.689	0.912	8.179	1.030	0.707	0.330	31.800	31.800	53800	239.302	57950.84	257.765	0.928
59	2790.00	19.237	1.846	0.908	8.279	1.047	0.704	0.400	31.290	31.290	46800	208.166	47436.20	210.996	0.987
60	2920.00	20.133	2.095	0.906	8.405	1.068	0.699	0.500	30.370	30.370	38800	172.582	36834.14	163.838	1.053
61	3180.00	21.926	2.512	0.901	8.648	1.109	0.690	0.670	25.120	25.120	28600	127.213	26576.70	118.213	1.076
62	3270.00	22.547	3.690	0.962	8.729	1.123	0.687	1.000	9.340	9.340	17500	77.840	14372.03	63.927	1.218
63	2890.00	19.927	4.934	1.405	8.377	1.063	0.700	0.890	41.650	41.650	19000	84.512	16899.86	75.171	1.124
64	2910.00	20.064	6.049	1.400	8.396	1.066	0.700	0.890	41.800	41.800	22800	101.414	16959.96	75.438	1.344

204

Table 5.4.1 Section and Material Properties of Torsional Members

specimen	a (in)	b (in)	as (in)	bs (in)	fc psi	fls ksi	fts ksi	Long.	Trans.
B1	10.00	15.00	8.50	13.50	4000	45.5	49.5	4#4	#3@6.00
B2	10.00	15.00	8.50	13.50	4150	45.9	46.4	4#5	#4@7.13
B3	10.00	15.00	8.50	13.50	4070	47.5	46.4	4#6	#4@5.00
B4	10.00	15.00	8.50	13.50	4430	46.4	46.9	4#7	#4@3.63
B5	10.00	15.00	8.50	13.50	4210	48.2	46.6	4#8	#4@2.75
B6	10.00	15.00	8.50	13.50	4180	48.1	46.8	4#9	#4@2.25
B7	10.00	15.00	8.50	13.50	3770	46.4	46.2	4#4	#4@5.00
B8	10.00	15.00	8.50	13.50	3880	46.7	46.4	4#4	#4@2.25
B9	10.00	15.00	8.50	13.50	4180	46.3	49.7	4#6	#3@6.00
B10	10.00	15.00	8.50	13.50	3840	48.5	49.6	4#9	#3@6.00
D1	10.00	15.00	8.50	13.50	3860	48.3	49.0	4#4	#3@6.00
D2	10.00	15.00	8.50	13.50	3710	46.8	48.0	4#5	#4@7.13
D3	10.00	15.00	8.50	13.50	4120	49.5	48.3	4#6	#4@5.00
D4	10.00	15.00	8.50	13.50	4440	47.9	48.3	4#7	#4@3.63
M1	10.00	15.00	8.50	13.50	4330	47.3	51.2	4#5	#3@5.88
M2	10.00	15.00	8.50	13.50	4430	47.7	51.8	4#6	#3@4.13
M3	10.00	15.00	8.50	13.50	3880	46.7	47.3	4#7	#4@5.50
M4	10.00	15.00	8.50	13.50	3850	46.2	47.4	4#8	#4@4.13
M5	10.00	15.00	8.50	13.50	4060	48.6	48.0	4#9	#4@3.25
M6	10.00	15.00	8.50	13.50	4260	46.1	49.4	6#8	#4@2.75
I2	10.00	15.00	8.50	13.50	6560	47.2	50.6	4#5	#3@3.88
I3	10.00	15.00	8.50	13.50	6490	49.8	48.4	4#6	#4@5.00
I4	10.00	15.00	8.50	13.50	6520	45.7	47.3	4#7	#4@3.63
I5	10.00	15.00	8.50	13.50	6530	45.0	47.2	4#8	#4@2.75
I6	10.00	15.00	8.50	13.50	6640	47.2	47.7	4#9	#4@2.25
G1	10.00	20.00	8.50	18.50	4320	46.7	49.2	4#4	#3@7.38
G2	10.00	20.00	8.50	18.50	4480	46.8	48.4	4#5	#3@4.75
G3	10.00	20.00	8.50	18.50	3890	49.1	47.5	4#6	#4@6.13
G4	10.00	20.00	8.50	18.50	4100	47.2	49.6	4#7	#4@4.50
G5	10.00	20.00	8.50	18.50	3900	48.0	47.5	4#8	#4@3.38
G6	10.00	20.00	8.50	18.50	4340	48.5	50.7	6#4	#3@5.00
G7	10.00	20.00	8.50	18.50	4490	46.3	46.8	6#5	#4@5.75
G8	10.00	20.00	8.50	18.50	4110	46.7	47.7	6#6	#4@4.13
C1	10.00	10.00	8.50	8.50	3920	49.5	49.5	4#3	#3@8.50
CC2	10.00	10.00	8.50	8.50	3850	48.5	50.0	4#4	#3@4.63
C3	10.00	10.00	8.50	8.50	3900	48.0	47.8	4#5	#4@5.50
C4	10.00	10.00	8.50	8.50	3940	48.8	47.5	4#6	#4@3.88
C5	10.00	10.00	8.50	8.50	3950	47.6	47.7	4#7	#4@2.88
C6	10.00	10.00	8.50	8.50	4000	45.8	47.5	4#8	#4@2.13

Table 5.4.2 Comparison Between Measured and Predicted Ultimate Torsional Strength

specimen	I_p (in^2)	$a_s b_s (1+\frac{a_s}{b_s})$ (in^2)	Ψ_{sl}	Ψ_{st}	$\frac{T_u}{f_t^* I_p}$	T_u Measured (kips-in)	T_u Predicted (kips-in)	$\frac{T_u(\text{measured})}{T_u(\text{predicted})}$
B1	291.7	187.0	1.54	0.26	2.39	197	205.67	0.96
B2	291.7	187.0	2.38	0.63	2.84	259	258.87	1.00
B3	291.7	187.0	3.52	1.28	2.99	332	348.29	0.95
B4	291.7	187.0	4.58	2.45	3.64	419	475.64	0.88
B5	291.7	187.0	6.35	4.20	4.00	497	502.55	0.99
B6	291.7	187.0	8.04	6.48	4.00	546	499.75	1.09
B7	291.7	187.0	1.60	0.57	2.43	238	212.56	1.12
B8	291.7	187.0	1.60	1.28	3.80	288	340.00	0.85
B9	291.7	187.0	3.41	0.59	2.51	264	294.95	0.90
B10	291.7	187.0	8.31	1.31	3.03	304	353.99	0.86
D1	291.7	187.0	1.65	0.26	2.21	198	197.96	1.00
D2	291.7	187.0	2.51	0.62	2.53	245	244.71	1.00
D3	291.7	187.0	3.66	1.28	2.99	346	356.65	0.97
D4	291.7	187.0	4.73	2.45	3.62	424	473.84	0.89
M1	291.7	187.0	2.43	0.43	2.42	269	261.87	1.03
M2	291.7	187.0	3.45	0.87	2.81	359	347.11	1.03
M3	291.7	187.0	4.79	1.57	3.19	388	375.78	1.03
M4	291.7	187.0	6.25	2.75	3.85	439	450.72	0.97
M5	291.7	187.0	8.19	4.46	4.00	493	488.47	1.01
M6	291.7	187.0	12.11	3.44	3.96	532	502.10	1.06
I2	291.7	187.0	2.23	0.73	2.54	319	358.67	0.89
I3	291.7	187.0	3.35	1.46	3.12	404	496.95	0.81
I4	291.7	187.0	4.18	2.75	3.67	514	627.22	0.82
I5	291.7	187.0	5.42	4.78	4.00	626	684.25	0.91
I6	291.7	187.0	7.19	7.45	4.00	679	691.19	0.98
G1	416.7	229.5	0.97	0.19	2.04	237	260.35	0.91
G2	416.7	229.5	1.49	0.46	2.33	357	328.67	1.09
G3	416.7	229.5	2.31	0.89	2.73	439	382.64	1.15
G4	416.7	229.5	2.98	1.66	3.24	574	511.74	1.12
G5	416.7	229.5	4.05	2.89	3.99	637	674.23	0.94
G6	416.7	229.5	2.01	0.23	2.24	346	329.79	1.05
G7	416.7	229.5	2.95	0.56	2.49	466	420.33	1.11
G8	416.7	229.5	4.33	1.09	2.87	560	505.52	1.11
C1	166.7	144.5	1.99	0.14	2.13	100	115.52	0.87
CC2	166.7	144.5	3.57	0.46	2.49	135	159.36	0.85
C3	166.7	144.5	5.45	1.10	2.88	177	194.66	0.91
C4	166.7	144.5	7.84	2.21	3.63	224	247.36	0.91
C5	166.7	144.5	10.42	4.07	4.00	263	273.12	0.96
C6	166.7	144.5	13.15	7.27	4.00	303	275.86	1.10
							Average	0.98
							STD	0.09

References
(Part I)

ACI Committee 318, (1989). *Commentary on Building Code Requirements for Reinforced Concrete (ACI 318-89).* Detroit: American Concrete Institute;

Chen, W.F.(1961). "Limit analysis of reinforced concrete and the theorems of limit analysis." *Mem. Inc. Ass. Bridge struct. Eng.,* Vol 21, pp49-59;

Chen, W.F.(1975). *Limit Analysis and Soil Plasticity,* Elsevier Scientific Publishing Company;

Chen, W.F.(1982). *Plasticity in Reinforced Concrete.* McGraw-Hill Inc., pp 295-344

Collins, M.P.(1973). "Torque-twist characteristics of reinforced concrete beams." *Inelastic and non-linearity in structural concrete.* University of Waterloo Press, Waterloo, Ontario, Canada.

Coulomb, A. C. (1773). *Mém. Math. et Phys. 7 , p. 343,* see also, Hill, 1950

De Paiva, Rawdon, H.A. and Siess, Chester P.(1965). "Strength and behavior of deep beams in shear." *Proceedings, ASCE,* Vol 91., *ST*5, Oct., pp. 19-41;

Dettman, J.W.(1968) *Mathematical Methods in Physics and Engineering,* McGraw-Hill, New York.

Drucker, D.C., Greenberg, H.J., Prager, W.(1952). "Extended limit design theorems for continuos media." *Quart. Appl. Mech.,* vol. 9, pp. 381-389

Exner, H. (1979). "On the effectiveness factor in plastic analysis of concrete." *Plasticity in Reinforced Concrete, Introductory Report,* Int. Ass. Bridge Struct. Eng., *Reports of the WC,* Vol.29, pp.35-42;

References
(**Part I** Continued)

Gozdev, A. A.(1960). "The deformation of the value of the collapse load for statically indeterminate systems undergoing plastic deformation." Dec. 1936, p. 19, Akademiia Nauk SSR, Moscow-Lenigrad 1938, see also Haythornthwaite's translation in *Int. J. Mech. Sci.*, Vol. 1, pp.322-335.

Hason, J. A. (1961). "Tensile strength and diagonal tension resistance of structural light weight concrete." *ACI Journal*, Proceedings Vol. 58, No.1, July , pp. 1-40.

Hill, R.(1950). *The Mathematical Theory of Plasticity*, Oxford University Press, Ely House, London

Hillerborg, A.(1956). "Jämnviktsteori för armerae Betongplattor." *Betong*, vol. 41, No. 4, pp. 61-71

Hillerborg A.(1953). "Armering av Elsticitetsteoretiskt Beräknade Plattor, skivor och skal." *Betong*, 1953 no.2, pp. 101-109.

Hsu, T.T.C.(1968a). "Torsion of structural concrete-behavior of reinforced concrete rectangular members." *Torsion of Structural Concrete, SP-18,* American Concrete Institute, Detroit.

Hsu, T.T.C. (1988) "Softened truss model theory for shear and torsion." *Structural Journal, ACI*, 85(6), pp. 624-635.

Hsu, T.T.C.(1968b). "Ultimate torque of reinforced concrete beams." *J. Struct. Div.*, ASCE, vol.94, no.2, pp. 485-510

Hsu, T.T.C., Mau, S.T., and Chen, B. (1987). "The Theory of Shear Transfer Strength of Reinforced Concrete", *Structural Journal, ACI*, March-April, pp. 149-160.

Ivey, D.L. and Buth, E.(1966). "Shear capacity of light weight concrete beams." *ACI Journal, Proceedings,* vol. 63, No.6 June, pp. 634-643.

Jiang, D.H. and Shen, J.H.(1986). "Strength of concrete slabs in punching shear." *ASCE, ST 12,* pp.2578-2591;

References
(**Part I** Continued)

Johansen, K.W.(1931). "Beregning af krydsarmerede jernbetonpladers brudmoment." *Bygningsstatisk Meddelelser,* vol. 3, no.1, pp. 1-18

Johansen, K.W.(1932). "Bruchmomente der kreuzweise bewehrten platten." *Mem. Ass. Int. Ponts Charp.* vol. 1, pp.277-295

Klingroth, H.(1942). "Versuche an stahlbetontragwanden und deren auswertung." *Beton u. Eisen,* Vol.41, pp.91-98, 108-115, 130-136;

Kong, F.K., Robins, P.J.; and Cole, D.F.(1970). "Web reinforcement effects on deep beams." *ACI Journal, Proceedings,* Vol. 67, No.12, Dec., pp. 1010-1017;

Kupfer, H.(1969). *Das verhalten des betons unter zweiachsiger beanspruchung.* Techn. Hochsch. Munchen, Lehrstuhl Massivbau Ber. 18.;

Lampert, P. and Thurlimann, B.(1968). " Torsionsversuche an stahlbetonbalken." *Berich Nr. 6506-2,* Institute für Baustatik, ETH, Zurich, Switzerland.

Lampert, P. and Thurlimann, B.(1969). "Torsion-beige-versuche an stahlbetonbalken." *Bericht Nr. 6506-3,* Institute für Baustatik, ETH, Zurich, Switzerland.

Lessig, N.N. (1958). "Theoretical and experimental investigation of reinforced concrete elements subjected to combined bending and torsion." *Theory of Design and Construction of Reinforced Concrete Structures,* Moscow, USSR, 1958, pp. 73-84

Mast, R.F.(1968). "Auxiliary reinforcement in concrete connections." *ASCE, ST.* vol 96, st.6, June, 1968, pp. 1485-1504.

Mattock, R.H. and Hawinks,N.M.(1972). "Shear transfer in reinforced concrete-recent research." *PCI Journal,* March-April, pp. 55-75.

References
(**Part I** Continued)

Mau,S.T.,Hsu, Thomas T.C.(1989). "Formula for Shear strength of deep beams", ACI structural Journal, Sept.-Oct., pp.516-532;

Nielsen, M.P.(1961). "Limit analysis of reinforced concrete and the theorems of limit analysis." *Mem. Int. Ass. Bridge Struct. Eng.*, Vol 21, pp.49-59;

Nielsen, M.P.(1971). "On the strength of reinforced concrete discs", *Civil Engineering and Building Construction Series* No.70, ACTA Polytechnica Scandiavica;

Nielsen, M.P.(1984). *Limit analysis and concrete plasticity.* Prentice-Hall, Englewood Cliffs, N.J.

Nielsen, M.P., Braestrup, M.W., Jensen, B.C.,and Bach,F.(1978). "Concrete plasticity, beam shear,shear in joints, punching shear." *Danish Society for Structural Science and Engineering*, Copenhagen, Special Publication, pp 129;

Okaemure, H. and Maekawa K.(1991). *Nonlinear Analysis and Constitutive Models of Reinforced Concrete.* Tokyo University.

Ottosen, N. S.(1977). "A failure criterion for concrete." *J. Eng. Mech. ASCE,* vol. 103 (EM4). pp 527-535.

Paulay, T. and Locker, P.L.(1974). "Shear transfer by aggregate interlock." *Shear in Reinforced Concrete, ACI Special Publication 42,* vol.1, Detroit, pp. 1-5.

Prager, W.(1952). "The general theory of limit design." *Proc. 8th Int. Congr., Theor. Appl. Mech.*, Istanbul, vol. II, pp 65-72.

Raush, E.(1929). *"Design of reinforced concrete in torsion (Berechung des Eisenbeton gegen Verdrehung)."* Technische Hochshule, Berlin, Germany.

Richartm F.E., Brandtzaeg, A., Brown, R.L.,(1929). "A study of the failure of concrete under combined compressive stresses." *Univ. Ill. Eng. Exp. Bull. 185.*

References
(**Part I** Continued)

Sadowsky, M.A.(1941). "An extension of the sand heap analogy in plastic torsion application to cross-section having one or more holes." *Journal of Applied Mechanics,* Vol. 62.

Smith, K.N. and Fereig, S.M.(1974). "Effect of loading and supporting conditions on the shear strength of deep beam." *Shear in Reinforced Concrete,* Vol.3(SP-42). Detroit: American Concrete Institute, pp.441-460;

Smith, K.N. and Vansiotis, A. S.(1982). "Shear strength of deep beams." *ACI Journal, Proceedings* V.79, No.3 May-June, pp.201-213;

Spliiers, W.R.(1975). *Iterative Structural Design,North-Holland Monographs in Design Theory,* North-Holland Publishing-American Elsevier, New York.

Vechio, F. and Collins, M.P.(1981). "Stress-strain characteristics of reinforced concrete in pure shear." *Final report* IABSE Colloquium *Advanced Mechanics of Reinforced concrete,* International Association of Bridge and Structural Engineers.

Wang, W.(1988). "Limit analysis of steel and steel fiber reinforced concrete shear transfer and brackets." *Thechnical Report,* Department of Structural Engineering, Tongji University, Shanghai, China.

Wang, W., Jiang, D.H. and Hsu, C.T.T.(1993), "Shear strength of reinforced concrete deep beams." *Journal of Structural engineering, ASCE,* vol.119, No. 8, August, pp. 2294-2312.

Willam, K.J. and Warnke, E.P.(1975). "Constitutive model for the triaxial behavior of concrete." *International Association of Bridge and Structural Engineers, Seminar on Concrete Structure Subjected to Triaxial Stresses,* Paper III-1, Bergamo, Italy, May, 1974, IABSE Proc. 19

References
(**Part I** Continued)

Wischers, G. (1978). "Application of effects of compressive loads on concrete." *Betontech.*, Berlin, Nos. 2 and 3, Düsseldorf.

Yudin, V.K.(1962). "Determination of the load-carrying capacity of rectangular reinforced concrete elements subjected to combined torsion and bending." *Beton i Zhelezobeton (Concrete and Reinfroced concrete)* No. 6, Moscow, USSR, June, 1962, pp. 265-268

References
(Part II)

Baluch, M.H., A.B. Qureshy and A.K. Azad (1987). "Fatigue crack propagation in plain concrete." *SEM/RILEM International Conference on Fracture of Concrete and Rock*, Houston, Texas, June, Editor, S.P. Shah, and S.E. Swartz, Springer-Verglag, New York, pp. 80-87.

Barsom, J. M. and R.C. McNicol (1974). "Effective of stress concentration on fatigue-crack initiation in HY-130 steel." *ASTM STP 559*, American Society for Testing and Materials, Philadelphia.

Bazant, Z.P. (1985). "Mechanics of Fracture and Progressive Cracking in Concrete Structures." *Fracture Mechanics of Concrete, Engineering application of fracture mechanics*, v. 4, G.C. Sih and A. DiTommaso, editors, Martinus Nijhoff Publishers, The Hague, pp. 1-94

Bement, A.L.,Jr., Hoagland, R.G., Smidt, F.A.,Jr.(1971). "Fracture Mechanics and Radiation Effects." *Fracture, An Advanced Treatise*, Liebowitz (Editor), Volume III, Academic Press New York and London, pp.548-551.

Broek,D.(1986). *Elementary Engineering Fracture Mechanics*, fourth revised edition, Martinus Nijhoff Publishers, pp.261-266.

Broek, D., Leis, B.N.(1981). "Similitude and anomalies in crack growth rRate." *Material, Experimentation and Design in Fatigue*, Sherratt and Stargen Ed., Westburg House, pp. 126-146.

Carpinteri, A.(1986). *Mechanical Damage and Crack Growth in Concrete*. Martinus Nijhoff Publishers, pp44-46.

Carpinteri, A. (1985). "Scale Effects in Fracture of Plain and Reinforced Concrete Structures." *Fracture Mechanics of Concrete, Engineering application of fracture mechanics*, v. 4, G.C. Sih and A. DiTommaso, editors, Martinus Nijhoff Publishers, The Hague, pp. 95-140

References
(**Part II** Continued)

Chudnovsky, A. I.(1973). "On fracture of solids." *Investigation on Elasticity and Plasticity*, No. 9, Leningrad University Press, pp. 3-41.

Clark, W. G., Jr.(1974). "How Fatigue Crack Initiation and Growth properties Affect Material Selection and Design Criteria." *Metals Engineering Quarterly*, Aug.

Cooke, R.J., Beever, C.J.(1974). "Slow Fatigue Crack Propagation in Pearlitie Steels." *Material Science and Engineering*, Vol 13,p.201.

Davidson, D.L., Lankford, J.(1983). "Fatigue crack tip strain in 7075-t6 aluminum alloy by stereo imaging and their use in crack growth method." *ASTM STP 811*, American Society for Testing and Materials, Philadelphia, PP. 71-399.

Dugdale, D.S.(1960). "Yielding of steel sheet containing slits." *J. Mech, Phys.* Vol. 8, pp 100-108.

Ernst, H.A.(1989). "Further development on the modified J-integral." *Non-linear Fracture Mechanics, Volume II - Elastic-plastic Fracture, ASTM STP 995*, American Society for Testing and Materials, Philadelphia, pp. 306-319.

Fine,M.E., Davidson, D.L.(1983). "Quantitative measurement of energy associated with a moving fatigue crack." *Fatigue Mechanics in Quantitative Measurement of Physical Damage, ASTM STP 811*, American Society for Testing and Materials, Philadelphia, pp. 350-370.

Frost, E.N., Marsh, K.J., Pook, P.L.,(1974). *Metal Fatigue*, Clarendon Press, Oxford.

Griffith,A.A.(1920). "The phenomena of rupture and flaw in solids." *Transaction*, Royal society of London, A-22I, 1920.

Head, A.K.(1956). "The propagation of fatigue cracks." *Journal of Applied Mechanics*, September, pp 407-409.

References
(**Part II** Continued)

Hertzberg, R.W. (1976). *Deformation and Fracture Mechanics of Engineering Materials*, John Wiley & Sons, New York, pp. 5-38.

Hillerborg, A. (1985). "Numerical methods to simulate softening and fracture of concrete." *Fracture Mechanics of Concrete, Engineering application of fracture mechanics*, v. 4, G.C. Sih and A. DiTommaso, editors, Martinus Nijhoff Publishers, The Hague, pp. 141-170

Hilsdorf, H.K., and Brameshuber, W. (1991). "Code-type formulation of frcture mechanics comcept for concrete." *Internationsl Journal of Fracture*, Vol. 51, 61-72, pp. 61-72.

Irwin, G.R. (1960). "Plastic zone near a crack and fracture toughness." *Proc. 7th Sagamone Conference*, P IV-63.

Jenq, Y.S., Shah, S.P.(1985). "Nonlinear fracture parameters for cement based composites: theory and experiments." *Application of Fracture Mechanics To Cementitious Composites, NATO ASI series E, Applied Science*, No. 94 S.P.Shah(Editor), Martinus Nijhoff Publishers, pp. 319-360.

Jones, D. J., H. Liebowitz and J. Eftis (1974). "Fracture toughness characterization of several aluminum alloys in semi-brittle fracture." *Engineering Fracture Mechanics*, Vol. 6, No. 4, pp. 639 - 652.

Kachanov, L.M. (1986). *Introduction to Continuum Damage Mechanics*. Martine Nijhoff Publishers, Dordrecht, Boston and Lancaster, pp.2-10.

Karsan, P., and Jirsa, J.O. (1969). "Behavior of concrete under compression loading." *J. Struct. Div. ASCE*, Vol. 95, No. ST12, Proc. pap6935, December pp.2543-2563.

Kovalenko, A. D. (1969). *Thermoelasticity*, Translated from Russian by D. B. Macvean, Wolters-Noordhoff Publishing Groningen, The Netherlands, pp. 21-26.

References
(**Part II** Continued)

Leis, B.N., Forte, T.P.(1986). "Fatigue growth of initially short cracks in notched aluminum and steel plates", from *Elementary Engineering Fracture Mechanics*, by David, B. pp. 288-290.

Loye, C., Bathias, C. (1983). "The Plastic Zone ahead of a Fatigue Crack in 316 Stainless Steel." *Fatigue Mechanics, Advances in Quantitative Measurement of Physical Damage, ASTM STP 811*, American Society for Testing and Materials, Philadelphia, pp.427-444.

Miller,M.S., Gallagher, P. (1981). "An analysis of several fatigue crack growth rate (FCGR) description." *Fatigue Crack Growth Measurement and Data Analysis, ASTM STP 738*, American Society for Testing and Materials, Philadelphia, pp.205-251.

Murakami, S. and Ohno, N. (1981). "A continuum theory of creep and creep damage." *Creep in Structures*, A. R. Ponter and D. R. Hayhurst (Eds.), Springer-Verlag, Berlin, pp. 422-444.

Nielsen, M. P. (1990). "An energy balance crack growth formula." *Bygningsstatiske Meddelelser*, Danish Society for Structural Science and Engineering, vol. 61, No. 3-4, pp. 71-125.

Paris, P.C. (1957). "The mechanics of fracture propagation and solutions to fracture arrested problems." *Document D2-2195*, The Boeing Company, USA.

Paris, P.C. and F. Erdogan (1963). "A critical analysis of crack propagation laws." *Trans. American Soc. Mechanical Engineers (ASME), J. Basic Engng 85D*, pp. 528 -534.

Paris, P.C.(1962). *The growth of fatigue cracks due to variations in load. Ph.D. Thesis*, Lehigh University.

Rice, J.R. (1968). "Mathematical analysis in the mechanics of fracture." *Fracture, An Advanced Treaties Vol II, Mathematical Foundations*. pp. 191-311.

References
(**Part II** Continued)

Rice, J.R. (1966), "Mechanics of crack tip deformation and extension by fatigue." *Fatigue Crack Propagation, Symposium of Fatigue Crack Propagation (1966: Atlantic city) ASTM STP 415*, American Society for Testing and Materials, Philadelphia, pp. 247-309.

Rice R.J. (1967). "Stress due to a sharp notch in a work-hardening elastic-plastic material loaded by longitudinal shear." *J. appl Mech.*, Vol 34 P.287-98.

Shah,S.P. (1990). "Fracture process zone and parameters." *Engineering Fracture Mechanics,* Vol. 35, No. 1/2/3, pp. 1-14.

Shah, S.P. (1984). "Dependence of concrete fracture toughness on specimen geometry and on composition." *Fracture Mechanics of Concrete, Engineering application of fracture mechanics,* v. 3, A. Carpinteri and A.R. Ingraffea, editors, Martinus Nijhoff Publishers, The Hague, pp. 111-138

Sih, G.C. (1984). "Mechanics of material damage in concrete, fracture mechanics of concrete." *Engineering application of fracture mechanics,* v. 3, A. Carpinteri and A.R. Ingraffea, editors, Martinus Nijhoff Publishers, The Hague, pp. 1-30

Stark, E.A.Jr., and Williams, J.C. (1984). "Microstructure and the fracture mechanics of fatigue crack propagation." *ASTM STP 1020,* American Society for Testing and Materials, Philadelphia, P.193.

Tada,H., Paris, P., Irwin, G. (1973), *The Stress Analysis of Cracks Handbook,* Del Research Corporation.

Tanak, K. (1989). "Mechanics and micromechanics of fatigue crack propagation." *Fracture Mechanics: Perspective and Dircetion, (Twentieth Symposium) ASTM STP 1020,* R.P. Wei and R.P. Gangfloff, eds. American Society for Testing Materials, Philadelphia, pp.151-183.

References
(**Part II** Continued)

Timoshanko, S.P. (1953). *History of Strength of Materials,* McGraw-Hill Book Company, New York, Toronto, London, pp. 162-167.

Vakulenko, A. A. and Kachanov, M.L. (1971). "Continuum model of medium with cracks." *Mekhanika Tverdogo Tela,* No. 4, 1971, pp. 159-166.

Wang, W. and Hsu, C.T.T.(1994). "Fatigue crack propagation rate by damage accumulation theory." *Journal of Engineering Mechanics,* ASCE, Vol. 120, No.4, April., pp. 776-795.

Wang, W., Hsu, C.T.T. and Blackmore, D.(1994), "Mathematical treatments of a generalized process zone theory in fracture mechanics." Unpublished report, *Technical Report Structural Series,* Dept. of Civil & Enviro. Engrg., NJIT.

Weertman, J. (1978). "True stress intensity fctor rtionalization of a 2nd and 4th power Paris fatigue crack growth equation." *Fracture Mechanics,* Perrone et al. (Eds.), University Press of Virginia, Charlottesville, pp. 193 - 204.

Weibull, W.(1939). "Statistical theory of srength of materials." *Proc. Roy. Acad. Eng. Sci.* No. 151.